2018

Friction and wear mechanisms of high performance polyetheretherketone and silicone

Mark Placette
Iowa State University

Friction and wear mechanisms of high performance polyetheretherketone and silicone

by

Mark Daniel Placette

A dissertation submitted to the graduate faculty

in partial fulfillment of the requirements for the degree of

DOCTOR OF PHILOSOPHY

Major: Mechanical Engineering

Program of Study Committee:
Christian J. Schwartz, Major Professor
Michael Bartlett
Jonathan Claussen
Adarsh Krishnamurthy
Pranav Shrotriya

The student author, whose presentation of the scholarship herein was approved by the program of study committee, is solely responsible for the content of this dissertation. The Graduate College will ensure this dissertation is globally accessible and will not permit alterations after a degree is conferred.

Iowa State University

Ames, Iowa

2018

DEDICATION

To my wife, Dan Li and the Li family, to my brother, Joel, and to my sister, Claire.

TABLE OF CONTENTS

ACKNOWLEDGMENTS v

ABSTRACT vi

CHAPTER 1: GENERAL INTRODUCTION 1

1.1 Motivation 1

1.2 Literature Review 2

1.2.1 Modeling of Rough Surfaces 2

1.2.2 Polymer Tribology: Wear Modes 3

1.2.3 PEEK Wear and the Role of Transfer Film 6

1.2.4 Implantable Cardiac Device (ICD) Wear 8

1.3 Research Objectives and Dissertation Organization 10

1.3.1 Research Objectives 10

1.3.2 Dissertation organization 11

1.4 References 12

CHAPTER 2: A COMPUTATIONAL INVESTIGATION OF FRICTION AND WEAR-RELEVANT ASPERITY BEHAVIOR USING CLASSICAL AND FRACTAL SURFACE REPRESENTATIONS 17

2.1 Introduction 18

2.2 Mathematical Models and Procedures 22

2.2.1 Two-dimensional Approximation of the Greenwood-Williamson Model 22

2.2.2 Surface Generation 25

2.2.3 Finite Element Analysis 29

2.3 Results and Discussion 31

2.3.1 Comparison to Modified GW Model 31

2.3.2 Comparison of Surfaces with Same Average Roughness 33

2.3.3 Observations and Possible Limitations of Modeling Approach 38

2.4 Conclusions 39

2.5 References 40

CHAPTER 3: THE EFFECT OF SURFACE ROUGHNESS ORIENTATION ON PEEK (POLYETHERETHERKETONE) TRANSFER FILM IN MULTI-DIRECTIONAL SLIDING 43

3.1 Introduction 44

3.2 Materials and Methods 47
3.2.1 Experimental Materials 47
3.2.2 Wear Testing 47
3.2.4 Chemical Etching and Micro-Scratch Testing 52
3.2.5 Infrared Radiometry 54
3.3 Results and Discussion 55
3.3.1 Wear, Friction Coefficient, and Transfer Film Observations 55
3.3.2 Dark Deposition Investigation 61
3.3.3 Directional Strengthening Hypothesis: Scratch Tests and Chemical Etching 62
3.3.4 Thermal Softening Hypothesis: Transfer Film Analysis 64
3.3.5 Bulk Temperature Rise 66
3.4 Conclusions 67
3.5 References 67

CHAPTER 4: THE WEAR REDUCING ATTRIBUTES OF POLYETHERETHERKETONE (PEEK) TRANSFER FILM AS A RESULT OF LARGE INITIAL WEAR 71
4.1 Introduction 72
4.2 Materials and Methods 75
4.2.1 Testing Materials 75
4.2.2 Wear Testing 76
4.2.3 White Light Profilometry 78
4.2.4 Thermal Behavior 79
4.2.5 Finite Element Contact Model 82
4.3 Results and Discussion 83
4.3.1 Wear Results 83
4.3.2 Coefficient of Friction and Frictional Heating 89
4.3.3 Counterface and Transfer Film Roughness 91
4.3.4 DMA Cyclic Heating 93
4.3.5 Finite Element Contact Model 95
4.4 Conclusions 96
4.5 References 97

CHAPTER 5: TRIBOLOGICAL TESTING OF SILICONE IMPLANTABLE CARDIAC DEVICE LEADS BY INVESTIGATING LOAD, TESTING FLUID, AND SILICA ABRASIVE....101

5.1 Introduction....102

5.2 Materials and Methods....105

5.2.1 Experimental Materials....105

5.2.2 Wear....108

5.2.3 Wear Analysis....109

5.3 Results....110

5.3.1 Wear Results....110

5.3.2 Wear Scar Analysis....113

5.3.3 Optical Microscopy of Silicone Leads....116

5.4 Conclusions....117

5.5 References....118

CHAPTER 6: GENERAL CONCLUSIONS....120

ACKNOWLEDGMENTS

I am fortunate to have received incredible support with my research from numerous people and institutions. I want to first express my deepest thanks to Dr. Cris Schwartz for his wisdom and patience. I would not have been able to accomplish this dissertation without his guidance.

I would like to extend my gratitude to my graduate committee members: Dr. Michael Bartlett, Dr. Jonathan Claussen, Dr. Adarsh Krishnamurthy, and Dr. Pranav Shrotriya for their support and advice in completing my graduate work.

Additionally, I would like to acknowledge Joshua DeLarm, Craig Severson, Jim Shelledy, and Wyman Martinek for assisting in the fabrication of my experiments. I would also like to thank John Howell, Jim Dautremont, and Taylor Schweizer for advice on the electronic aspects of this work. I want to acknowledge staff that continuously assisted me throughout my studies: Deb Schroeder, Joel Buehler, and Nate Jensen. Furthermore, I am thankful for Dr. Warren Straszheim and Dr. Dapeng Jing for their guidance of electron microscopy techniques. I would also like to acknowledge Medtronic for their financial support for parts of this work.

I would like to extend my gratitude to my fellow tribology lab members for their guidance and companionship including: Dr. Kevin Plumlee, Dr. Matthew Darden, Dr. Geetha Chimata, and Thomas Wilde. I also appreciate Dr. Sougata Roy and Derek White for their assistance in parts of this work.

Finally, I would also like to thank my undergraduate research mentor, Dr. Xuejun Fan, who continued to support me during my graduate studies along with many friends and family members.

ABSTRACT

This work examines two high performance polymer tribology systems. Polyetheretherketone (PEEK) is a high temperature, low wear thermoplastic that has potential for several modern industries, but the understanding of its wear mechanisms in relation to transfer film is not well understood. An investigation into these mechanisms would benefit the utility of PEEK in several applications. The second polymer system investigated is high performance silicone used in implantable cardiac devices (ICDs). Understanding the wear mechanisms of silicone *in-vivo* is challenging, and examining the fundamental causes of wear would benefit device design in surgical implantation methods. First, the viability of using finite element analysis as a way to understand fundamental contact behavior is investigated. It was found that for high-level contact models, average roughness is a weak sole descriptor of contact behavior. Next, two PEEK studies in dry sliding were conducted. The first study examined multi-linear and reciprocating sliding in relation to roughness orientation, while proposing hypotheses to explain transfer film behavior. The second PEEK study, examined the development of transfer film and wear with respect to roughness orientation for a variety of sliding distances. From these studies, it was found that frictional heating affects the volume of transfer film, multi-directional sliding and reciprocation play a role in wear and transfer film development, and roughness orientation can greatly impact both wear and transfer film of PEEK. Lastly, a silicone lead in implantable cardiac devices was studied by using three key parameters thought to affect its wear: load, albumin protein, and silica abrasive. It was found that none of these parameters greatly impacted the wear scar metrics, but silica and albumin can lead to wear mechanisms that might impact long-term wear or other wear modes.

CHAPTER 1: GENERAL INTRODUCTION

1.1 Motivation

This dissertation examines the friction and wear of two high-performance polymer tribology systems. One system investigated consists of a self-lubricating thermoplastic known as polyether-ether-ketone (PEEK) in dry sliding. The other system examined is a silicone composite in aqueous solution used in implantable cardiac devices (ICDs). These fundamentally dissimilar systems represent two extremes in polymer tribology behavior which will provide this study with an extensive look into polymer friction and wear mechanisms.

Poly-ether-ether-ketone (PEEK) is a polymer with several favorable wear properties. It has excellent mechanical strength, chemical and moisture resistance, and high thermal stability. These properties make PEEK ideal for industries in need of light-weight bearing materials which are reliable in harsh environments. PEEK is replacing metal materials that require liquid lubricants in automotive, aviation, and commercial mining industries. Like other polymers, PEEK forms a transfer film, a self-lubricating solid which replaces the need for liquid lubricant [1, 2]. The fundamental understanding of PEEK's transfer film would benefit numerous technologies that are limited by material performance.

From 1993-2006, the United States saw 2.4 million heart pacemakers implanted in patients with an average age of 75.5 years. In addition, 0.8 million implantable cardioverter defibrillators devices were implanted at this time. These implantable cardiac devices (ICD) raise the quality of life for patients with cardiac arrhythmia disorders by monitoring and regulating heart rate with electrical impulses. Currently, about 13% (396,000) of implanted pacemakers and 10.8 % (74,000) of defibrillators have been replaced from failure [3]. A large portion of these failures are normal battery depletion. However, one study showed out of 2,562 surgeries to

replace the depleted battery, 16% identified imminent lead failure caused by wear resulting in surgical [4]. Silicone is also used in other biomedical implants, sealants, and coatings, but its tribological performance limits its functionality since silicone has a high friction coefficient [5]. Investigating the wear mechanisms of this elastomer would assist in the design of safer and more reliable ICD insulation and other silicone tribology systems.

1.2 Literature Review

1.2.1 Modeling of Rough Surfaces

Since contact area and contact pressure are two vital factors affecting wear of all contacting materials, modeling of rough surfaces in contact is imperative to understanding mechanisms of tribology. The foundation for modeling of rough surfaces is Hertzian contact mechanics. Hertz developed equations for contact area, stress, and strain in relation to load and simple asperity geometry. The Hertzian equations make several assumptions worth noting. The contacts are assumed to be spherical or cylindrical, and the contact radius is assumed to be significantly less than the overall body length. The theory also assumes all materials must be linearly elastic and isotropic, ignores friction and adhesion, and is exclusively static or quasi-static [6]. Given these assumptions, Boussinesq theorized elastic spheres with an applied load cannot have a greater contact area than what Hertzian contact predicts, which was later proved by Johnson [7, 8].

The Greenwood-Williamson (GW) model is one of the most empirically tested models in literature, and uses Hertzian contact as a basis for modeling entire rough surfaces. The GW model predicts the contact area and pressure for a surface by statistically applying the Hertzian model to every asperity on an ideal surface [9]. Several iterations of the GW model exist that incorporate adhesion and other minor factors, but the fundamental approach is still considered to

have strong prediction power [10-12]. Nevertheless, the GW model has several intrinsic weaknesses. The GW model inherits most of the assumptions in the Hertzian equations such as identical asperities, rigid, undeforming bodies, and linear elasticity. The bodies in contact are also assumed to be have mechanically independent asperities, which, as the authors noted, is perhaps its greatest weakness [13]. Another important characteristic of the GW model is that friction arises from topography and not adhesion of asperities, although these were added in later studies [11]. Despite these limitations, the GW model was successful in two key areas: the prediction of contact area/pressure and the prediction of plastic/elastic deformation. The latter was included in the "plasticity-index" and ended a long-held debate of the plasticity of contacts in sliding [14]. Real surface asperities are not geometrically regular as described by the GW model. Surfaces typically have slope, curvature, and distribution of heights that are dependent on resolution and length of sample measurement [15]. This has led some researchers to develop more complex fractal surface models since they are scale independent and more accurately represent the geometry of real surfaces [16-18]. The asperity tips for fractal surfaces are much smaller, so fractal models typically predict more plastic deformation then the GW model [16]. Several wear modes are dependent on contact area and roughness of asperities, so both fractal and GW models find utility in tribology as a basis to explain wear behavior.

1.2.2 Polymer Tribology: Wear Modes

Polymer tribology is a multi-disciplined field that focuses on the wear and friction of polymer surfaces in contact. Studies have focused on a variety of tribological phenomenon such as contact mechanics, crystallography of wear debris, viscoelasticity or plastic flow at the interface, and many more. Polymers experience three fundamental wear modes and sometimes have self-lubrication properties that can greatly impact the wear cycle. In this section, the

fundamentals of polymer tribology are summarized, and focus is given to polymer-on-metal interactions in dry sliding.

Perhaps the most intuitive wear mode of polymers is abrasive wear, which is the result of differential hardness of the metal counterface and polymer surfaces. Some researchers have suggested to categorize all abrasion into general categories of low and high stress regimes, gouging, and polishing [19]. However, Myshkin et al. categorize two main forms of abrasive wear specific to polymers: ploughing and cutting [20]. Regardless of categorization, the two major factors that influence abrasive wear of polymers are the hardness of the counterface and counterface roughness. In addition, angle of asperities and yield strength can have significant abrasive effects [19-21]. Abrasion can be described experimentally by the Lancaster-Ratner correlation, the reciprocal of ultimate stress and corresponding strain compared to its wear coefficient [22]. One form of abrasion is known as third-body abrasive wear which can occur when particles either from the application or relocated wear debris, collect at the interface. If the particles are harder than the polymer or roughen the existing interface, significant wear can occur [23]. The effect of third-body wear is described more detail in a later section as it is most relevant to ICDs in this study.

The second mode of polymer wear is adhesion, and it is particularly important to the wear of polymers given the weak intermolecular bonding between two polymer chains. Adhesion wear is produced when van der Waals, hydrogen, or sometimes electrostatic bonds form between the polymer and counterface during sliding. As the polymer continues to slide over the metal counterface, the bond can pull polymer material from the bulk if the adhesive energy of the polymer-on-metal bond is higher than the cohesive strength of the bulk polymer. The shearing or drawing of these polymer particles will form wear debris and possibly transfer film [24]. The

adhesive forces are also responsible for friction in polymers and are influenced by temperature, pressure, and surface energy [25]. Since adhesion is a fundamental mechanism of surface science, several approaches exist for modeling adhesive forces as a source for friction ranging from simple to complex. Desagulier did the first work with lead spheres and estimated the contribution of adhesion to friction [26]. Johnson et al. proposed a model that used surface energy combined with elastic effects of the Hertzian model [27]. The bond interactions outside Hertzian contact are were later considered by Derjaguin et al. [28]. The latter two models were later united by Tabor as he explained both were extreme ends of a spectrum of adhesive behavior [29]. Bowden and Tabor proposed a simple adhesion model that defined friction as a ratio of asperity elastic modulus and hardness, linking macro-scale properties to microscale adhesion [30, 31].

The third wear mode of polymers is fatigue initiated tearing or crack growth through cyclic loading. Fatigue wear is produced by repeated loading and unloading of asperities during sliding which initiate crack growth. Like bulk mechanical fatigue, the cracks are points of stress concentration. Upon tangential and normal stress caused by friction and contact pressures respectively, these cracks grow and collide until a particle is eventually removed from the bulk. Fatigue wear is affected by existing defects in the material such as topographical craters or by defects in fabrication of the polymer such as voids [25]. Fatigue wear is related to contact pressure and possibly surface roughness as fatigue is normally not seen in contact pressures less than 1 MPa. Above this regime, fatigue wear is a function of number of cycles for a given contact stress [32].

Other than these fundamental wear modes, other supplementary or specialized wear modes have also been established for polymers. One wear mode that has received more attention

in recent studies is fretting. Fretting occurs when polymers translate at very small amplitudes but with high contact pressures. This results in stick/slip adhesion which promotes severe cracking and fatigue [33]. Polymers have a low melting temperature and thermal conductivity, and it is therefore likely melting temperatures are reached at the interface for medium to high velocities. The melting polymer interface can have a profound effect on friction and wear. If the "PV limit" is reached, the polymer is thought to undergo rapid melting which results in substantial wear [34]. This type of wear occurs only at high pressures or high sliding speeds, but normal frictional heating promotes adhesion and thereby might increase friction below this limit [35].

One way to possibly lower wear in polymers is to promote development of transfer films. Transfer films are films of polymer material which are adhered to the metal counterface. The added material between asperities is thought to lower contact pressure, protect against abrasion, and reduce wear [36, 37]. Transfer films are then very desirable, and polymers can be filled with additives to promote transfer film formation [36]. The concern with studies on PEEK transfer films is they are qualitative and often lack fundamental physical explanations for transfer film development.

1.2.3 PEEK Wear and the Role of Transfer Film

PEEK is a thermoplastic polymer whose base unit consists of three aromatic rings connected by two ether groups and a ketone group. The aromatic rings are rigid, which accounts for its favorable mechanical, thermal, and chemical properties, but the ether and ketone groups can rotate freely about the backbone. PEEK can exist as semi-crystalline (spherulites/lamella) or amorphous depending on the rate of cooling during manufacturing [38, 39]. As a result of the favorable wear properties, PEEK has practical uses in complex and traditional environments which exclude many other wear materials including metals [1]. PEEK has also been known to be

biocompatible for decades and is a candidate for orthopedic and spinal implants [38]. However, it is rare PEEK or any other polymer is utilized in its unfilled form. PEEK typically has high wear resistance, but its coefficient of friction relatively high (~0.3). For this reason, it is common for PEEK to be blended with other polymers and reinforcing additives to reduce friction and wear [39].

Compared to other classic tribological polymers, the effect of PEEK's crystalline structure and changes in phase on wear behavior is not clearly understood. Unlike PTFE, PEEK does not have lamella shearing that produces transfer film and substantial wear [40, 41]. Plasma etching and SEM imaging revealed ultra-high molecular weight polyethylene (UHMWPE) can orient surface chains in the direction of sliding which produces directional strengthening. It is this strengthening which makes linear UHMWPE reciprocating wear rates several times less than in multi-directional sliding [42]. PEEK is known to be directional strengthened during a specialized process referred to as roll-trusion, but it is unknown whether this occurs during the wear process [43]. There is, however, evidence to suggest wear debris and surface polymer all undergo phase changes. Chemical etching of PEEK has revealed it's crystalline structure may become amorphous under plastic deformation when undergoing sliding [44]. Transversely, PEEK can exist in amorphous structures which can crystallize during the wear process [45]. PEEK transfer film itself has displayed orientation, but it is more likely this is a result of drawing polymer chains out of the bulk rather than bulk polymer orienting in the direction of sliding [46]. The exact effect of these phase changes in relation to wear and friction is not clear. For spherulite polymers, it has been speculated wear debris size is governed by the size of the spherulites and are formed by crack growth [47]. There is evidence that suggests smaller spherulite size, which also corresponds to higher molecular weight, increases wear resistance in PEEK [48].

While there have been some studies to suggest PEEK wear is not lowered by transfer film, PEEK transfer film development has been shown to depend on several factors. Transfer film appears to be assisted by roughness regimes where wear debris can by confined between asperities [49]. Roughness is also highly deterministic of wear, and a number of polymers display a transition point above which roughness values will cause considerable abrasion [50]. An early work on PEEK revealed sliding direction with respect to roughness orientation can greatly affect wear in a block-on ring system [51]. It is clear the direction of sliding relative to roughness orientation plays a role in transfer film and wear, but there is currently no theoretical explanation for why this occurs. Several studies suggest frictional heating is playing a significant role in inducing chemical and adhesive effects. Wear debris, for example, has been shown to have been generated near the melting temperature of PEEK [52, 53]. In a recent work, the temperature rise of PEEK during pin-on-disc sliding was analyzed by infrared thermography. The temperature rise matched closely with those predicted by Blok's flash temperature theory, and there was significant evidence to suggest PEEK films form due to localized zones of heated material undergoing shear [46]. The above PEEK studies indicate there is much to be learned about the thermal aspects and roughness orientation of transfer film and how it pertains to wear.

1.2.4 Implantable Cardiac Device (ICD) Wear

ICD lead wear studies are rare and little is known about the cardiac implant wear mechanisms. However, silicone wear it has been acknowledge as a severe tribology-based problem [54]. The few studies on this subject investigate the wear of the internal layers of the outer insulating layers or 'sleeve'. The sliding of insulating layer material (silicone, ethylene, and tetraflouroethylene) showed no thermal dependence on wear rate [55]. A similar study investigated the wear of internal sleeve layers consisting of polyurethane/silicone copolymers

and silicone elastomer contacts [56]. It is clear from the previous two studies of ICD lead wear and clinical studies is 1) frictional heating is not playing a dominant role in wear and 2) The ICD wire is expected to experience low loads and frictional heating. The general notions of silicone rubber friction and wear under lubricated sliding are well established so an understanding of fundamentals of these materials would benefit any proposed study.

The ICD leads are expected to experience the "mild wear" of rubbery materials. Rubber mild wear is defined as wear on the order of $\leq 10^2 \mu g$ cm^2 m^{-1}. Mild wear in rubbery polymers is mostly a factor of low frictional heating and relative velocity. This applies to ICD leads, especially considering the applied load is thought to be very low. Fatigue and tearing perpendicular to maximum shear stress are often associated with rubbery polymers since there are no natural shear planes. Rubbery polymers can experience wear in three subsequent stages: mechanical weakening, aging and fatigue, and crack formation [57]. However, another key characteristic of rubbery materials is rolling of material. This wear mode is governed by the adhesion between the rubber and metal surfaces. [24]. The ridges produced by this process are not to be confused with Schallamach waves which are the result of strong adhesion, large contact area, and viscoelasticity of rubbery polymers. These waves move rapidly across the rubbery surface and at high sliding velocities can move at very high speeds [58].

Although the ICD studies suggest that frictional heating is not a factor in its wear profile, but it still cannot be dismissed given the profound effect on the wear cycle. Frictional heating can promote material flow and adhesion which results in low coefficient of friction at lower temperatures. As temperature rises, the friction increases until a maximum coefficient is achieved. Then friction declines when temperature rises beyond this maximum [59]. This is profoundly affected by lubrication through cooling effects, and the cardiac implant is surrounded

by fluids *in vivo*. However, it is reasonable to assume the sliding speeds of ICDs are very small, and the effect of aqueous solutions on rubbery polymer sliding is sometimes hydrodynamic resulting in friction coefficients similar to dry sliding [60].

Another potential wear mode that could affect ICDs is known as third-body abrasion or third-body damage. One of the first to systematically explore this concept in metals was Rabinowicz et al. who slid surfaces in contact while providing large amounts of powder abrasive grit to the interface. Wear rates were reduced by the sand abrasion because, as speculated by the authors, only a small percentage of powder was abrading while the rest of the powder rolled with sliding providing a reduction in friction and lowering of contact pressure [61]. An increase in particle size and hardness will increase abrasion significantly, and third-body particles can be embedded in the contacting surfaces [62]. For polymers, third body abrasion is complex since third body debris can constitute solid lubrication as well as abrading particles. What complicates this matter further is the fact most polymers in practice are blends or composites which means debris particles may be composed of multiple materials in different concentrations. The result are wear particles that may vary in hardness and size and abrade at far different rates or in some cases act as transfer film [63]. This explains in part why adding strengthen particulates to the polymer matrix may actually increase wear since it allows harder wear particles at the interface [64, 65]. Since ICD leads are composites immersed in an active environment, particularly silicone which is mechanically strengthened with silica, third-body effects may play an important in the unusual wearing of the insulation. It is important to consider all the above factors in the ICD system considering the lack of empirical data relating to ICD wear.

1.3 Research Objectives and Dissertation Organization

1.3.1 Research Objectives

The purpose of this dissertation is to investigate two research areas in polymer tribology to examine the fundamental friction and wear mechanisms of each system.

1. Determining the primary causes of PEEK transfer film and its effect on wear from changes in roughness orientation
    a. To develop and verify a Finite Element Analysis of a 2D Greenwood Williamson Model to evaluate rough surface contact area and friction
    b. To develop quantitative methods of evaluating PEEK transfer film
    c. To determine causes of transfer film volume gradient in multi-directional sliding
    d. To determine the relationship between transfer film development and wear in regards to roughness orientation and frictional heating
2. Determining the factors of ICD lead wear in linear sliding by developing testing apparatus and procedure
    a. To simulate wear of field retrieval ICD sleeves using a developed testing apparatus
    b. To determine amount of wear from ICD sleeves for comparison amongst tests
    c. To examine the effects of traditional and biological tribology parameters such as load, third-body abrasion, bodily fluid, and sliding path on wear behavior
    d. To determine wear mode mechanisms of silicone lead sleeves

1.3.2 Dissertation organization

The chapters in this dissertation are organized according to the topic of study. Chapters 2-4 presents work conducted to accomplish research objective ‘1’. Chapter 5 presents work relating to research objective 2. Chapter 2 investigates the impact of a fundamental roughness parameter Ra by proposing a finite element analysis model of contacting surfaces and comparing

two different surface generation types' contact area. Chapter 3 discusses the research completed to explore the effects of PEEK wear and transfer film development in regards to sliding direction relative to roughness orientation in linear and multi-directional sliding. Chapter 4 extends the work done in Chapter 3 by implementing new wear paths and cataloging the wear of PEEK for varied sliding distances, while investigating wear debris and proposing a model to explain the observed frictional temperatures. Chapter 5 investigates the wear of silicone ICD lead wires via simulating *in vivo* conditions by using a full factorial matrix to observe interactions of three key tribological parameters. Chapter 6 summarizes the conclusions of all the studies in this dissertation and proposes future work.

1.4 References

[1] M. Zalaznik, M. Kalin, and S. Novak, "Influence of the processing temperature on the tribological and mechanical properties of poly-ether-ether-ketone (PEEK) polymer," *Tribology International,* vol. 94, pp. 92-97, 2016.

[2] R. Schroeder, F. W. Torres, C. Binder, A. N. Klein, and J. D. B. de Mello, "Failure mode in sliding wear of PEEK based composites," *Wear,* vol. 301, no. 1-2, pp. 717-726, 2013.

[3] S. M. Kurtz *et al.*, "Implantation Trends and Patient Profiles for Pacemakers and Implantable Cardioverter Defibrillators in the United States: 1993-2006.(Report)," *Pacing and Clinical Electrophysiology,* vol. 33, no. 6, p. 705, 2010.

[4] R. G. Hauser *et al.*, "Clinical experience with pacemaker pulse generators and transvenous leads: An 8-year prospective multicenter study," *Heart Rhythm,* vol. 4, no. 2, pp. 154-160, 2007.

[5] N. W. Khun, H. Zhang, J. L. Yang, and E. Liu, "Tribological performance of silicone composite coatings filled with wax-containing microcapsules," *Wear,* vol. 296, no. 1-2, pp. 575-582, 2012.

[6] H. Hertz, "Über die Berührung fester elastischer Körper und über die Härte," ed: Univ.-Bibliothek Frankfurt am Main, 1882.

[7] J. Boussinesq, Paris : Gauthier-Villars, 1885.

[8] K. L. Johnson, "Anote on the adhesion of elastic solids," *British Journal of Applied Physics,* vol. 9, no. 5, pp. 199-200.

[9] J. A. Greenwood and J. B. P. Williamson, "Contact of Nominally Flat Surfaces," *Proceedings of the Royal Society of London. Series A, Mathematical and Physical Sciences,* vol. 295, no. 1442, pp. 300-319.

[10] M. Ciavarella, V. Delfine, and G. Demelio, "A “re-vitalized” Greenwood and Williamson model of elastic contact between fractal surfaces," *Journal of the Mechanics and Physics of Solids,* vol. 54, no. 12, pp. 2569-2591, 2006.

[11] M. Ciavarella, J. A. Greenwood, and M. Paggi, "Inclusion of “interaction” in the Greenwood and Williamson contact theory," *Wear,* vol. 265, no. 5, pp. 729-734, 2008.

[12] J. A. Greenwood, C. Putignano, and M. Ciavarella, "A Greenwood & Williamson theory for line contact," *Wear,* vol. 270, no. 3, pp. 332-334, 2011.

[13] J. A. Greenwood and J. J. Wu, "Surface Roughness and Contact: An Apology," *International Journal of the Italian Association of Theoretical and Applied Mechanics AIMETA,* vol. 36, no. 6, pp. 617-630, 2001.

[14] R. A. Onions and J. F. Archard, "The contact of surfaces having a random structure," *Journal of Physics D: Applied Physics,* vol. 6, no. 3, pp. 289-304, 1973.

[15] R. S. Sayles and T. R. Thomas, "Surface topography as a nonstationary random process," *Nature,* vol. 271, no. 5644, p. 431, 1978.

[16] A. Majumdar and B. Bhushan, "Fractal Model of Elastic-Plastic Contact Between Rough Surfaces," *J. Tribol.,* vol. 113, no. 1, p. 1, 1991.

[17] B. B. Mandelbrot, "Self-Affine Fractals and Fractal Dimension," *Physica Scripta.,* vol. 32, no. 4, pp. 257-260, 1985.

[18] W. Yan and K. Komvopoulos, "Contact analysis of elastic-plastic fractal surfaces," *Journal of Applied Physics,* vol. 84, no. 7, pp. 3617-3624, 1998.

[19] K. G. Budinski, *Surface Engineering for Wear Resistance / Kenneth G. Budinski*. Englewood Cliffs, N.J.: Englewood Cliffs, N.J. : Prentice Hall, 1988.

[20] N. K. Myshkin, M. I. Petrokovets, and A. V. Kovalev, "Tribology of polymers: Adhesion, friction, wear, and mass-transfer," *Tribology International,* vol. 38, no. 11-12, pp. 910-921, 2005.

[21] L. W. McKeen, *Fatigue and Tribological Properties of Plastics and Elastomers Laurence W. McKeen*, 2nd ed.. ed. Amsterdam ; Oxford: Amsterdam ; Oxford : William Andrew, 2010.

[22] N. Chand, P. Sharma, and M. Fahim, "Correlation of mechanical and tribological properties of organosilane modified cenosphere filled high density polyethylene," *Materials Science & Engineering.*, vol. 527, no. 21, pp. 5873-5878, 2010.

[23] A. Birkett and J. K. Lancaster, "Counterface effects on the wear of a composite dry-bearing liner," *Wear,* vol. 110, no. 3, pp. 345-357, 1986.

[24] G. W. Stachowiak and G. W. Stachowiak, *Engineering Tribology*. Amsterdam ; Boston: Butterworth-Heinemann, 2005.

[25] B. J. Briscoe, *Polymer Tribology*. Singapore: Singapore World Scientific, 2009.

[26] D. Dowson, *History of Tribology / Duncan Dowson*. London: London : Professional Engineering Publishing, 1998.

[27] K. L. Johnson, K. Kendall, and A. D. Roberts, "Surface Energy and the Contact of Elastic Solids," *Proceedings of the Royal Society of London. Series A, Mathematical and Physical Sciences,* vol. 324, no. 1558, pp. 301-313, 1971.

[28] B. V. Derjaguin, V. M. Muller, and Y. P. Toporov, "Effect of contact deformations on the adhesion of particles," *Journal of Colloid And Interface Science,* vol. 53, no. 2, pp. 314-326, 1975.

[29] D. Tabor, "The hardness of solids," *Review of Physics in Technology,* vol. 1, pp. 145-179, 1970.

[30] F. P. Bowden and D. Tabor, "Mechanism of Metallic Friction," *Nature,* vol. 150, no. 3798, p. 197, 1942.

[31] F. P. Bowden, *The Friction and Lubrication of Solids, / by F.P. Bowden and D. Tabor*. Oxford: Oxford, Clarendon Press, 1950.

[32] J. R. Atkinson, K. J. Brown, and D. Dowson, "The Wear of High Molecular Weight Polyethylene—Part I: The Wear of Isotropic Polyethylene Against Dry Stainless Steel in Unidirectional Motion," *Journal of Lubrication Technology,* vol. 100, no. 2, p. 208, 1978.

[33] I. Etsion, "Revisiting the Cattaneo--Mindlin concept of interfacial slip in tangentially loaded compliant bodies.(Author abstract)(Report)," *Journal of Tribology,* vol. 132, no. 2, p. 20801, 2010.

[34] J. K. Lancaster, "Estimation of the limiting PV relationships for thermoplastic bearing materials," *Tribology,* vol. 4, no. 2, pp. 82-86, 1971.

[35] C. M. McC. Ettles, "Polymer and Elastomer Friction in the Thermal Control Regime," *A S L E Transactions,* vol. 30, no. 2, pp. 149-159, 1987.

[36] S. Bahadur, "The development of transfer layers and their role in polymer tribology," *Wear,* vol. 245, no. 1, pp. 92-99, 2000.

[37] J. M. Blakely, *Surface Physics of Materials / edited by J. M. Blakely*. New York: New York : Academic Press, 1975.

[38] S. M. Kurtz, *PEEK Biomaterials Handbook* (Plastics Design Library). Burlington: Burlington : Elsevier Science, 2011.

[39] L. Mu *et al.*, "Comparative Study of Tribological Properties of Different Fibers Reinforced PTFE/PEEK Composites at Elevated Temperatures," *Tribol. Trans.,* vol. 53, no. 2, pp. 189-194, 2010.

[40] S. Biswas and K. Vijayan, "Changes to near-surface region of PTFE during dry sliding against steel," *Journal of Materials Science,* vol. 23, no. 5, pp. 1877-1885, 1988.

[41] S. K. Biswas and K. Vijayan, "Friction and wear of PTFE — a review," *Wear,* vol. 158, no. 1, pp. 193-211, 1992.

[42] A. Wang *et al.*, "Orientation softening in the deformation and wear of ultra- high molecular weight polyethylene," *Wear,* vol. 203, pp. 230-241, 1997.

[43] R. Ciora and J. Magill, "Rolltruded poly(aryl ether ether ketone) (PEEK) for membrane applications," *Sep. Sci. Technol.,* vol. 32, no. 5, pp. 899-923, 1997.

[44] Q. Wang, Y. Wang, H. Wang, N. Fan, M. Wang, and F. Yan, "Evaluation of fretting Wear Behavior of PEEK by Analyzing the Change of Crystallinity: The High Temperature Effect," *Polymer Engineering and Science,* 2017.

[45] G. Zhang, H. Yu, C. Zhang, H. Liao, and C. Coddet, "Temperature dependence of the tribological mechanisms of amorphous PEEK (polyetheretherketone) under dry sliding conditions," *Acta Materialia,* vol. 56, no. 10, pp. 2182-2190, 2008.

[46] K. A. Laux, A. Jean-Fulcrand, H. J. Sue, T. Bremner, and J. S. S. Wong, "The influence of surface properties on sliding contact temperature and friction for polyetheretherketone (PEEK)," *Polymer,* vol. 103, pp. 397-404, 2016.

[47] F. J. Clauss, *Solid Lubricants and Self-lubricating Solids / [by] Francis J. Clauss*. New York: New York, Academic Press, 1972.

[48] Z. P. Lu and K. Friedrich, "On sliding friction and wear of PEEK and its composites," *Wear,* vol. 181, pp. 624-631, 1995.

[49] A. E. Hollander and J. K. Lancaster, "An application of topographical analysis to the wear of polymers," *Wear,* vol. 25, no. 2, pp. 155-170, 1973.

[50] T. C. Ovaert and H. S. Cheng, "Counterface topographical effects on the wear of polyetheretherketone and a polyetheretherketone-carbon fiber composite," *Wear,* vol. 150, no. 1, pp. 275-287, 1991.

[51] K. Friedrich, J. Karger-Kocsis, and Z. Lu, "Effects of steel counterface roughness and temperature on the friction and wear of PE(E)K composites under dry sliding conditions," *Wear,* vol. 148, no. 2, pp. 235-247, 1991.

[52] M. Q. Zhang, Z. P. Lu, and K. Friedrich, "On the wear debris of polyetheretherketone: fractal dimensions in relation to wear mechanisms," *Tribology International*, vol. 30, no. 2, pp. 87-102, 1997.

[53] M. Zhang, L. Song, H. M. Zeng, K. Friedrich, and J. Kargerkocsis, "Frictional surface temperature determination of high-temperature-resistant semicrystalline polymers by using their double melting features," *J. Appl. Polym. Sci.*, vol. 63, no. 5, pp. 589-593, 1997.

[54] B. Małecka *et al.*, "Endocardial silicone lead wear: description of tribological phenomena on the basis of microscopic examination of removed leads. Preliminary report," *Kardiologia Polska*, vol. 72, no. 10, p. 960, 2014.

[55] A. Himes and C. Wilson, "Wear of cardiac lead outer insulation due to internal cable motion," *Tribol. Int.*, vol. 62, pp. 177-185, 2013.

[56] C. Wilson and A. Himes, "Tribology of INsulation Materials Within Implantable Cardioverter-Defibrillator Leads," in *International Joint Tribology Conference*, Denver, Colorado, USA, 2012.

[57] J.-Å. Schweitz and L. Åhman, "Mild Wear of Rubber-Based Compounds-Chapter 9," *Composite Materials Series*, vol. 1, pp. 289-327, 1986.

[58] A. Schallamach, "How does rubber slide?," *Wear*, vol. 17, no. 4, pp. 301-312, 1971.

[59] K. A. Grosch, "Visco-Elastic Properties and the Friction of Solids: Relation between the Friction and Visco-elastic Properties of Rubber," *Nature*, vol. 197, no. 4870, pp. 858-859, 1963.

[60] S. C. Cohen and D. Tabor, "The Friction and Lubrication of Polymers," *Proceedings of the Royal Society of London. Series A, Mathematical and Physical Sciences*, vol. 291, no. 1425, pp. 186-207, 1966.

[61] E. Rabinowicz, L. A. Dunn, and P. G. Russell, "A study of abrasive wear under three-body conditions," *Wear*, vol. 4, no. 5, pp. 345-355, 1961.

[62] A. Misra and I. Finnie, "An experimental study of three-body abrasive wear," *Wear*, vol. 85, no. 1, pp. 57-68, 1983.

[63] J. Bijwe, S. Sen, and A. Ghosh, "Influence of PTFE content in PEEK–PTFE blends on mechanical properties and tribo-performance in various wear modes," *Wear*, vol. 258, no. 10, pp. 1536-1542, 2005.

[64] N. Chand, A. Naik, and S. Neogi, "Three-body abrasive wear of short glass fibre polyester composite," *Wear*, vol. 242, no. 1, pp. 38-46, 2000.

[65] A. P. Harsha, U. S. Tewari, and B. Venkatraman, "Three-body abrasive wear behaviour of polyaryletherketone composites," *Wear*, vol. 254, no. 7, pp. 680-692, 2003.

CHAPTER 2: A COMPUTATIONAL INVESTIGATION OF FRICTION AND WEAR-RELEVANT ASPERITY BEHAVIOR USING CLASSICAL AND FRACTAL SURFACE REPRESENTATIONS

A paper submitted to *Tribology International*

Mark D. Placette and Christian J. Schwartz

Abstract

One of the most fundamental challenges of modeling sliding tribological contact is accurately representing real surfaces. The major difficultly being that real surfaces are often composed of complex, and potentially random geometries. It is conceptually impossible to mimic real contact behavior in a deterministic manner given the dependence of asperity interactions and shapes as well as the vast number of engaged surface features during a sliding event. Traditionally, roughness parameters like average roughness (Ra) have been used as convenient and somewhat useful way of describing surfaces. The flaw in using a global average of asperity heights is it does not account for the size or shape of asperities. It is possible that two surfaces with similar Ra will behave extremely differently, because of gross underlying differences in their asperity geometry. Theoretical approaches to surface modeling have used relatively simple geometries like the Greenwood-Williamson (GW) model or fractals, in order to estimate bulk frictional behavior and asperity behavior as it relates to the potential for sliding wear. In this study, finite element (FE) modelling was employed to explore the differences in asperity behavior for surfaces with nearly equivalent average roughness but with vastly different asperity geometries and height distributions. It was found that the FE model is very comparable to the classic GW model at practical loads encountered in most applications, but at extremely

high loads the GW model predicts contact lengths much higher than the FE results. Two surfaces types (equivalent semi-circular geometries and fractals) with an array of different Ra values were studied for their contact behavior. The effects of an array of surface parameters (asperity tip angle, asperity length, distribution of heights, Ra) on contact length were studied, with a focus on their impact on wear-relevant parameters such as contact stresses and shear strains. It was found that Ra was a weak, but essential descriptor. The parameter which had the most explanatory power for the surfaces investigated was asperity tip angle. Although the surfaces presented here were idealistic, this work is an initial step in modeling complex sliding contact.

2.1 Introduction

One of the fundamental challenges in understanding tribological behavior is predicting macro-scale phenomena, such as friction coefficient, from the amalgamation of behaviors taking place at the micro-scale involving the numerous individual asperities. This challenge partly stems from the difficulty in accurately representing surface topology in a way that is amenable to analytical or computational models, furthered by the difficulty in bridging between the vastly different size scales involved. It is difficult to characterize the complexity of a real surface by using a small number of parameters versus a point-by-point height map. However, it would be extraordinarily useful to tribologists to be able to accurately predict phenomena such as friction coefficient from some small set of topological parameters. The result of this tradeoff is the definition of simple metrics that give some idea of surface topology. The most commonly used practice is to describe the surface using an algorithm based on asperity heights, such as the arithmetic average roughness (Ra), which is the arithmetic average of asperity heights over a selected lateral distance. Use of Ra as a topology parameter is extremely commonplace due to its simplicity of measurement and clarity of interpretation. In some cases, Ra can be useful in

predicting tribological behavior. For example, the wear rate of diamond-like carbons and polymers has been shown to depend heavily on a critical Ra value [1, 2]. The adhesion of rubber on a hard counterface has been shown to be influenced by average asperity height and has been well modelled when Ra is lower than 0.1 μm [3]. Additionally, topological metrics such as Ra can correlate mechanical and thermal behavior during sliding. It has been shown that increasing Ra can boost temperature rise in metals [4], but it also can reduce friction and slow contact area growth at moderate roughness ranges [5, 6].

Though the simplicity of calculating Ra can be useful for surface characterization, its lack of complexity often makes it impossible to compare real surfaces with similar roughness average. Furthermore, because it is a simple average of asperity heights, there are an infinite number of different surface topologies that possess the same Ra value [7]. This indicates the challenges in developing a predictive friction model from Ra, or any other single surface parameter. Conversely, it has been shown that surfaces of the same material with very different Ra have can produce nearly identical coefficients of friction [8]. The implication of this is that while parameters such as Ra enjoy widespread use in the representation of surface roughness, they can be a poor way of quantitatively representing real surfaces. Therefore, the ability to reliably predict frictional behavior from Ra is questionable in real surfaces, though it is a parameter that is very often employed in tribological studies. While many other global surface parameters have been proposed, many of them have no clear influence on contact behavior [9]. Therefore, it is essential to determine how effectively Ra can be used to predict macro-scale friction coefficient and to clearly indicate where it becomes less effective.

Predicting friction behavior from surface topology also involves the ability to model not only the contact mechanics involved in asperity-on-asperity contact, but also the ability to

aggregate these myriad asperity interactions into the observable macro-scale phenomenon. This modeling effort must trade fidelity for analytical tractability thus producing: 1) moderately accurate analytical friction models using idealized surfaces; or 2) specialized computational friction models requiring the processing of a multitude of data representing surface topology, thus only applicable to atomic-scale surfaces due to computational expense. The need continues to exist for a means to bridge the divide between these two extremes.

The majority of classic analytic contact models involve idealized surfaces consisting of spherical asperity tips, which allows for simplifications and reduced model complexity. Some early models that attempted to predict friction coefficient from surface topology were developed by Archard [10, 11]. Perhaps the most widely used contact model from this paradigm is the Greenwood-Williamson (GW) model which has been expanded and modified frequently since its creation [12-15]. Part of the simplicity of the GW model is its treatment of asperities as mechanically independent of each other and with a stochastic distribution of heights [16]. While this allows for qualitative assessment and comparison among conceptual surfaces, the GW model tends not to give fundamental insight into asperity-scale behavior [13]. Another limitation of the GW approach, and others, comes back to the simplified asperity characteristics that do not closely match real surfaces. More recent work has focused on creating higher fidelity topological representations of surfaces, yet still minimizing the number of parameters used. One such approach has been to use fractal mathematics to describe rough surfaces. Fractals can be effective at multiple size regimes because of their scale-independence [17], and thus fractal-generated surfaces can be made to visually resemble real surfaces. Another benefit to the fractal approach of surface representation is that it can be used to model irregular sizes and spacing of asperities, which is a challenge for a GW modeling approach [18]. However, despite the

usefulness of fractal surface modeling, it still suffers from issues related to information reduction in going from a complex three-dimensional topology to a few quantitative parameters [19]. Whether surfaces are represented using the stochastic spherical assumptions or fractal generation, there is still the question of how well either of these approaches can be used to develop a useful predictive model of contact and friction behavior. Thus, a computational modeling approach can give insights into how well either of the two analytical modeling approaches can describe the true group behavior of asperities, and can highlight whether there may be other asperity-level parameters that play a dominant role in the manifestation of macro-scale friction behavior.

It is likely that better predictive contact models will need to rely on capturing the contact mechanics of individual asperities, no matter what method is used for topological representation. Finite Element Analysis (FEA) is a potentially useful tool to address mechanics issues in high complexity problems. FEA has the ability to investigate nodal interactions as well as global deformation, making multi-scale modeling possible. Multi-scale FEA models have already been developed for sheet metal forming and nanoscale effects of hysteresis and microscopic adhesion [20, 21], to name a few. In addition, FEA has been utilized for roughness studies in micro-machines as well as fundamental roughness studies of simple triangular asperities and fractals [22-24]. Because of the ability to develop computational models of widely varying asperity characteristics, it has the potential to be a useful platform for exploring the impact of various asperity topological parameters on macro-scale friction coefficient. However, the use of FEA must be validated against empirically validated classic friction models, such as GW, before it can be deployed for more complex studies. The GW model is one of the most successful models in

literature with a long history of empirical confirmation and would be sufficient in validating the FEA models presented in this work.

The primary purposes of this work were threefold: 1) to develop a robust computational model to explore the observable macro-scale contact behavior generated by fundamental asperity-level contact mechanisms, 2) then to apply this model as a means to evaluate the impact of various asperity geometry parameters on contact as it relates to tribological applications, and 3) to assess the usefulness and shortcomings of a commonly used surface topology parameter. This was accomplished by producing idealized surfaces as FEA models using two generation methods: a) a 'Duplicated Shape' (DS) asperity profile similar to those used in the development of GW models, and b) a Fractal Based (FB) asperity profile based on the stochastic application of a common fractal generation algorithm. Complementary DS and FB surfaces of the same Ra values were generated and incorporated into a two-body finite element model which simulated the compression and sliding of the subject surface against an idealized flat and rigid body. Normal loads and asperity parameters were varied in the simulation to observe the impacts on actual contact length and number of asperities in contact. These data indicated the ranges where the GW contact model, as well as the use of Ra as a roughness measure, went from reasonable to erroneous. This paper presents the details of the investigation as well as the results.

2.2 Mathematical Models and Procedures

2.2.1 Two-dimensional Approximation of the Greenwood-Williamson Model

A linear elastic finite element modeling approach was developed to investigate the collective behavior of numerous individual asperities against a flat surface. In an effort to manage the computational complexity of this investigation, the investigators employed plane strain, purely elastic finite element models to simulate the compression and sliding event

between two bodies. There were preliminary steps that were developed, however, because of this conceptual decision. The Greenwood-Williamson model was originally formulated as a three-dimensional representation of a rough-on-flat surface whose asperities were simplified as spheres [12]. More recently, a two-dimensional approximation of the model was developed by Greenwood et al. [13]. It was this approximation that was used to assess the FEA models studied in this investigation. In two dimensions, the asperity tips were approximated as cylinders rather than spheres. According to the modified GW model, every asperity on the surface deforms as a cylinder-on-plane predicted by Hertzian contact mechanics. The load is linearly related to indention and independent of radii, and the equation resembles two parallel cylinders in contact with the distinction of one radii being infinite.

$$b = \sqrt{Rd_s} \tag{2.1}$$

$$P = \frac{\pi}{4} E^* d_s L \tag{2.2}$$

Where b is the contact half length. One point must be clarified when moving from the classic three-dimensional GW model to this plane strain modification. In the plane strain model of cylinder-on-flat contact, the zone of contact is assumed to be a rectangle with a dimension of $2b$ in the lateral direction (and a long dimension equal to the axial length of the cylinder). R is the radius of the cylinder being deformed, and d_s is the indention depth. E^* and L are the equivalent Young's modulus and axial length of the cylinder, respectively. As per the GW model, all cylinders on the rough surface are assumed to have identical radii. The flat surface and the rough surface are brought together until their reference planes are separated by distance, d. If an asperity's height relative to the reference plane, z is greater than d, then the asperity will be in contact. Both z and d are measured from the reference planes, and it is the difference in these values that is important as opposed to the absolute position of the planes. However, it is

conceptually convenient to have the reference plane of the cylindrical surface located at the mean asperity height, and the reference plane of the flat body located at the body's surface. If the asperity heights follow a Gaussian probability distribution function, $\phi(z)$, then the probability of any asperity is easily found by integrating that function. With the reference planes are located as proposed, then when d = 0 the chance of choosing any asperity in contact will be 50%. Similarly by applying Equations 2.1 and 2.2 with a normalized Gaussian distribution of heights, the total contact length (A_c), force (P_c), and number of asperities in contact (N_c) are given by:

$$A_c = \sqrt{\frac{2}{\pi}} NR^{1/2}\sigma \int_d^\infty (w(x))^{1/2} e^{\frac{1}{2}z^2} dz \tag{2.3}$$

$$\mathrm{P}_c = \sqrt{\frac{\pi}{32}} NE^* \sigma \int_d^\infty w(x) e^{\frac{1}{2}z^2} dz \tag{2.4}$$

$$N_C = N \int_d^\infty e^{\frac{1}{2}z^2} d(z) \tag{2.5}$$

Where N is the number of asperities on the surface, and σ is the standard deviation of asperity heights. $w(x)$ is the compliance of the asperity geometry as a function of d. For asperities with spherical tips (three-dimensional) this compliance is easily found as $w(x)=z-d$. In two dimensions, the compliance is problematic. The shape of asperities changes from spherical to cylindrical when shifting the problem to two dimensions. Thus, the shape of the contact region also shifts from circular to rectangular, and the thickness of the counterface becomes significant [13]. The authors pursued the use of the GW model to validate the FEA results, so the model also included the effect of a finite depth of the counterface. The compliance becomes a direct result of the thickness of the flat surface as proposed by Johnson [25]. It has been shown that this complicated compliance can be estimated as a simple power function [13].

$$w(x) = \alpha(z-d)^m \tag{2.6}$$

As suggested by Greenwood et al., α and m are found by the equations below where D is the thickness of the finite flat surface.

$$\alpha = 0.230 + \frac{1}{(0.799 + 0.444\ln(D/\sqrt{R\sigma}))} \tag{7}$$

$$m = 0.501 + \frac{1}{(3.730 + 4.404\ln(D/\sqrt{R\sigma}))} \tag{8}$$

This model has several important simplifications which diverge from the complex asperity-scale contact mechanics that the FEA model was developed to address. Firstly, the analytical GW model does not include adjacent asperity interaction. When one asperity comes into contact, it is assumed to have no influence on neighboring contacts. Thus, the relationship of d with either contact length or force is assumed negligible in the GW approach. As suggested by Greenwood et al., the force-per-length curve will still be viable for predicting behavior since the effect is cumulative [13]. Some have included mechanical interaction in later versions of the model, but the original still produces reasonable results without its inclusion [26]. Secondly, the contact length must be small compared to the asperity geometry. Thirdly, the bodies in contact are also assumed to deform completely elastically in the GW model. Real contacts typically experience plastic deformation, but the GW is purely elastic and still has great predictive power. It was expected that these assumptions would lead to a divergence in results between the predictions of the FEA and GW models at higher loads where contact length and deformation are very large.

2.2.2 Surface Generation

Two classes of surfaces were mathematically generated for incorporation into finite element models: 1) a series of ‘Duplicated Shape’ (DS) surfaces which had groups of asperities that had identical arc-tipped profiles but of stochastically varying heights, similar to a two-

dimensional analogue of the idealized spherical asperities in the GW models; and 2) a series of fractal based (FB) surfaces which collected asperities of varying radius tips and of different stochastically generated heights, as described in the next section. Both DS and FB surfaces were generated with computer algorithms that produced a surface profile which was imported into finite element modeling software to create a surface model. These two surfaces were chosen because of their dissimilar geometry and completely different input parameters as well as their relatively common usage for surface representation in tribological investigations. The DS surface was also useful in validating the FEA model proposed in this paper since it corresponds well with the idealized surface employed in the development of the two-dimensional GW model. An example of a Duplicate Shape surface is illustrated in Figure 2.1. This series of surfaces had asperities with 90 degree tip angles with equivalent radii of 1 μm. The height distribution was generated to be Gaussian with a known mean and standard deviation (SD) from a reference plane. Caution was taken to make certain the asperities did not collide upon deflection by separating the asperities by a center-to-center distance of 4 μm. Six surfaces of this type were generated with varying values of Ra. Each generated surface had 250 asperities and a nominal length of 1,000 μm. The summary of Ra and asperity heights is recorded in Table 2.1. The mean height for each surface was nearly identical, and the Ra was controlled by changing the standard deviation.

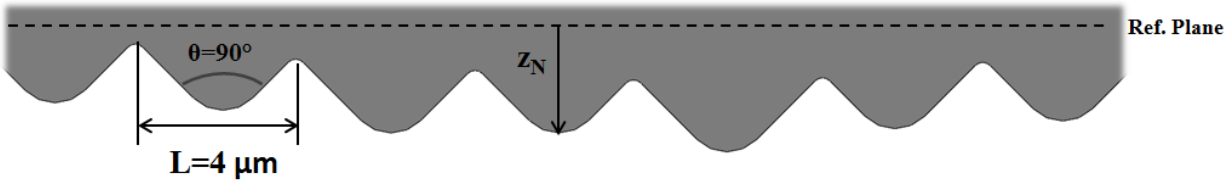

Figure 2.1: Duplicate Shape (DS) surface with identical asperities with tip radius of 1 μm and heights, Z_N.

Table 2.1: Duplicated Shape surface data containing the roughness, average asperity height, and standard deviation.

	Asperity heights (μm)	
Ra (μm)	**Mean**	**SD**
0.46	0.99	0.26
0.55	0.97	0.51
0.68	1.0	1.1
0.71	0.97	0.76
0.85	1.0	0.95
0.92	1.0	1.2

A computational algorithm was used to generate the Fractal Based (FB) surfaces as follows. The nominal surface length (1000 μm) was divided into segments by 2^9 equally-spaced points. A stochastic algorithm was used to assign each point a random height from the reference plane, based on a Gaussian distribution with a prescribed mean and standard deviation. The allowable range of these random heights was constrained to be within a percentage of the segment length, to avoid producing asperity tip angles which were too sharp for convergence of the finite element model. The generated surface was then further segmented and smoothed with b-splines to ensure a continuous surface when imported into FEA. The average roughness (Ra) of the trial surface was then calculated in order to either accept the trial surface or discard it and generate a new trial surface of a target roughness. Varying ranges of Ra were produced by modifying the allowable asperity height to segment length percentage. This class of surfaces is termed ‘fractal based’ because of the generation process used, even though it does not produce a mathematically precise fractal surface (as it has no fractal dimension and was constrained). Several fractal-based surfaces were generated and validated so that each had Ra values that corresponded to previously generated Duplicate Shape surfaces, thus producing sets of surface pairs (one DS and one FB surface per pair) of nearly equivalent average roughness. Figure 2.2 displays a portion of an FB surface generated with the above methods. The fractal-based models

were analyzed by an algorithm that recorded the height, tip angle, and length of each asperity. Because of the varying height and angles of asperities, it was necessary to develop an objective algorithm to count the number of asperities. Local minima and maxima were found for the entire surface where the second derivative equaled zero. An asperity was then defined as a local minima set between two local maxima. The asperity length (L_N) was defined as the distance between the local maxima, and the asperity tip angle (θ_N) was defined as the angle between the tangent lines of the asperity. The summary of FB surface data is displayed in Table 2.2. Generally, the average tip angle decreased as Ra increased, but there is a large standard deviation of tip angles on a given surface. The lengths of asperities and number of asperities are consistent despite Ra.

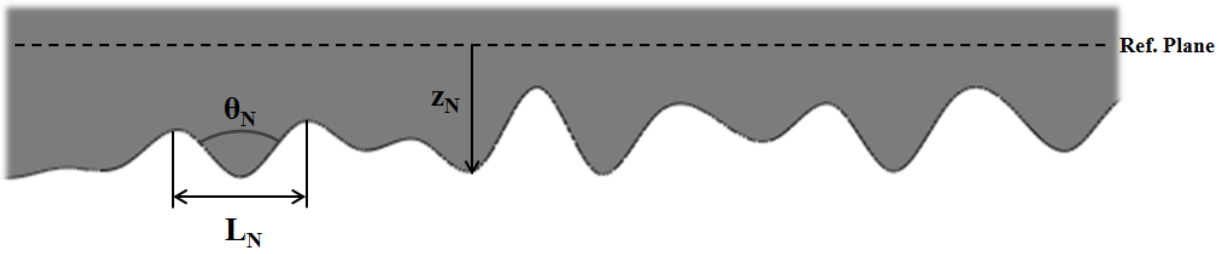

Figure 2.2: Fractal surface with tip angle, (θ_N) asperity length (L_N), and height (z_N) measured for every asperity with a total of N asperities.

Table 2.2 Fractal surface asperity data containing asperity length, height data, and total number of asperities.

Ra	Asperity Tip Angle		Asperity Length (μm)		Heights (μm)		No. of Asperities
	Mean	SD	Mean	SD	Mean	SD	
0.47	144	16.20	10.5	3.2	0.48	0.51	93
0.54	144	17.35	11.2	3.6	0.63	0.51	89
0.69	132	19.13	11.17	3.7	0.80	0.65	88
0.73	132	20.36	10.7	3.5	0.75	0.76	93
0.87	126	23.43	10.53	3.7	0.94	0.91	94
0.94	117	20.02	10.8	3.4	1.1	0.95	92

2.2.3 Finite Element Analysis

2.2.3.1 Model Validation

In order to gain confidence in the performance of the FEA model, simulations of surfaces with Duplicated Shape (DS) asperity profiles were run which closely adhered to the fundamental assumptions of the modified Greenwood-Williamson model described above. The results were compared to GW model predictions for contact force, number of asperities in contact, and total contact length. Because the DS surfaces have a Gaussian distribution of asperity heights, the analytical predictions can be directly obtained by use of the relations cited above, (Equation 2.3 through Equation 2.5). Figure 2.3 displays an overview of the FEA simulation scenario and surface configuration. The DS surface was placed above a rectangular counterface with a thickness of 10 μm. The bottom of the counterface was fully constrained while the top of the DS surface is constrained to prohibit rotation as well as displacement in the horizontal direction. To mimic the assumptions of the GW contact model, the interaction of the counterface and top surface were made frictionless. There is then no resulting tangential resistance at the interface, and the asperity-level friction coefficient is equivalent to zero. In this model validation, the DS surface was assumed rigid, while the counterface had properties similar to a tribologically relevant polymer, ultra-high molecular weight polyethylene (UHMWPE), using a linear elastic modulus of 690 MPa and a Poisson's ratio of 0.45. The simulation involved the application of increasing normal load until the FEA model failed to converge to a solution. Mesh refinement was conducted and tested for the parameters of contact area and contact stress. In this case, care had to be taken since a high number of elements increases stiffness and lowers chances of convergence in such a large model. The elements were refined until the contact pressure at specific point varied less than 0.4 % when the mesh density was reduced by a factor of 8.

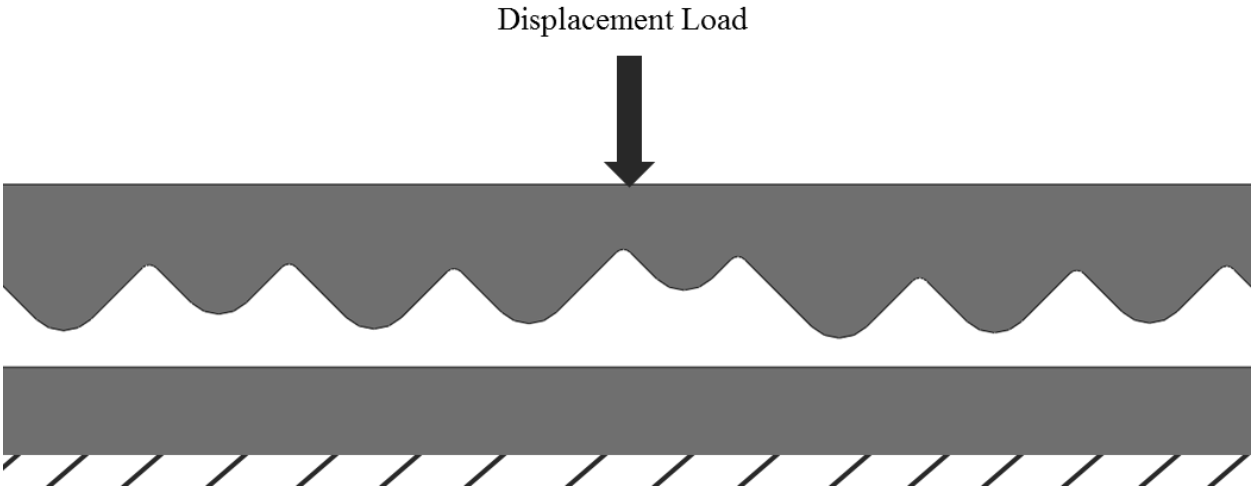

Figure 2.3: Configuration of bodies in FEA investigation. The top body is the bulk with the chosen topology (DS in this case), while the bottom is a rigid counterface whose bottom surface is completely fixed. Normal load is applied perpendicular to the top body.

2.2.3.2 Investigation of Average Roughness

To explore the usefulness of employing Ra as a simple roughness parameter for prediction of friction and contact behavior, simulation results of surfaces with the same Ra values were compared to each other. Each comparison involved one DS and one FB surface of the same roughness. While the spatial arrangement and boundary conditions were identical to that of Figure 2.3, the material properties were reversed to better represent a polymer on ground metal tribological scenario. Because the future goal is to use FEA for more complicated interactions, the surfaces' material properties were assigned for materials of interest to the authors. The counterface was modeled to be steel with an elastic modulus of 180 GPa and a Poisson's ratio of 0.3. The top body was modeled to have material properties of UHMWPE, as stated above. In addition, a simple asperity-level Coulombic friction behavior was added to the models using the computational penalty method formulation. The penalty method allows for the simultaneous solution of deformation and contact in the numerical model and is highly stable when implementing Coulombic friction [27, 28]. The global friction coefficient was taken to be 0.2, based upon a high estimate of dry sliding of steel and UHMWPE. To compare the macro-

scale friction coefficient generated by each surface type described in Tables 2.1 and 2.2 (either DS or FB), the surfaces were initially compressed and then modeled by simulating reciprocated sliding for a multitude of loads. Each surface in this analysis was then compressed and slid until numerical computational non-convergence of solution. The principle strain at failure was noted to determine if the models' computational failure was correlated to excessive strain or other material parameters.

2.3 Results and Discussion

2.3.1 Comparison to Modified GW Model

Figures 2.4 and 2.5 indicate the contact length and number of asperities in contact, respectively, for the computational results as well as the analytical modified Greenwood-Williamson model. Because a plane-strain approach was used with cylindrical asperities (as opposed to spherical asperities), the contact length reported indicates that the cylinder-on-flat contact zones are lines of growing length. The length shown is the sum of the contact lengths for all asperities. Furthermore, the load reported is expressed in load per length, as the two-dimensional analogue of stress. The contact length for the FEA model was approximately proportional to load for several orders of magnitude. As can be seen in the figures, the results of the modified GW model and the computational simulation of a Duplicated Shape asperity profile agreed reasonably well at low to moderate loads. The GW model overestimated contact length at very high loads, however. This deviation at higher loads is similar to that noted by other studies when FEA results are compared to GW [29]. In Figure 2.5, the number of asperities in contact predicted by both models agreed remarkably well up to moderate loads. The formulation of the GW model suggests a general linear trend of contact length versus load due to the balance of growing asperities and new asperities coming into contact [30]. This behavior was directly

observed in the FEA simulations. Interestingly, the rate at which asperities came into contact decreased significantly around 40,000 N/m. This was where the contact length also started to deviate significantly from GW and becomes less linear. This implies that high deformations began to invalidate the assumptions of a linear increase in number of asperity contacts to distribute the increase in normal load. The compliance of the counterface body in the FEA model might also have been the cause of increasing nonlinearity. Figure 2.6 displays the von Mises stress distribution in a section of the model at an applied force load of 50,000 N/m. It can be seen that the counterface deformed considerably around the hard asperities. Thus, the assumption of non-interacting asperities and relative small contact length in the GW model was violated at these very high loads. However, the strong agreement between the analytical and computational models, along with the observations of simulation behavior during load application, suggested that the FEA model was a suitable instrument for use in the remainder of the investigation.

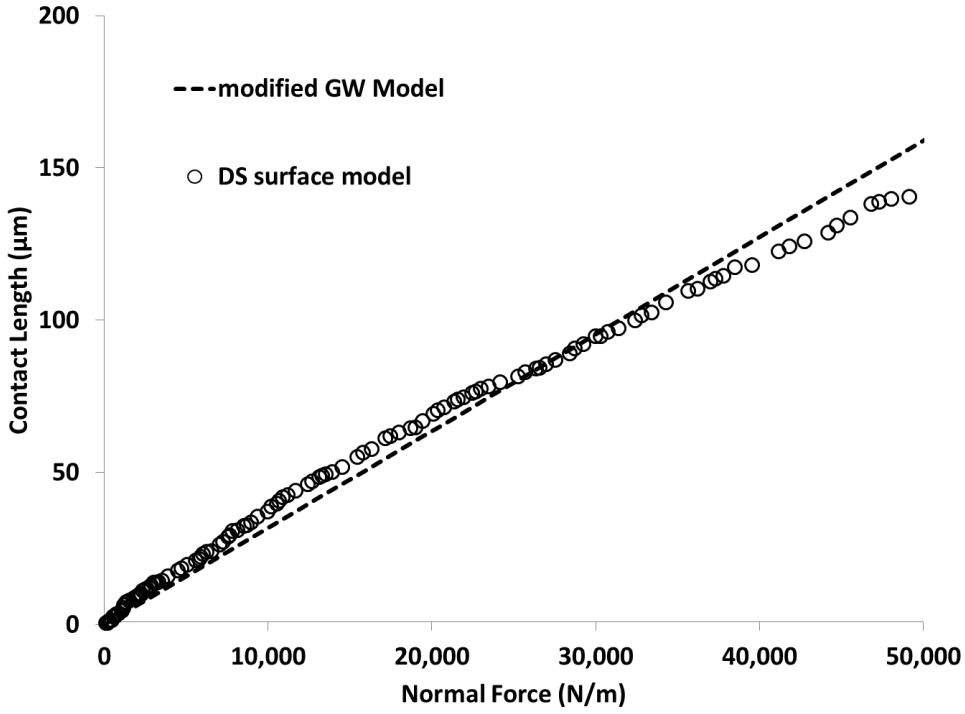

Figure 2.4: The contact length of the GW model compared to the results of the duplicated shape FEA model.

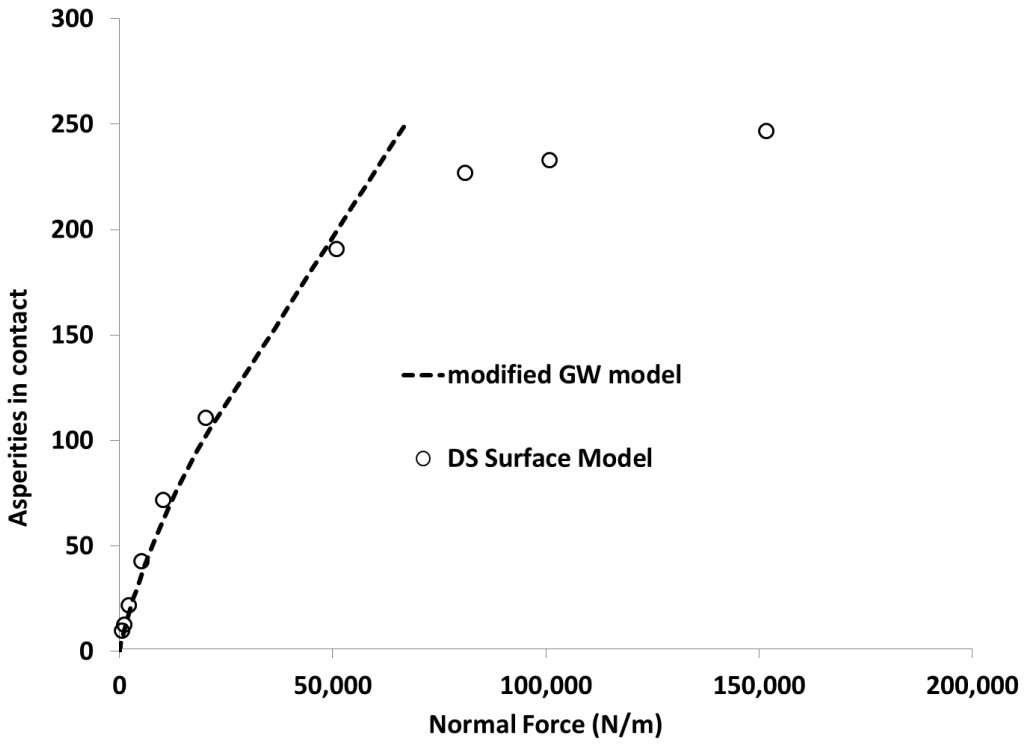

Figure 2.5: The number of asperities in contact predicted by GW is compared to FEA model.

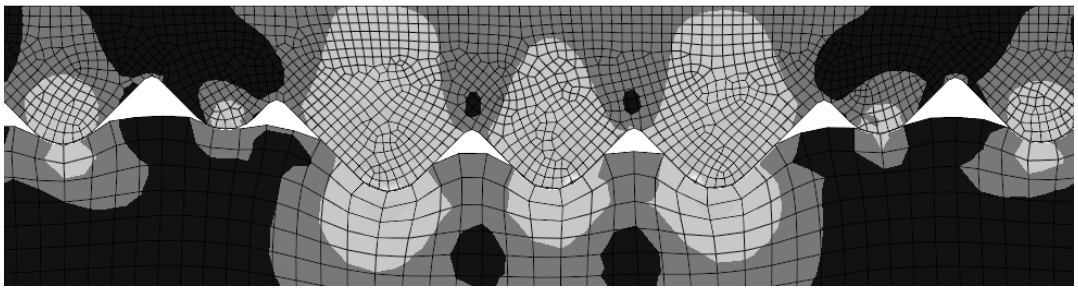

Figure 2.6: Shaded map of von Mises stress levels produced during FEA modeling of a DS surface against a flat counterface. Lighter shades indicate high stress areas.

2.3.2 Comparison of Surfaces with Same Average Roughness

As stated above, sample length and standard deviation of asperity heights can have an effect on roughness, and that this can lead to surfaces with the same average roughness (Ra) but with drastically differing features [31]. The FEA models used in this work all had the same sample length of 1,000 μm. As indicated in Tables 2.1 and 2.2, the standard deviations of asperity heights of the two surface types, DS and FB, were not significantly different for a given Ra value, and the mean heights were within a reasonable range of each other. The results for the

surfaces with the highest and lowest Ra are shown in Figure 2.7. Clearly, surfaces with approximately the same Ra exhibited extremely different contact lengths for a given load. Contact length was consistently found to be greater for the Fractal Based (FB) surfaces than the Duplicated Shape (DS). In fact, reducing the roughness of an FB surface by half (0.94 to 0.47) still produced a greater contact length than a DS surface with Ra = 0.92. One clue to this behavior is that the asperity lengths and tip angles were typically much larger for the FB surfaces than the corresponding DS surfaces. The computational modeling showed that this had a large effect on how the asperities deformed and thus contact length. Acute, smaller asperities on the FB surfaces tended to deform much like axially loaded columns. After initial contact was made with such asperities, the contact zone grew rather slowly in a mechanism dominated by the Poisson effect in response to the stress being transmitted deeply into the asperity. On the other hand, large and obtuse asperities had contact zones which grew somewhat faster under increasing load because of direct compression and deformation of material near to the contact surface. Such observations about the impact of asperity tip angle affecting friction and contact area have been previously observed [6, 32]. However this investigation allowed for the direct observation of the phenomenon. These results confirm the hypothesis that different asperity profiles can produce disparate results, even with the same average roughness. Thus, Ra tends to be a weak predictor of contact length unless the surface topology closely matches the idealized conditions proposed by the classical analytical contact models.

Conceptually, increasing Ra can potentially reduce the contact length for a given normal load. However, the magnitude of this reduction is different between the two surface types as shown in Figure 2.8. It is evident that there was a more drastic reduction in contact length for fractal based surfaces than for the duplicated shape asperity profiles. Furthermore, the contact

lengths predicted for the FB models are substantially higher than DS surfaces until the highest roughness was attained. In the FB surfaces, the contact length decreased steadily and had an overall decrease of 37% over a doubling of average roughness. However, the DS surfaces exhibited a general decreasing trend but with some localized variations. The resulting decrease in contact length was only 29% for the full range of roughness values. The explanation of this behavior was again related to the geometry of asperities. As Ra increased in the FB surfaces, the asperity angles that were generated by the algorithm became gradually more acute, and this effect on contact behavior was quite large. It is clearly seen in Figure 2.7, that asperity angle in the FB surfaces had a major impact on contact length. This suggests that asperity angle was a strong predictor of contact length; however, it was also important to note that this angle is not fully independent from Ra due to the surface generation algorithm used. These results reaffirm that Ra must be used cautiously as a roughness parameter for any application involving contact mechanics or friction.

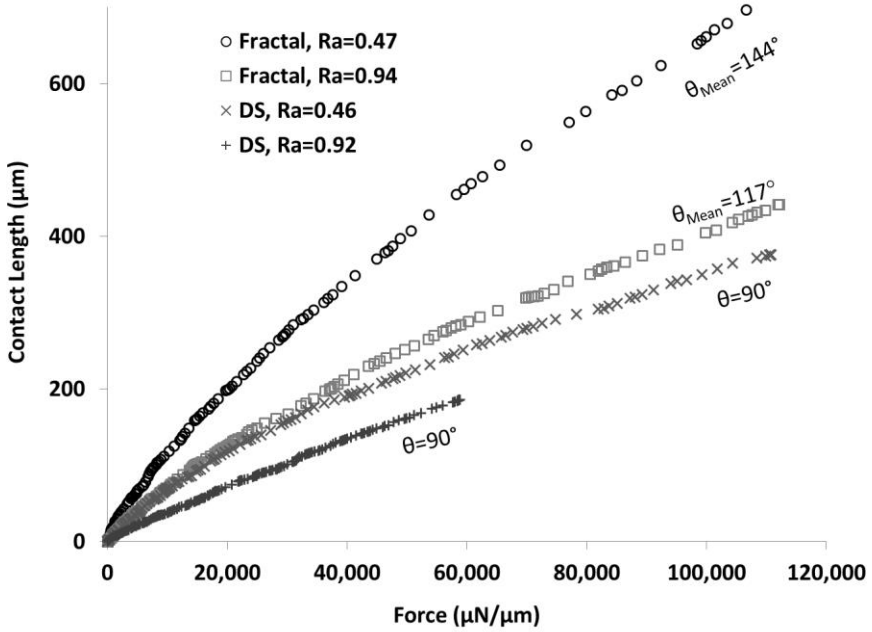

Figure 2.7: Contact length of Duplicated Shape (DS) and Fractal Based (FB) surfaces of equivalent average roughness. The surfaces shown had the highest and lowest Ra values of surface pairs investigated in this work.

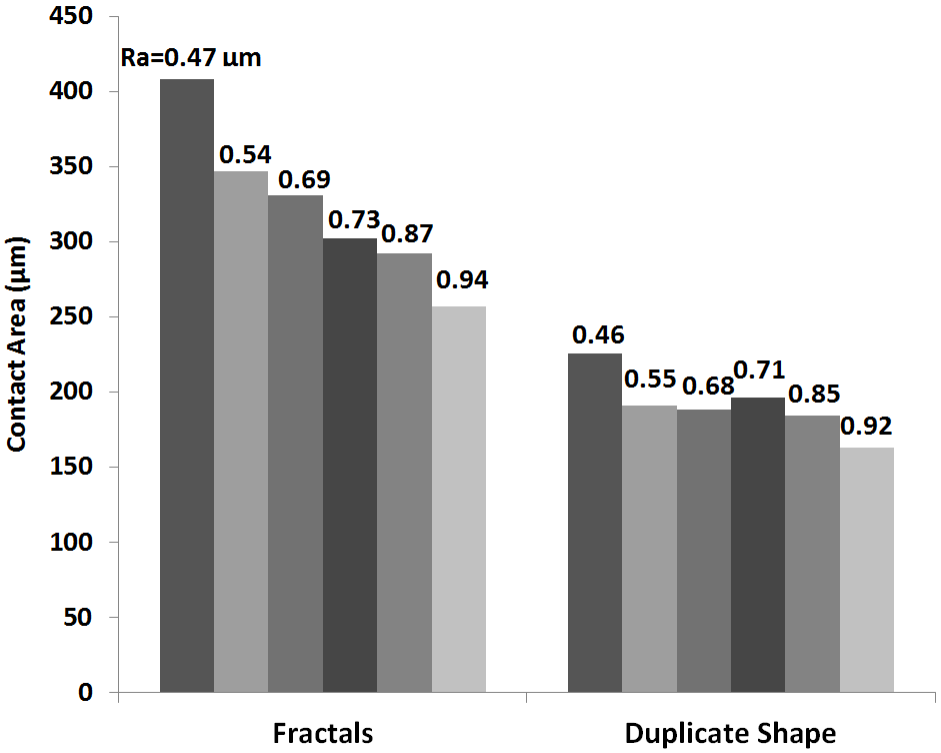

Figure 2.8: The total lineal contact length exhibited by the computational model at a load of 50,000 N/m for both surface types (DS and FB) and all roughness values investigated

While actual contact length has direct ties to friction and wear, both conceptually and borne out experimentally, the number of distinct zones of contact is a more indirect relationship and more difficult to quantify based on analytical models. Modeling of both surface types, especially the fractal based asperity profiles, highlighted an important behavior. The multiple contact regions of adjacent asperities began to merge into conjoined zones under increasing load. What may have originated as several distinct asperities in contact with separate contact regions eventually became one contiguous contact zone. In this situation, the concept of number of asperities in contact then becomes somewhat ambiguous. Figure 2.9 presents the number of contact zones resulting from the computational simulation of multiple FB and DS surfaces under increasing normal loads. An attempt was made to systematically interpret these results to determine whether contact zone was a useful parameter for complementing Ra or other single-dimension metrics. Close observation of the contact zone number revealed that there was no

overarching trend for either the DS or FB surfaces investigated here. This appeared to be largely due to the fact that there was still significant stochastic variation in the surfaces produced via the generation algorithms. In general, it did appear that the number of contact zones for the duplicated shape surfaces was much more sensitive to applied load than were the fractal based surfaces. This was likely due to the wide diversity of asperity geometries found in the FB surfaces versus the fairly restricted nature of the DS asperity shapes and its quantized deformation behavior as additional asperities came into contact with the counterface.

The ability to successfully model the surface interactions in this study depended on using modeling techniques, and model configurations, which would attain computational convergence on solutions as load was increased. In all cases, the models were developed to converge under increasing load; however for the analysis conducted in Section 3.2, once sliding was initiated some of the surfaces encountered convergence problems. This appeared to be most pronounced with high asperity angle fractal based surfaces. To better understand the cause of this behavior, the various DS and FB surfaces were slid after compression at multiple loads to determine the parameters most responsible for non-convergence. The computed principle strain at model failure was recorded for each simulation, and the means and standard deviations are reported in Table 2.3. The table reveals that both surface types consistently failed at a maximum principle strain of approximately 0.4. This consistent behavior suggests that the cause of convergence failure was excessive strain and that more sophisticated material models may need to be employed in future studies.

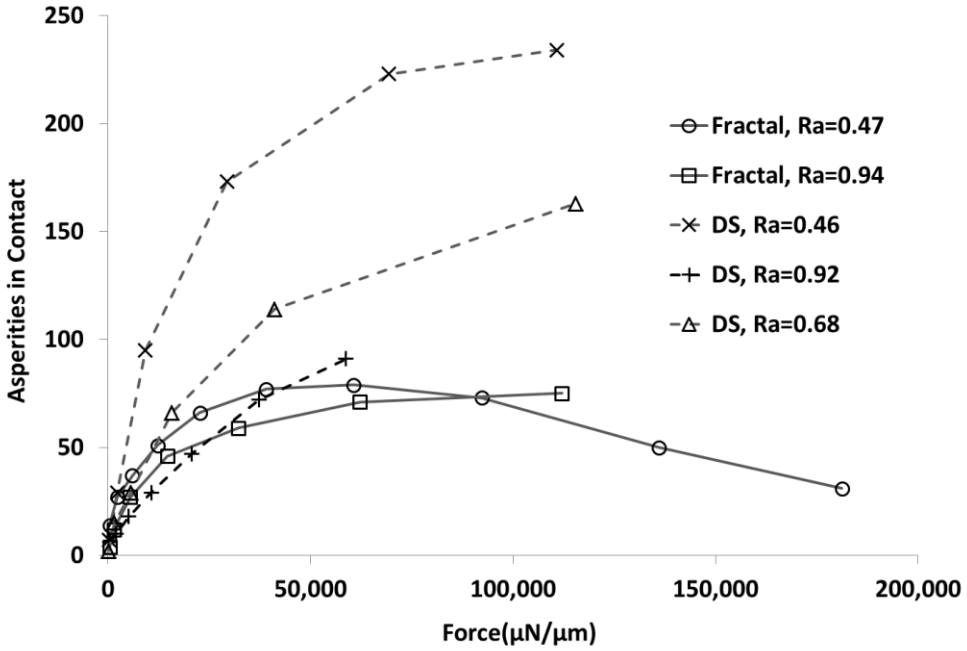

Figure 2.9: Number of contact zones predicted by the FEA model for surfaces of both types under varying loads. Not all surfaces were able to be taken to maximum load because of non-convergence of the model under extreme deformation at some asperity tips.

2.3.3 Observations and Possible Limitations of Modeling Approach

Finite element analysis has many subtle aspects that could potentially affect the outcome of these results, especially in the plane-strain formulation. The most important consideration was element type and integration order. Because the models were constitutively simple (linear elastic), most of the problems that arose involved nodal constraints. Contact with friction adds several constraints to a model which are vital to the possibility of convergence. The pressure in a contact zone produced by circular/spherical shaped asperities must be continuous and fall to zero at the edge of contact. Furthermore, the use of plain-strain elements also added a constraint on deformation to occur only within the plane. Given all of these restrictions to degrees of freedom, the risk of non-convergence and element locking can be very high. This risk was addressed by using linear elements instead of quadratic. There were other FEA considerations that are worthy of note. A surface-to-surface discretization was chosen for the contact pairs because it has been

generally shown to be more accurate than a node-to-surface or node-to-node approach. During preliminary model development for this work, the node-to-surface discretization was shown to be negligibly different, likely due to the fine mesh size. For the penalty method employed here, the matrix storage must be asymmetric since it applies an extra stiffness parameter at the surface nodes. FEA contact is also nonlinear so there is no direct relationship with displacement and force. When using force as the loading parameter, this could produce inaccuracies since the model sometimes struggled to obtain force equilibrium, especially for the large surfaces used in this study. It became necessary to use displacement control rather than load control because of this issue. Although this is not directly equivalent to most empirical approaches, it produces much more accurate results in terms of force and contact length relationships for computation models. The resultant normal force, however, was still obtainable as an output of the simulation, and this could be used as an experimental factor.

Table 2.3: Principle strain at FEA failure when sliding.

	Max. Principle Strain		**Min Principle Strain**	
	Average	**SD**	**Average**	**SD**
Fractals	0.3738	0.0623	-0.0587	0.0052
Semi-Circular	0.4266	0.0425	-0.0172	0.0081

2.4 Conclusions

The purposes of this study were to develop a useful computational model to understand the impact of asperity geometry on contact behavior and to use this model to assess the appropriateness of using simple topology parameters – such as average roughness – as an input parameter for contact mechanics and friction models. This was accomplished by employing finite element analysis to query the behavior of both duplicated shape and fractal based asperity geometries with similar average asperity heights. While these results are confined to a relatively

simple linear elastic material model, they provide a foundation for future, more complex surface studies. The following conclusions have been drawn from this investigation:

- A linear elastic finite element model can be used to simulate and confirm the basic assumptions of asperity behavior in a modified Greenwood-Williamson (GW) contact model. However, the computational and analytical models diverged at very high loads.
- Average Roughness (Ra) is not suitable as a sole descriptor of surface topology for higher level friction models, unless the surfaces under consideration have very similar asperity profiles. Surfaces of duplicated asperity shapes exhibited markedly different contact length to load behavior than did surfaces consisting of fractal based asperity geometry.
- Excessive principal strain of the deformed surfaces is a fundamental cause of computational non-convergence in linear elastic finite element models such as those used in this work. This behavior was exhibited in both duplicated shape and fractal based surface topologies.

2.5 References

[1] J. Jiang and R. D. Arnell, "The effect of substrate surface roughness on the wear of DLC coatings," *Wear,* vol. 239, no. 1, pp. 1-9, 2000.

[2] T. S. Barrett, G. W. Stachowiak, and A. W. Batchelor, "Effect of roughness and sliding speed on the wear and friction of ultra- high molecular weight polyethylene," *Wear,* vol. 153, no. 2, pp. 331-350, 1992.

[3] K. N. G. Fuller and D. Tabor, "The Effect of Surface Roughness on the Adhesion of Elastic Solids," *Proceedings of the Royal Society of London. Series A, Mathematical and Physical Sciences,* vol. 345, no. 1642, pp. 327-342.

[4] D. Guha and S. K. Roy Chowdhuri, "The effect of surface roughness on the temperature at the contact between sliding bodies," *Wear,* vol. 197, no. 1, pp. 63-73, 1996.

[5] H. Jiang, R. Browning, J. Fincher, A. Gasbarro, S. Jones, and H.-J. Sue, "Influence of surface roughness and contact load on friction coefficient and scratch behavior of thermoplastic olefins," *Applied Surface Science,* vol. 254, no. 15, pp. 4494-4499, 2008.

[6] S. R. Ghabrial and S. A. Zaghlool, "The effect of surface roughness on static friction," *International Journal of Machine Tool Design and Research,* vol. 14, no. 4, pp. 299-309, 1974.

[7] D. J. Whitehouse, *Surfaces and Their Measurement*. London: Kogan Page Science, 2002.

[8] M. Sedlaček, B. Podgornik, and J. Vižintin, "Influence of surface preparation on roughness parameters, friction and wear," *Wear,* vol. 266, no. 3, pp. 482-487, 2009.

[9] A. J. Terry and C. A. Brown, "A Comparison of Topographic Characterization Parameters in Grinding," *CIRP Annals - Manufacturing Technology,* vol. 46, no. 1, pp. 497-500, 1997.

[10] J. F. Archard, "Single Contacts and Multiple Encounters," *Journal of Applied Physics,* vol. 32, p. 1420.

[11] J. F. Archard, "Contact and Rubbing of Flat Surfaces," *Journal of Applied Physics,* vol. 24, p. 981.

[12] J. A. Greenwood and J. B. P. Williamson, "Contact of Nominally Flat Surfaces," *Proceedings of the Royal Society of London. Series A, Mathematical and Physical Sciences,* vol. 295, no. 1442, pp. 300-319.

[13] J. A. Greenwood, C. Putignano, and M. Ciavarella, "A Greenwood & Williamson theory for line contact," *Wear,* vol. 270, no. 3, pp. 332-334, 2011.

[14] M. Ciavarella, V. Delfine, and G. Demelio, "A “re-vitalized” Greenwood and Williamson model of elastic contact between fractal surfaces," *Journal of the Mechanics and Physics of Solids,* vol. 54, no. 12, pp. 2569-2591, 2006.

[15] J. I. McCool, "Extending the Capability of the Greenwood Williamson Microcontact Model," *J. Tribol.,* vol. 122, no. 3, p. 496, 2000.

[16] J. A. Greenwood and J. J. Wu, "Surface Roughness and Contact: An Apology," *International Journal of the Italian Association of Theoretical and Applied Mechanics AIMETA,* vol. 36, no. 6, pp. 617-630, 2001.

[17] A. Majumdar and B. Bhushan, "Fractal Model of Elastic-Plastic Contact Between Rough Surfaces," *J. Tribol.,* vol. 113, no. 1, p. 1, 1991.

[18] A. Goedecke, R. L. Jackson, and R. Mock, "A fractal expansion of a three dimensional elastic–plastic multi- scale rough surface contact model," *Tribology International,* vol. 59, pp. 230-239, 2012.

[19] T. M. David, K. Eng-Keng, and P. Tod, "Application of fractals to the contact of carbon-carbon surfaces," *Journal of Applied Physics,* vol. 100, p. 124913, 2006.

[20] D. K. Karupannasamy, M. B. de Rooij, and D. J. Schipper, "Multi- scale friction modelling for rough contacts under sliding conditions," *Wear,* vol. 308, no. 1-2, pp. 222-231, 2013.

[21] L. Yang and A. Martini, "Nano- scale roughness effects on hysteresis in micro- scale adhesive contact," *Tribology International,* vol. 58, pp. 40-46, 2013.

[22] D. Hong Liu *et al.*, "Finite Element Based Surface Roughness Study for Ohmic Contact of Microswitches," ed, 2012, pp. 1-10.

[23] B. Chatterjee and P. Sahoo, "Finite Element Based Contact Analysis of Fractal Surfaces – Effect of Varying Elastic Modulus," *Procedia Engineering,* vol. 90, pp. 116-122, 2014.

[24] D. Diao and A. Kandori, "Finite element analysis of the effect of interfacial roughness and adhesion strength on the local delamination of hard coating under sliding contact," *Tribology International,* vol. 39, no. 9, pp. 849-855, 2006.

[25] K. L. Johnson, *Contact Mechanics*. Cambridge University Press.

[26] M. Ciavarella, J. A. Greenwood, and M. Paggi, "Inclusion of "interaction" in the Greenwood and Williamson contact theory," *Wear,* vol. 265, no. 5, pp. 729-734, 2008.

[27] J. C. Simo and T. A. Laursen, "An augmented lagrangian treatment of contact problems involving friction," *Computers and Structures,* vol. 42, no. 1, pp. 97-116, 1992.

[28] T. Shimizu and T. Sano, "An application of a penalty method contact and friction algorithm to a 3-dimensional tool surface expressed by a B-spline patch," *Journal of Materials Processing Tech.,* vol. 48, no. 1, pp. 207-213, 1995.

[29] K. Poulios and P. Klit, "Implementation and applications of a finite-element model for the contact between rough surfaces," *Wear,* vol. 303, pp. 1-8, 2013.

[30] J. F. Archard, "Elastic Deformation and the Laws of Friction," *Proceedings of the Royal Society of London. Series A, Mathematical and Physical Sciences,* vol. 243, no. 1233, pp. 190-205.

[31] R. S. Sayles and T. R. Thomas, "Surface topography as a nonstationary random process," *Nature,* vol. 271, no. 5644, p. 431, 1978.

[32] T. Hisakado, "Effect of surface roughness on contact between solid surfaces," *Wear,* vol. 28, no. 2, pp. 217-234, 1974.

CHAPTER 3: THE EFFECT OF SURFACE ROUGHNESS ORIENTATION ON PEEK (POLYETHERETHERKETONE) TRANSFER FILM IN MULTI-DIRECTIONAL SLIDING

A paper to be submitted to *Wear*

Mark D. Placette, Sougata Roy, Derek White, and Christian J. Schwartz

Abstract

Polymer transfer films are thought to reduce friction and wear during sliding. In such cases, a continuous, uniform transfer film is thought to yield better wear performance. However, several polymers, including the thermoplastic polyetheretherketone (PEEK), do not always display this behavior. Recent works analyzing transfer film quality of PEEK resulted in no clear correlation to wear. Currently, the mechanisms for PEEK transfer film development are unknown, but there is evidence suggesting roughness orientation relative to sliding and frictional heating play key roles. In this work, the development of PEEK transfer film is explored in relation to multi-directional versus linear sliding, roughness orientation, and temperature rise. These factors were examined by performing three distinct wear paths were chosen for wear tests. The transfer film of the square wear paths was analyzed using white light profilometry and imaging software to obtain the volume and area coverage by the film. The temperature rise during sliding of the bulk polymer pin was recorded with infrared camera radiometry for linear reciprocating tests. Scratch tests and chemical etching were conducted on the polymer pin surface to evaluate any directional bias or crystallinity orientation induced by sliding. It was found that wear debris and polymer chain orientation play no noticeable role in PEEK's transfer film formation. The transfer film gradient increased with frictional heating, and transfer film

color changed under certain conditions. This color changed also correlated to reduced wear. This study also confirms that transfer film development is strongly dependent on roughness orientation, and its effects are examined.

3.1 Introduction

PEEK (polyetheretherketone) is a semi-crystalline polymer that has a large industrial interest. Not only is PEEK a high strength and wear resistance material, but it also has low moisture absorption and low chemically reactivity. In addition, PEEK is able to operate over 220°C while still maintaining its high wear resistance [1, 2]. These properties give PEEK practical use in environments that exclude many other materials. It is a biomaterial being considered in spine, hip, and cranial implants [3] and has found utility in cryogenics and aerospace applications [4]. In the automotive and aviation industries, metal parts are being replaced with PEEK for lower weight and higher wear performance [5]. PEEK also has high promise for improved efficiency in large industrial applications while reducing adverse environmental effects [6]. PEEK, like several other polymers, forms a transfer film upon sliding which is thought to be self-lubricating, but the mechanisms for the development of this film is not well understood despite being an intimate part of the wear process.

Polymer transfer film forms when polymer material is transferred and attached to a metal counterface, but it is inconsistent in its relationship to wear. Generally, transfer film is thought to reduce wear of several common polymers by lowering contact pressure and protecting the polymer surface from further abrasion from a hard counterface [7]. A classic example is Polytetrafluoroethylene (PTFE) whose high-wear, neat form can be filled with certain additives thought to allow stronger adhesion to the metal counterface which reduces wear [8-11]. Nylon when blended with copper monosulfide and polyphenylene filled with sulfide will both generate

a better quality transfer film and reduce wear by the same hypothesized mechanism [12, 13]. PEEK wear can also be decreased when filled with PTFE and zirconium dioxide, both transfer film enhancing additives [9] [14]. However, the role of transfer film as a wear-reducing agent is not universal, and the effect of transfer film may sometimes have adverse effects. There are instances where a transfer film develops, but wear is increased. For example, when transfer film is formed in ultra-high-molecular-weight polyethylene (UMWPE), the film can increase roughness and abrade the polymer surface [15]. The bond of transfer film to the counterface can be poor, as in neat PTFE, resulting in transfer film but also considerable wear [8]. It has also been suggested that increased load and velocity can melt transfer film and remove it from the counterface, and in lower load/velocity cases provide a thermal barrier, increasing interfacial temperature [16]. PEEK transfer film in particular does not have a clear relationship to wear. Studies that have attempted to examine this relationship have yielded inconsistent or unexpected results when using quantitative metrics. Laux and Schwartz measured transfer film thickness and found no strong correlation to wear when introducing different molecular weights and suppliers [17]. Zalaznik et al. inspected wear tracks with scanning electron microscopy (SEM) and found that a thin transfer film reduces wear significantly [5]. An extensive quantitative approach was conducted by Haidar et al. who analyzed images of the transfer film for several PEEK composites to produce several variables for comparison including percent area coverage. Although there was a broad trend amongst all the PEEK blends examined that a thinner, more continuous film reduces wear, it is possible to achieve over an order of magnitude difference in wear with similar transfer film quality [18].

Nevertheless, PEEK transfer film development has been shown to be influenced by two factors: roughness orientation and reciprocation when sliding. PEEK transfer film is more likely

to develop when sliding perpendicular to roughness orientation compared to parallel, and under reciprocation a better quality transfer film of PEEK is generated [17]. PEEK wear is also well known to be dependent on roughness orientation above certain average roughness values [2]. Thermal effects also seem to play a key or auxiliary role. Increased temperature of the interface induced by frictional heating improved transfer film of unfilled PEEK [19]. The authors speculated that the increased temperature increased polymer-on-metal adhesion. The study also implied that the transfer film was able to cool interfacial temperatures below those predicted by flash temperature theory as the interface was lower than glass-transition of the PEEK [19, 20]. Wear mechanisms have been shown to shift after glass transition in PEEK, and investigators have speculated that thermal softening of PEEK could facilitate more material transfer [21]. There is a need to investigate these factors further as no clear, empirical explanation has been achieved for how they relate to transfer film and the wear cycle of PEEK.

The purpose of this study is to examine the fundamental effect of three tribological parameters - roughness orientations, reciprocation versus multi-directional sliding, and frictional heating - on the formation of PEEK transfer film and resulting wear. This was explored by using three distinct wear paths that isolated the effect of roughness orientation. In square wear path experiments, a transfer film volume gradient was notice on the legs perpendicular to roughness. Three hypotheses that could potentially explain this transfer film attribute were proposed and tested with the ultimate goal of exploring the mechanisms of transfer film development. First, due to the 90 degree shift in direction, trapped wear debris or debris loosely collected on the counterface could feasibly be compacted to form transfer film upon turning, and this is investigated by changing test parameters to isolate this effect. Secondly, directional strengthening via polymer chain alignment was investigated by chemical etching and scratch

tests. Lastly, thermal softening could be playing a role in PEEK transfer film deposition. Frictional heating was increased and decreased by altering the velocity in the above wear paths. Transfer film volumes and area covered are measured using a white light optical profilometer and imaging software. It was found for certain tests a dark film deposition was developed, and this was investigated with Raman spectroscopy.

3.2 Materials and Methods

3.2.1 Experimental Materials

A 6.35-mm diameter PEEK pin (Quadrant Plastics, Ketron PEEK 1000) was fabricated by cutting cylindrical stock at slow speeds. This PEEK is unfilled with a tensile strength of 115 MPa and melting temperature of 340°C. The pin was then polished with abrasive on a two-axis tribometer. This was to ensure the pin surface would mate well with the counterface surface during testing. The pin was then cleaned with an ultrasonic bath by sequentially bathing the sample in acetone, a soap-water mixture, and deionized water. Finally, the sample was rinsed with ethanol to evaporate all excess water. After air drying, the sample was then weighed. After the wear test, the cleaning procedure was repeated, and the sample was weighed again to determine wear loss. All counterface materials were A36 hot rolled-steel with a hardness of 62.4 HRB. The plates ground to a Ra roughness of approximately 1.1 μm as roughness below this threshold significantly reduces roughness orientation effects on wear in unfilled PEEK [2]. After the wear test, the counterfaces were carefully saved for transfer film analysis.

3.2.2 Wear Testing

All wear tests were conducted on a two-axis tribometer (Rtec Instruments, San Jose, California) represented by Figure 3.1. The stage was moved with two independent stepper motors (XY) controlled with motion software. Velocity and wear path were also regulated

through this motion control software. Load was applied in the z-axis by a controlled linear motor. The six-dimensional load cell was capable of measuring force in all three axes as well as measuring torque.

Three distinct wear paths were chosen to explore the effects of sliding direction with respect to counterface roughness. First, separate linear reciprocating tests biased perpendicular to roughness orientation and biased parallel to roughness orientation were conducted. The diagram of these wear paths are shown in Figure 3.2. The path length was 50 mm for a total of 100 mm for each cycle, and paths were traced with stops in the center to simulate the stops of square paths tests. This was to account for any effects these stops and acceleration would have on the transfer film development process when comparing to square tests. The average velocity and number of replications of these tests are shown in Table 3.1. Each test was run for a total sliding distance of 0.25 km at a contact pressure of 4.58 MPa. Next, square wear paths were traced with two legs perpendicular and two parallel to roughness, which simultaneously tested the effects of roughness orientation and multi-directional sliding. A diagram for this set of wear paths is shown in Figure 3.3. The square paths were traced with 45 mm side lengths for a total sliding distance of 180 mm per cycle. The square paths had two sides in the x-direction aligned perpendicular to roughness and two sides in the y-direction parallel to roughness. The velocity of the perpendicular sides was held constant, while the parallel side velocity was varied from 0.15 mm/s to 15 mm/s. The details of the square tests including velocities are located in Table 3.2. These tests were also run for a total sliding distance of 0.25 km at a contact pressure of 4.58 MPa. It was hypothesized that with load held constant, frictional heating is largely governed by sliding velocity. This was the purpose of using different velocities on the square wear paths to test the frictional heating hypothesis. In addition, a third wear path was included to further test

the probability of frictional heating effects, shown in Figure 3.4, by varying the average velocity from 0.14 mm/s to 11.58 mm/s. This path was linear reciprocating with no stops and a strictly parallel bias. Table 3.3 displays the testing parameters of this set of tests. Each distinct wear test was given test identification for brevity which is found in Tables 3.1-3.3. Parallel (∥) and perpendicular (⊥) symbols indicate the direction of sliding relative to counterface roughness which will be referred to as parallel biased and perpendicular biased respectively. The linear path lengths differed from the square path side lengths due to spatial limitations of the tribometer.

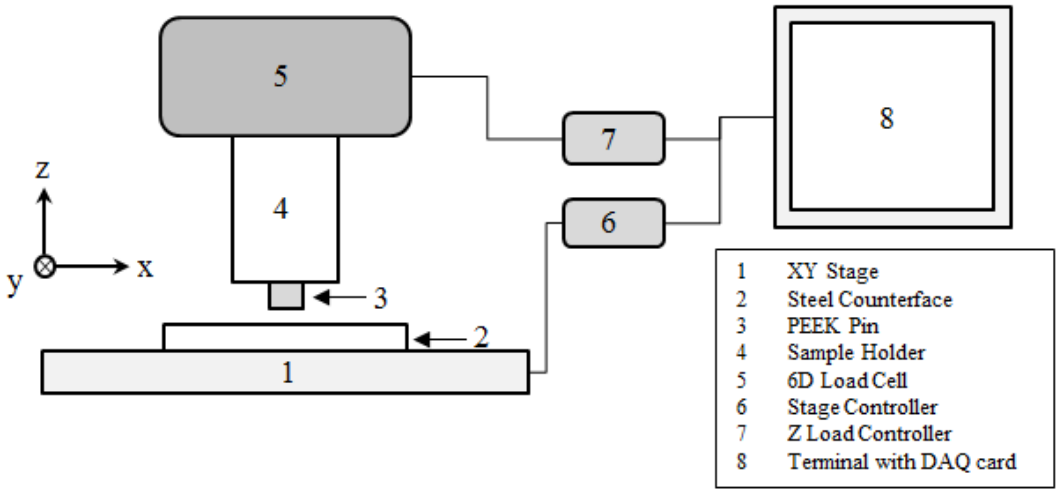

Figure 3.1: Schematic of tribometer with two-axis stage and 6-dimensional load cell used for all wear tests.

Table 3.1: Experimental parameters of the linear reciprocating with stops wear path shown in Figure 3.2.

Path Geometry	**Test ID**	**V_{avg} (mm/s)**	**No. of Tests**
Linear Recip. Stop (Parallel)	A∥	11.58 ∥	2
Linear Recip. Stop (Perpendicular)	A⊥	11.58 ⊥	2

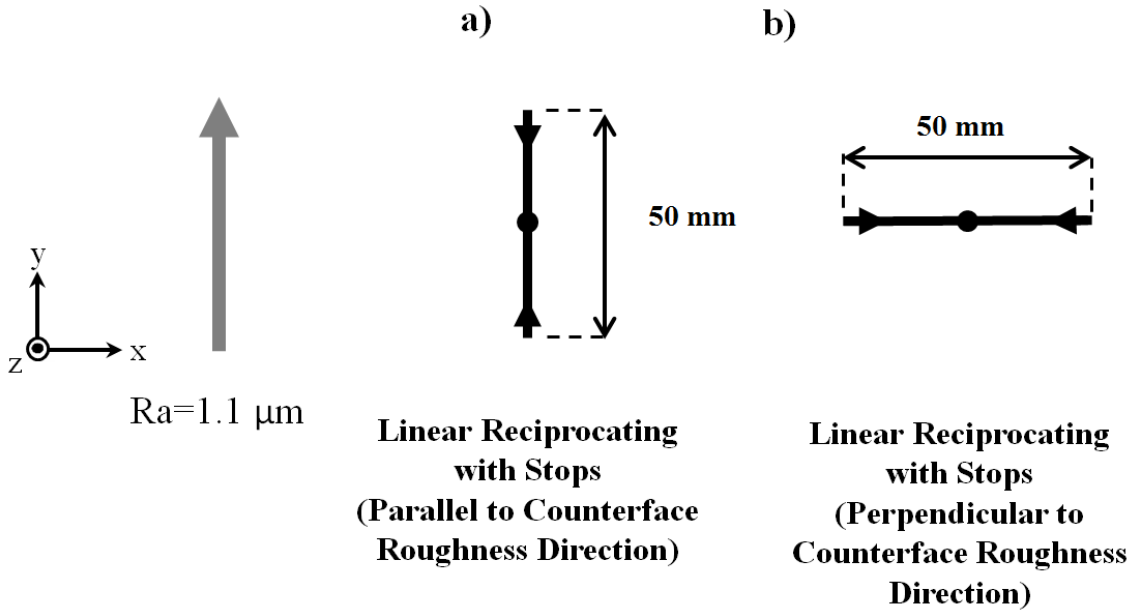

Figure 3.2: Diagram of linear reciprocating wear paths with central stops with a) a parallel roughness bias ($A_{\parallel}$) and b) perpendicular roughness bias ($A_{\perp}$). The sliding distance of one cycle was 100 mm, and the contact pressure was 4.58 MPa. Tests were conducted for a total sliding distance of 0.25 km

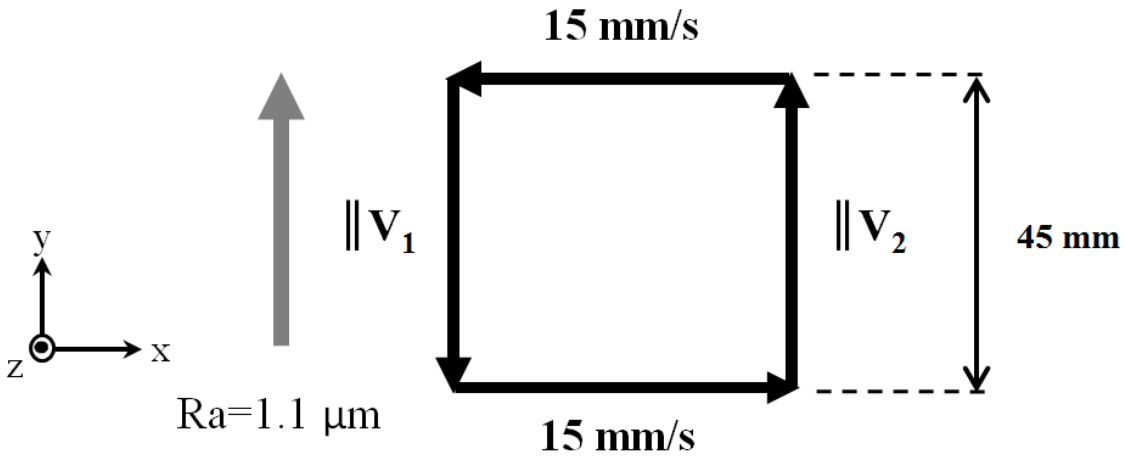

Figure 3.3: Diagram of square wear paths with side lengths of 45 mm and contact pressure of 4.58 MPa. Parallel sides had varied velocity (V_1, V_2) and perpendicular velocities were held constant. Tests were conducted for a total sliding distance of 0.25 km.

Table 3.2: Experimental parameters for square wear paths seen in Figure 3.3.

Path Geometry	Test ID	$\|\|V_1$ (mm/s)	$\|\|V_2$ (mm/s)	V_{avg} (mm/s)	No. of Tests
Square	S1	15 ‖	15 ‖	11.58	2
	S2	15 ‖	1.5 ‖	4.25	3

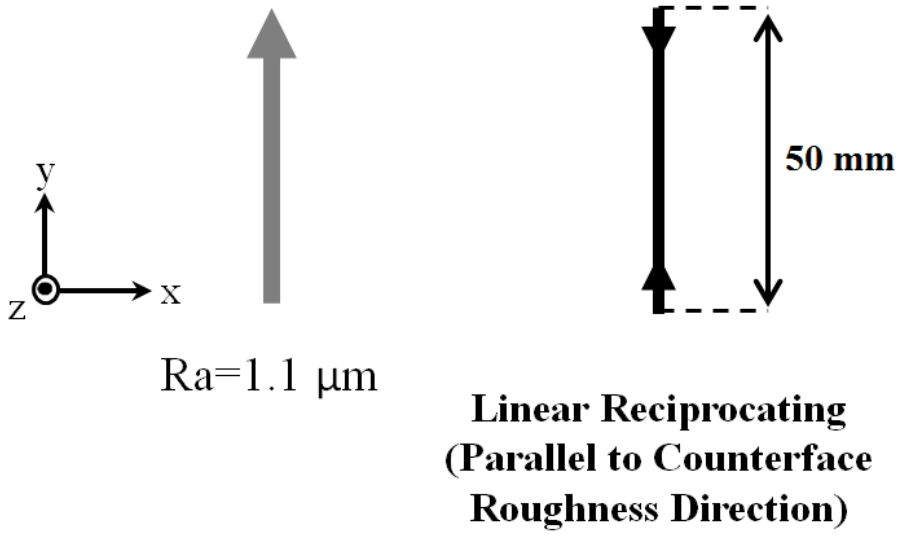

Figure 3.4: Diagram of simple linear reciprocating wear paths with a strictly parallel roughness bias. The path length was 50 mm and contact pressure was 4.58 MPa. The total sliding distance was 0.02 km.

Table 3.3: Experimental Parameters of the simple linear reciprocating wear paths shown in Figure 3.4.

Path Geometry	Test ID	V_{avg} (mm/s)	No. of Tests
Linear Recip. (Parallel)	B1‖	0.14 ‖	1
Linear Recip. (Parallel)	B2‖	11.58 ‖	1

3.2.3 Transfer Film Analysis

Because of the clear visible evidence of transfer film being deposited in perpendicular sliding and a visible gradient in film coverage, the transfer films of several tests perpendicular to roughness were analyzed with a white light interferometry based profilometer (Zygo

NewView700) to determine transfer film gradient volume. A special film application in the analysis software (MetroPro, Zygo Corp.) was used to measure the volume of transfer film deposited on the counterface by recognizing the separate fringes of polymer and metal. This generated a three-dimensional map which could differentiate between the areas occupied by the two separate materials, which could then be used to estimate the volume of transfer film on the counterface. An area analysis was conducted with the above surface maps using image analysis software (ImageJ) where the total area covered was calculated. To observe any gradient in volume or area in transfer film, the area and volume analysis was applied to the perpendicular biased legs of the square wear paths. Measurements of the entire wear path cross-section were taken at intervals along the perpendicular side. The corner of the square path where the pin changed directions was not considered in this analysis.

A dark deposition developed on the counterface in certain linear reciprocating tests. To determine the nature of this deposition, an attempt was made to replicate this deposition without sliding. PEEK samples and steel counterface were clamped together and soaked in an isolated convection oven. The assembly was soaked for two hours at 100 °C, 200 °C, 218°C, 237 °C, and 275 °C to determine if a thermally activated film developed and at what temperature. Raman spectroscopy was performed to determine the chemical composition of both the soaked samples and the actual deposition formed during the wear test.

3.2.4 Chemical Etching and Micro-Scratch Testing

A hypothesis was proposed to explain the transfer film gradient found in the perpendicular biased legs of the square wear paths. It is known that some polymers like UHMWPE can orient surface chains in the direction of sliding, and thus directionally strengthen its surface. This can reduce wear in linear reciprocation or increase wear in multi-directional

sliding [22]. PEEK is known to be directionally strengthened in bulk by a specialized process [23]. To test this hypothesis of directional strengthening in PEEK, chemical etching and micro-indenter scratch tests were conducted to determine if the surface exhibited any evidence of chain orientation. Permanganate etching was done by the method described by Olley et al. [24]. Two PEEK pins were cut, polished, and etched. One pin was etched but not wear tested and served as a control, and one pin was etched after wear testing with S1 test parameters. These samples were investigated with SEM at various magnifications to determine microstructure and chain orientation.

For scratch tests, a total of eight pins were prepared to further explore directional strengthening. Four pins were prepared but not wear tested and served as a control group, and four pins were worn by a wear test. The friction and tangential forces during scratch were acquired using a custom-built micro-tribometer used in a previous study (apparent area ~1,000 μm) [25]. A schematic of the micro-indenter components is shown in Figure 3.5. A 75 micron diameter probe is placed at the end of a crossed I-beam structure, which is lowered using a linear stage. The normal and the friction (lateral) forces are measured using semiconductor strain gages on the cantilevers. The resolution of frictional force is approximately ±5 μN, and the normal force resolution is approximately ±15 μN. The signal from the normal load is monitored and used in a simple proportional-integral (PI) feedback loop to maintain the desired normal force regardless of any slope or waviness in the surface of the sample. PEEK pins were then loaded with a 0.225 N load with a sliding distance of at least 4 mm at 0.05 mm/sec.

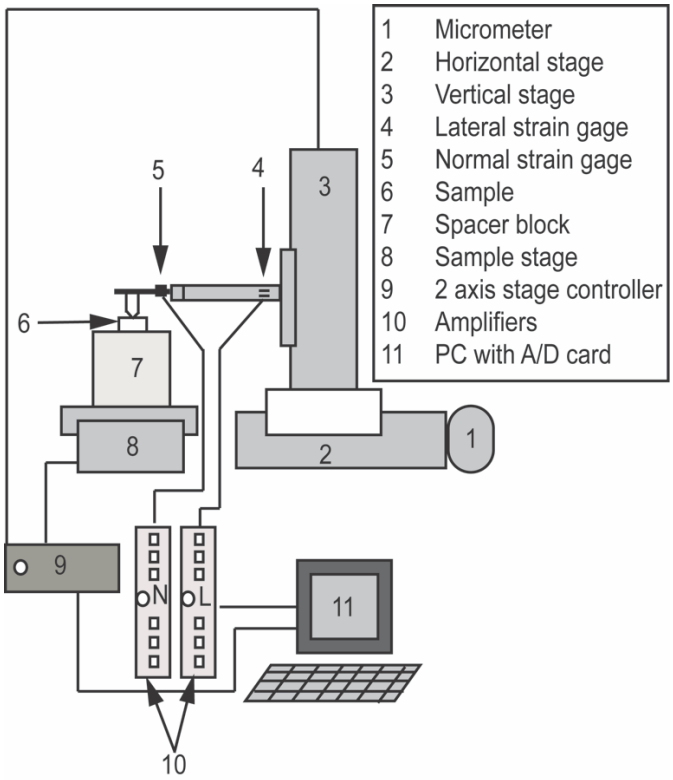

Figure 3.5: Schematic of custom-built micro-indenter used for scratch tests [25].

3.2.5 Infrared Radiometry

A thermal camera (FLIR A600) was used to investigate the temperature rise of pins during linear reciprocating sliding tests. To calibrate the emissivity for the PEEK pin as described by the manufacturer, a cleaned PEEK pin was partially covered with black electrical tape and was thermally soaked for two hours at 40°C. The pin was quickly removed and thermal images were quickly recorded for the sample. The emissivity was changed until the PEEK pin agreed with the known temperature of the electrical tape (emissivity ~0.95). This emissivity was found to be approximately 0.44. During each test, black electrical type was applied to the sample holder thermally isolated from the pin. This temperature was recorded for an ambient reference. The emissivity and reference temperature was then entered into the thermal camera software to ensure the temperature of the pin would be accurate. For wear tests, the thermal camera was

positioned perpendicular to sliding, and periodically temperature videos lasting 60s were recorded. Maximum, minimum, and mean temperature for each video sample was gathered.

3.3 Results and Discussion

3.3.1 Wear, Friction Coefficient, and Transfer Film Observations

Three distinct wear paths were chosen to test the influence of roughness orientation and multi-directional sliding on the wear process of PEEK. The wear volume of the linear reciprocating tests with intermediate stops is found in Figure 3.6. The wear of the parallel bias test ($A_{\parallel}$) had higher wear on average compared to the perpendicular bias test ($A_{\perp}$). However, the wear for the parallel bias also had greater variance. The parallel bias overall generated less transfer film, but the potential for wear was greater which suggests transfer film was wear reducing. The coefficient of friction of the perpendicular bias was greater (0.33) than the parallel case (0.40), possibly due to increased adhesive forces of polymer-on-polymer film interactions. These results indicated roughness orientation had significant effect on transfer film volume and wear, but why this occurred is unknown. Three hypotheses are proposed in this paper to explain film formation and the possible effect of roughness orientation and multi-directional sliding. First, as PEEK is worn and wear debris forms, the debris could be trapped at the interface where it is compacted, compressed, and adhered during sliding. In multi-directional sliding, this could produce more film upon changing direction, and sliding with a perpendicular bias might produce more wear and thus more transfer film. Secondly, directionality of polymer chains is known to effect the wear cycle in other polymer materials such as UHMWPE where the polymer chains can align in the direction of sliding, strengthening the polymer and reducing wear. However, in circular paths, this has an increased wear effect since the direction of sliding is not constant [26]. If this occurs in PEEK, multi-directional sliding could produce disparities in transfer film

depending on roughness bias by the same mechanism. The third hypothesis involves frictional heating. Upon frictional heating, the PEEK at the interface would soften, the contact area and adhesion forces would increase, and then a transfer film would be formed. Roughness orientation could possibly change the frictional heating at the interface as well as the available area for adhesion to take place, and thus have a large impact on film development.

The wear results of the square wear path tests are shown in Figure 3.7, and the average coefficient of friction for each square test was 0.33. S1 and S2 had comparable wear, though the average velocity of S1 was over twice as high with one parallel side an order of magnitude lower (1.5 mm/s) than the baseline (15 mm/s). Comparing the square to reciprocating tests, the square wear tests had greater wear than the linear reciprocating tests, though both tests had the same total sliding distance, contact pressure, and in the case of S1, average velocity. The difference in wear within square and linear path tests was greater than the difference in wear between just linear path tests. This indicates reciprocation had a more dominant effect on wear than roughness orientation. The authors hypothesize that this could be related to transfer film and the mechanical aspect of reciprocation versus non-reciprocation. In reciprocation, the transfer film can be mechanically smoothed by the constant backward-forward motion of the pin which would lower contact stress while still protecting from abrasion. It is important to note that neat PEEK adhesion to metal is generally thought to be weak [27], so without reciprocation, the continuous, unidirectional mechanical pushing of the pin could detach transfer film from the counterface forming wear debris or simply push transfer film in the direction of sliding. The latter could increase roughness of the film and thereby increase contact stress and wear.

To investigate the third hypothesis, linear reciprocating tests without stops were conducted to test the effect of frictional heating, and these results are displayed in Figure 3.8.

The 0.15 mm/s test produced a very small amount of wear when compared to the 15 mm/s test. Visually investigating the wear debris fields of these tests showed no significant difference in loose wear debris despite having significant disparity in wear results. Therefore, there is no evidence for the wear debris compaction hypothesis discussed previously in this section, so it was rejected. However, wear was highly dependent on velocity in these tests. In square path tests, wear showed a lower dependence on velocity. These observations indicate that reciprocation has the most dominant effect on the wear cycle followed by velocity of sliding. This is not unexpected because polymers are well-known to have operating limitations based on velocity. Roughness orientation seemed to be the least influential of the factors investigated. The results also indicate another potential mechanisms affecting wear. In Figure 3.8, the linear reciprocating with stops produced greater wear than linear reciprocating without stops, bearing in mind, however, that the sliding distance for the later was greater. In Figure 3.7, the linear reciprocating tests had substantially less wear than the square tests. The linear reciprocating tests had stops with no change of direction in sliding, while the squares had stopping points at the corners and change of direction. The change in direction of sliding and stopping points seemed to increase wear. The authors speculate the stops in the wear path might be causing stick-slip damage as this is a known wear mechanism of polymers [28, 29]. The increased wear for change in sliding direction could be due to the fact asperities experience shear in two orthogonal axes cyclically. This may create a fatigue cycle and increase fatigue wear.

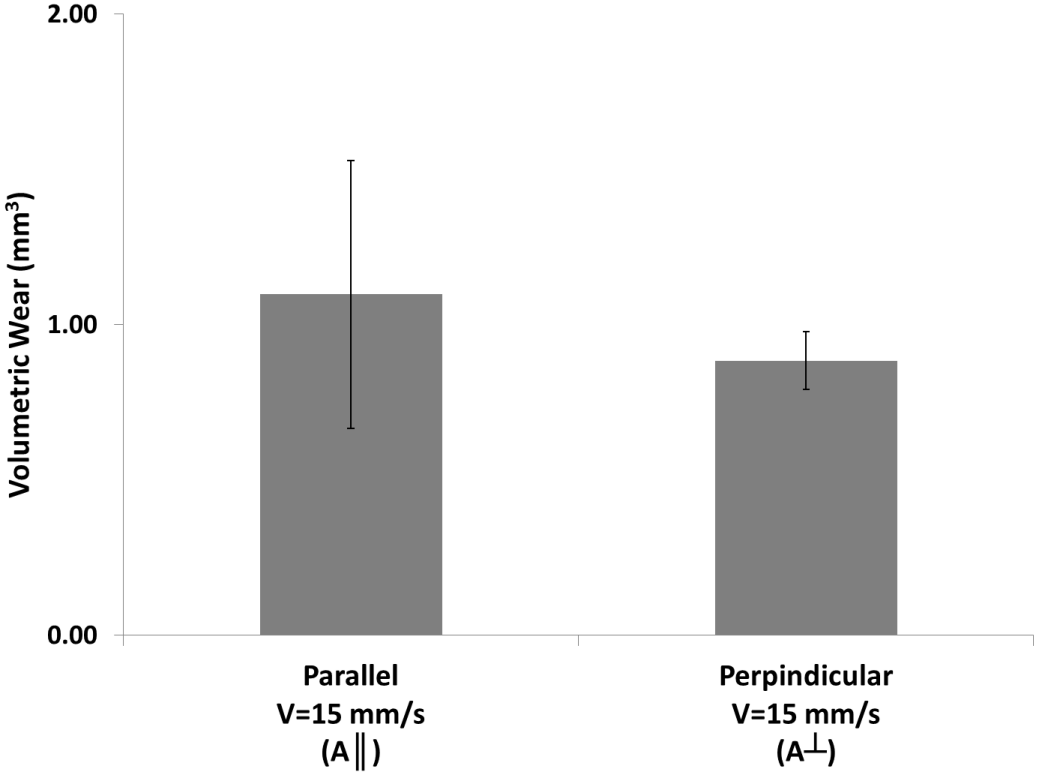

Figure 3.6: Wear volume of linear reciprocating wear paths with stops. Error bars indicate mean standard error.

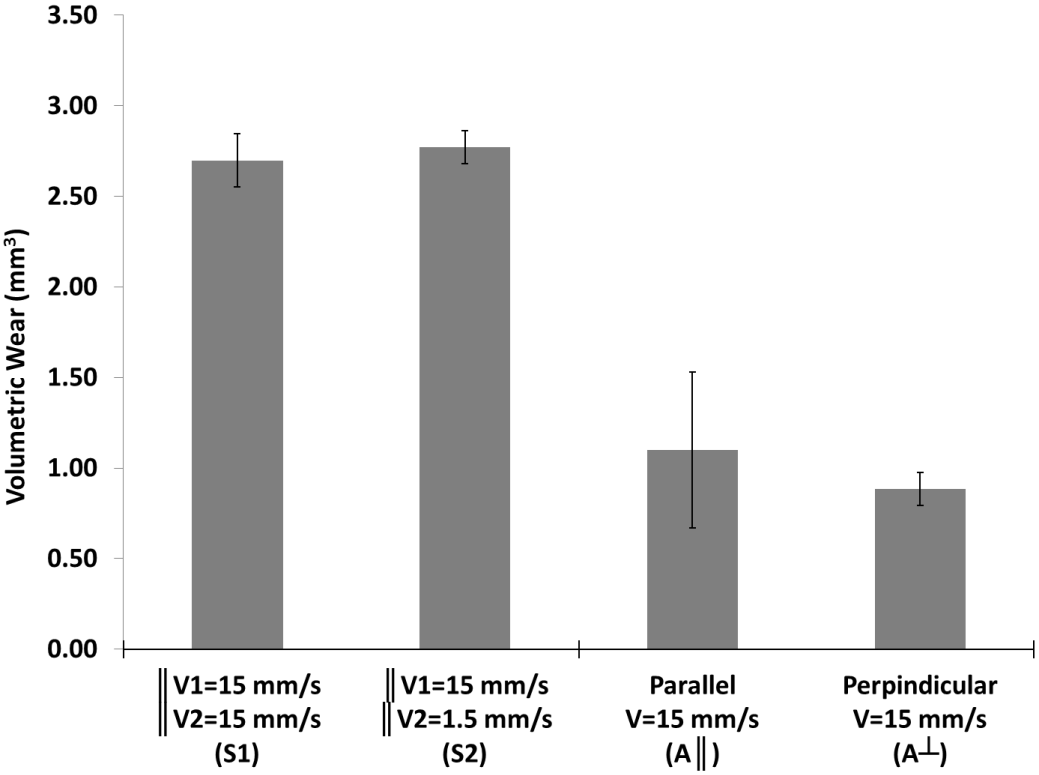

Figure 3.7: Wear volume of square wear tests. Error bars indicate mean standard error, and wear volume of $A_{\parallel}$ and $A^{\perp}$ is graphed for reference.

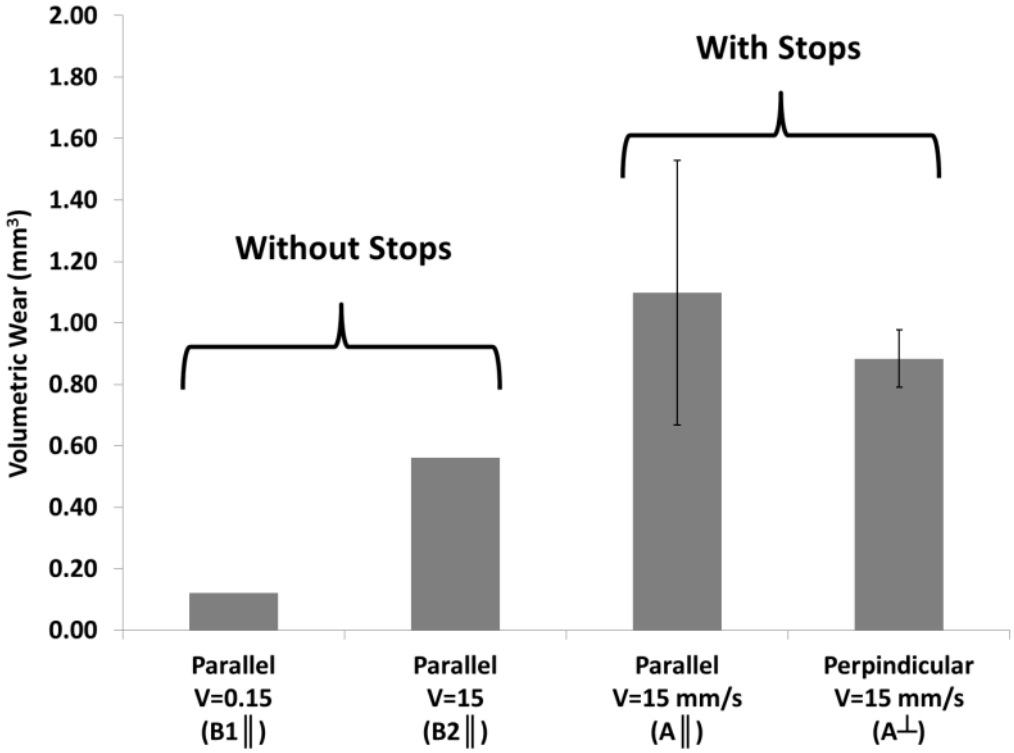

Figure 3.8 Volumetric wear for simple linear reciprocating wear paths. Linear reciprocating wear paths slid for a total of 0.02 km distance. Wear volume of $A_{\parallel}$ and $A^{\perp}$ is graphed for reference (total sliding distance 0.25 km), and error bars indicate mean standard error when applicable.

While not quantitative, observation of transfer film can lead to valuable information about the wear cycle and nature of transfer film. Figure 3.9 displays the wear track of a square wear test with velocities of 15 mm/s on all sides (S1) and two linear reciprocating tests with a perpendicular bias ($A^{\perp}$). The transfer film had a clear disparity between perpendicular and parallel biased legs of the square wear paths as seen previous studies. However, a clear gradient of film can be seen in Figure 3.9a from Point 1 to Point 2. Compared to Figure 3.9b, the square transfer film was more discontinuous and had a lumpy appearance. Figure 3.10 displays white light profilometry images of transfer film for a square and linear reciprocating wear path. The average roughness of the square and linear tests were Ra=3.46 μm and Ra=2.71 μm respectively. The Ra measurement for the square path was higher, and the film appeared to be thicker and less continuous according to Figure 3.10. Given the wear results of the tests corresponding to these films, the transfer film for non-reciprocating sliding was not as effective in preventing wear as

reciprocating sliding despite appearing to have more volume. These observations and wear results seem to suggest volume and thickness of transfer film was not a good predictive metric for wear. In fact, a thin, more continuous film seemed to indicate less wear. Therefore, transfer film quality must be viewed in terms of factors such as reciprocation, sliding velocity, and roughness orientation.

The linear reciprocating tracks with stops and a parallel bias (A‖) are shown in Figure 3.11. A dark deposition was formed on this counterface, and the nature of this film was closely investigated. This film appeared to have wear reducing effects as the film in Figure 3.11a had more developed dark deposition and lower wear than the film in Figure 3.11b. Figures 3.9 and 3.11 show two distinct types of deposition were developed in the wear tests. Both the dark deposition and transfer film gradient were then analyzed.

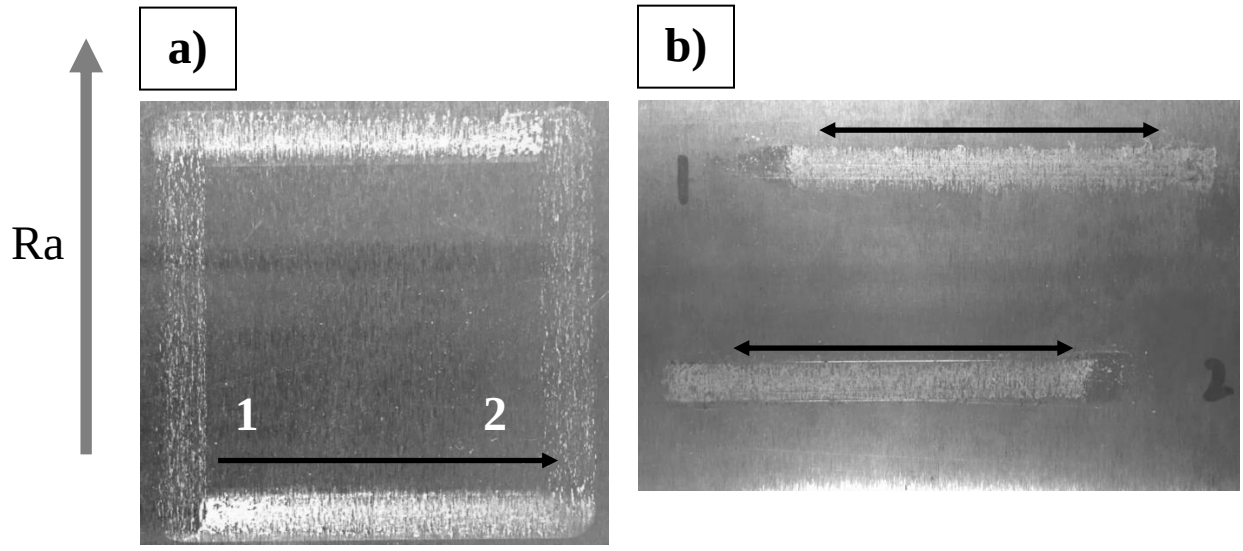

Figure 3.9: Wear tracks of a) S1 square tests where parallel sides had velocities of 15 mm/s and b) LS2 linear reciprocating tests with a perpendicular roughness bias. Arrows represent roughness direction and sliding direciton.

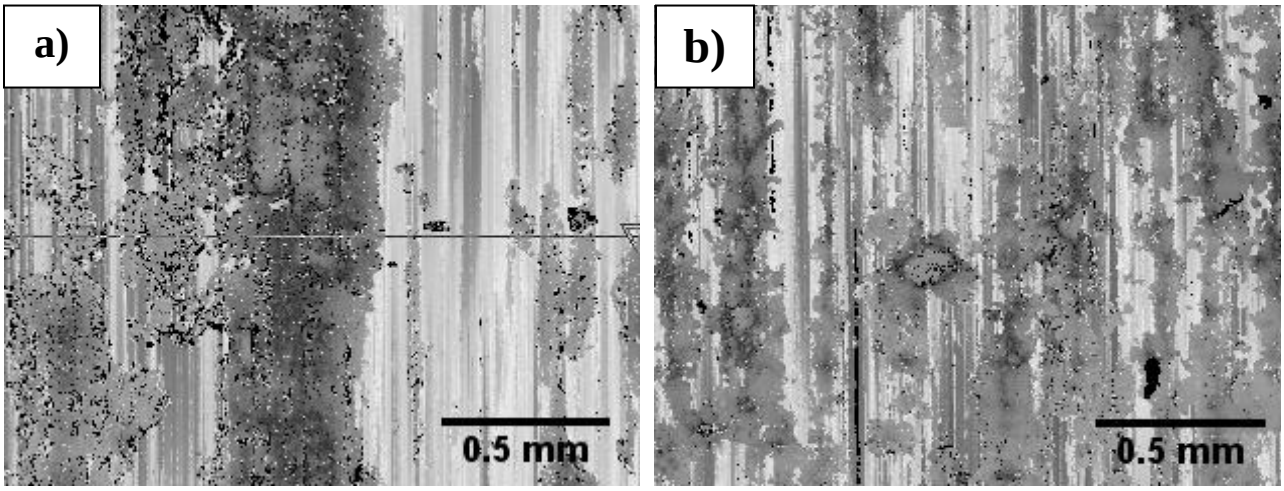

Figure 3.10: Three-dimensional profilometer maps of the a) square wear track and b) linear reciprocating perpendicular track corresponding to Figure 3.9.

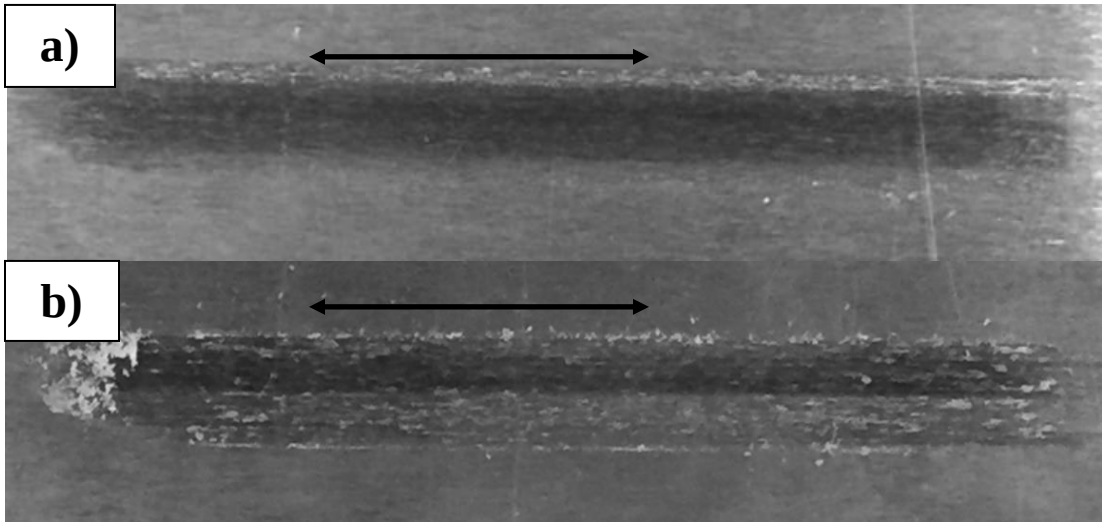

Figure 3.11: Wear scars of LS1 parallel linear reciprocating tests with stops. A dark deposition is formed in both, but wear was reduced for the sample with more deposition coverage (top).

3.3.2 Dark Deposition Investigation

In linear reciprocating tests, transfer film was present in some cases, but the least wear occurred when the wear track had a dark deposition as seen in Figure 3.11. Based on the replicate experiment performed in the oven, the results in Figure 3.12 showed that at 218°C, a white film developed, while at 275°C a darker deposition was partially formed. A Raman shift at 1200 cm^{-1} and 1600 cm^{-1} was observed for the films deposited in Figure 3.11 as well as the films in Figure 3.12. The results indicated that the dark deposition is in fact PEEK that has changed

color. Given that the deposition is transfer film and its presence corresponds to lower wear, it gives more evidence that suggests a thinner, more continuous transfer film was more effective of reducing wear in PEEK.

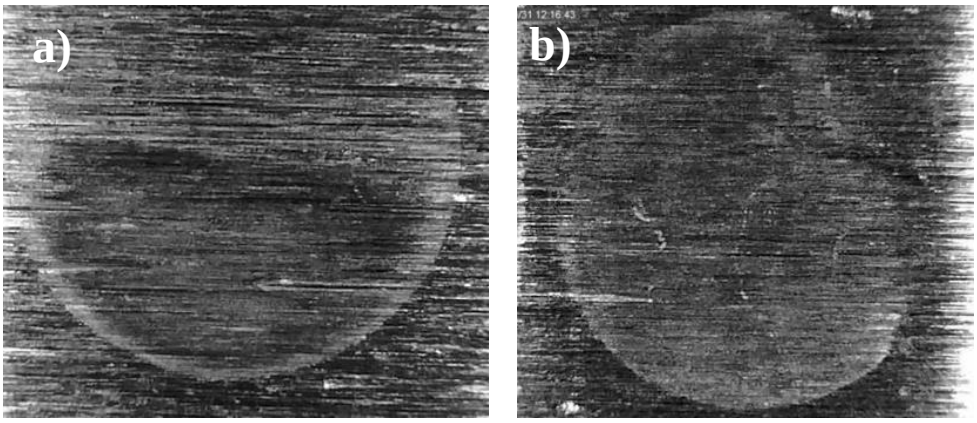

Figure 3.12: PEEK pins were clamped to steel counterfaces and heated to a) 275°C and b) 218° for two hours in a forced convection oven.

3.3.3 Directional Strengthening Hypothesis: Scratch Tests and Chemical Etching

Scratch tests and chemical etching were conducted to test the hypothesis of direction strengthening of PEEK in order to determine the cause of the transfer film gradient seen in Figure 3.9a. SEM images for the chemically etched PEEK pins are shown in Figure 3.13. Figure 3.13a and 3.13b show the pins which were not worn and those that were wear tested respectively with scale indicated. There were no spherulites visible on either surface, and no directionality in polymer crystallinity was apparent after the wear test. The lack of crystal structure demonstrates that both surfaces were amorphous before and after being worn as etching removes the amorphous phases. These results were also in agreement with previous studies [30].

Scratch tests were also conducted to further confirm that no directional strengthening occurred during wear tests. The forces required to scratch the PEEK surface are compiled in Figure 3.14. There was no clear correlation with direction of the scratch tests and force. From the control samples that were prepared, but not worn, there were instances of greater force at certain

angles, and this was also true for the worn samples. The directional strengthening hypothesis was proposed to explain the gradient of transfer film found in the square paths. Chemical etching revealed no visible chain orientation, and scratch tests on worn pins compared to unworn control samples showed no indication of directionality. Together, these two procedures gave no evidence of directional strengthening and falsified the directional strengthening hypothesis.

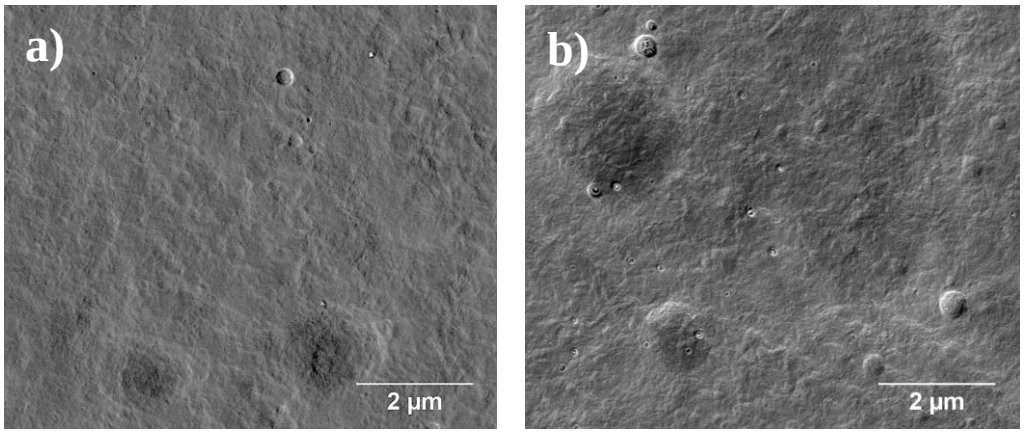

Figure 3.13: Permanganate chemical etching of PEEK pins for a) not wear tested pins and b) wear tested

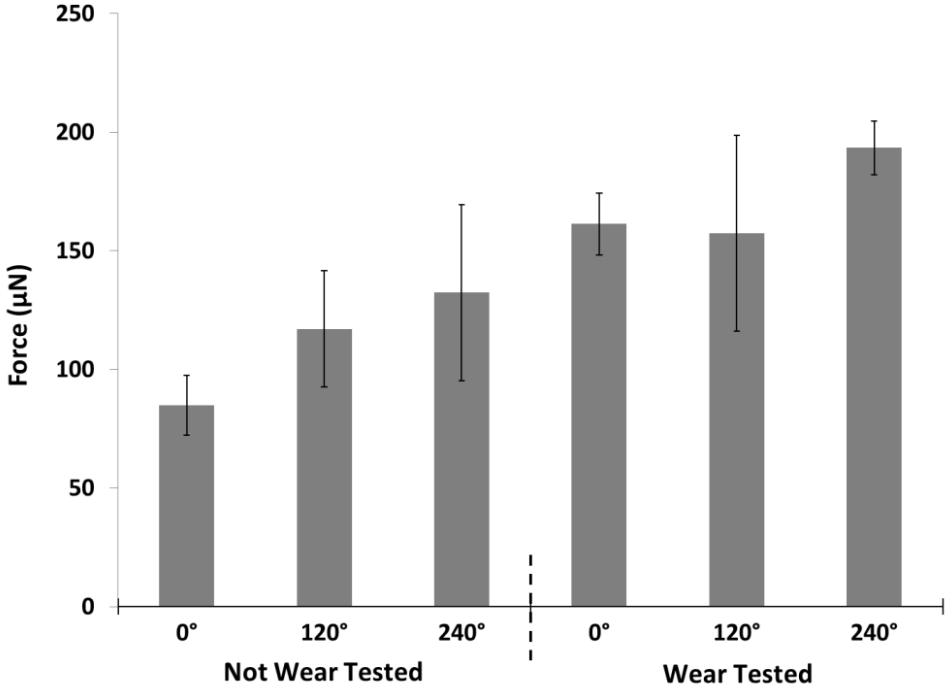

Figure 3.14: Scratch test results for unworn control samples and wear tested samples from square tests (S1). The average force needed to slide a 75 micron diameter indenter at a 0.255 N load is plotted for each direction. The probe was slid at 0.05 mm/s for approximately 4 mm. Tests were conducted three times at different angles along the PEEK pin at 0, 120, and 240 degrees. 0 degrees is in the x-direction indicated by Figure 3.3.

3.3.4 Thermal Softening Hypothesis: Transfer Film Analysis

The transfer film deposited by the square tests was analyzed with the optical profilometer, and the software was able to produce three-dimensional height maps that could estimate the PEEK volume on the steel counterface. Figure 3.15 displays the results of this analysis. The transfer film volumes in Figure 3.15 were taken from square tests at the perpendicular to roughness sides only. The velocities indicate the speed of the preceding parallel side leg of the square. The transfer film after the 15 mm/s leg had a clear gradient which decreased from initial value, indicating a larger volume of film just after the pin changed direction. No definitive gradient was present in the 1.5 mm/s test volume results given the mean standard error. A right-sided, one-tailed T-test was conducted on the data in Fig. 3.15 by comparing the film volume difference at 0 mm and 36 mm for both sets of data. It was found that for 15 mm/s, the P-value was 0.0253 with α=0.05. For 1.5 mm/s, this P-value was 0.190. Therefore, there was statistical confirmation that a gradient likely existed for the 15 mm/s case, whereas it was unlikely a gradient to exist for 1.5 mm/s case. Figure 3.16 presents the percent area coverage of the transfer film for each velocity case. There was no indication of gradient in area coverage in any transfer film examined, and percent coverage lies between 70-90% in all cases. Therefore, area covered by transfer film did not seem to correlate to wear in these tests.

The thermal softening hypothesis proposed here states that transfer film is the result of frictional heating of PEEK that is then deposited by adhesion. For square wear paths, this means when sliding with a parallel bias, little film is deposited and the heated volume of PEEK is accumulated on the tip of the pin. This accumulated volume is deposited on the area of counterface just after the corner of the wear path upon perpendicular sliding. Decreasing frictional heating by decreasing the velocity on the parallel sides of the square path would then

decrease the film gradient. Since Figure 3.15 does not falsify this statement, the thermal softening hypothesis was not rejected as were the previous explanations. However, more study is needed to confirm this hypothesis. It is important to note that depositions can be developed without sliding as demonstrated in Figure 3.12, but at elevated temperatures. This gives further evidence that the temperature generation at the interface was playing a key role in transfer film development.

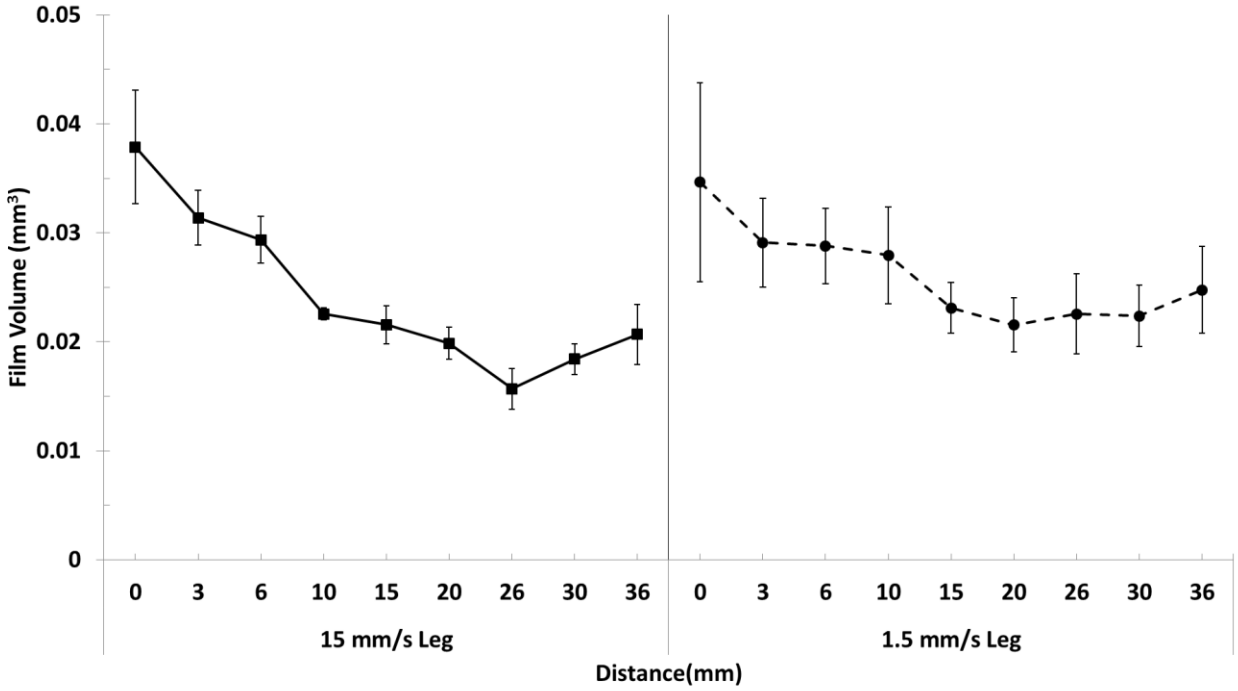

Figure 3.15: Transfer film volume analysis for perpendicular legs on square wear path after the 15 mm/s parallel legs and after the 1.5 mm/s parallel legs in square tests. Error bars indicate mean standard error.

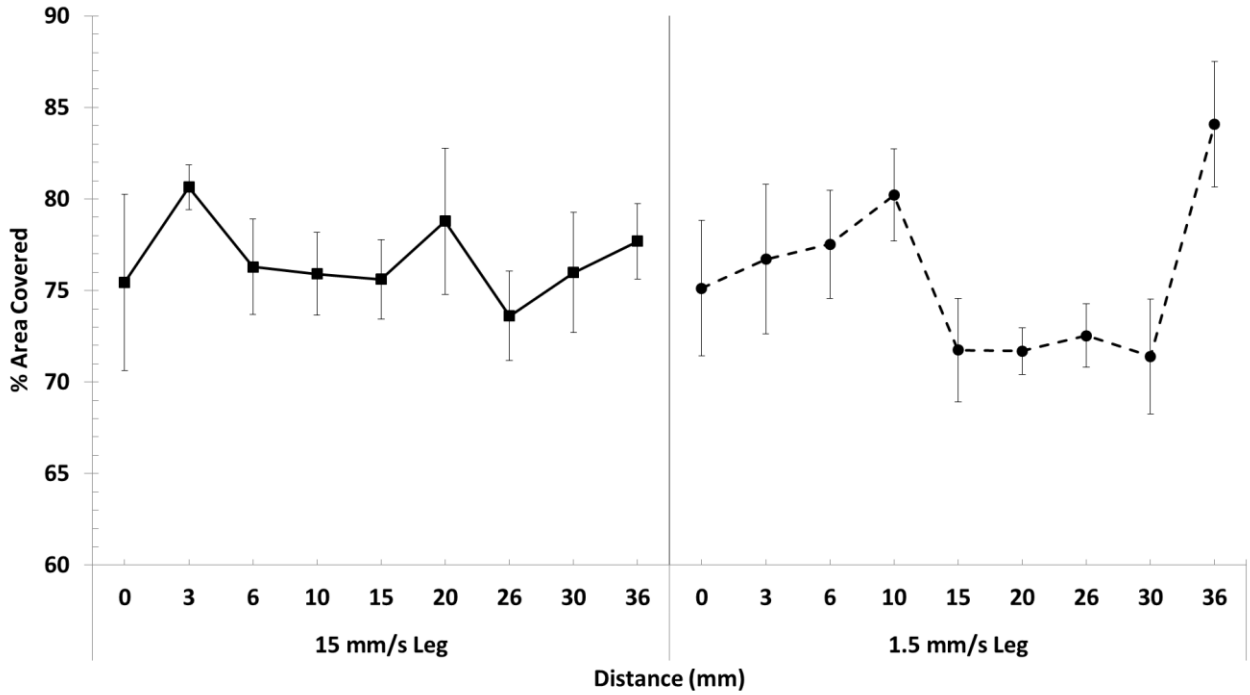

Figure 3.16: Percent area coverage by transfer film on perpendicular square legs after the 15 mm/s legs and after the 1.5 mm/s legs in square tests. Error bars indicate mean standard error.

3.3.5 Bulk Temperature Rise

Bulk temperature rise was obtained during linear reciprocating tests with stops ($A_{\parallel}$, $A_{\perp}$) by a thermal imaging camera and software. The mean temperature of the bulk polymer pin is shown in Figure 3.17. The temperature increased with time for all tests, but perpendicular sliding had a higher temperature even early in the test where little transfer film has been developed. The increased bulk temperature strongly suggests a higher interfacial temperature in the perpendicular test than in the parallel test. Given that film volume was visibly greater in the perpendicular case, this gives more evidence that interfacial temperature rise was correlated with transfer film development. Despite an increase in coefficient of friction, temperature rise, and film deposition, the perpendicular test had lower potential for wear than the parallel test indicating that transfer film has a wear-reducing effect that compensated for these factors.

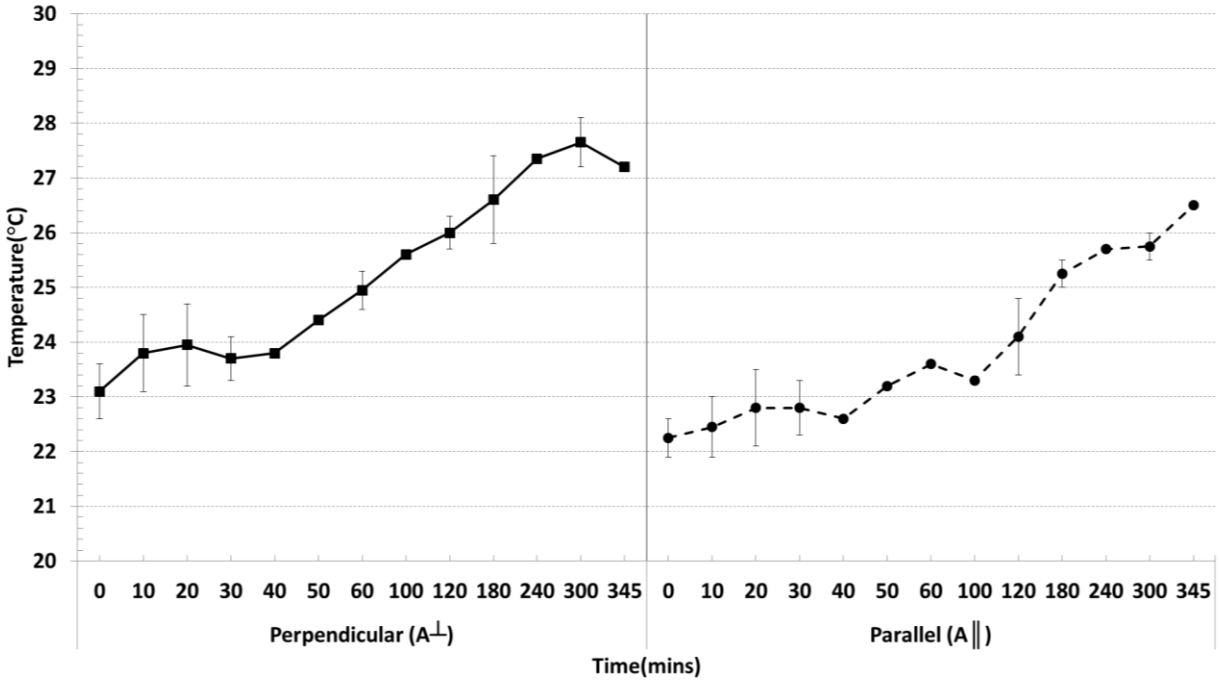

Figure 3.17: Bulk PEEK pin mean temperature rise during linear reciprocating stop tests. Error bars indicate mean standard error. Lack of error bar indicates one measurement taken at the specified time.

3.4 Conclusions

- Reciprocation plays a dominant role in the wear cycle followed by sliding velocity, while the least influential factor is roughness orientation.
- Transfer film reduces wear in PEEK, but the volume and area covered by transfer film when it is present is not indicative of wear. In this study, thin, continuous films correspond to less wear.
- There is no indication of directional strengthening of the PEEK surface during wear testing, or any evidence transfer film is primarily the result of free wear debris.
- Frictional heating is playing a key role in PEEK transfer film mechanisms and can influence transfer film volume and development.

3.5 References

[1] S. M. Kurtz, *PEEK Biomaterials Handbook* (Plastics Design Library). Burlington: Burlington : Elsevier Science, 2011.

[2] K. Friedrich, J. Karger-Kocsis, and Z. Lu, "Effects of steel counterface roughness and temperature on the friction and wear of PE(E)K composites under dry sliding conditions," *Wear,* vol. 148, no. 2, pp. 235-247, 1991.

[3] M. Abdullah, A. Goharian, M. Kadir, and M. Wahit, "Biomechanical and bioactivity concepts of polyetheretherketone composites for use in orthopedic implantsa review," in *J. Biomed. Mater. Res. Part A* vol. 103, ed, 2015, pp. 3689-3702.

[4] X. X. Chu, Z. X. Wu, R. J. Huang, Y. Zhou, and L. F. Li, "Mechanical and thermal expansion properties of glass fibers reinforced PEEK composites at cryogenic temperatures," *Cryogenics,* vol. 50, no. 2, pp. 84-88, 2010.

[5] M. Zalaznik, M. Kalin, and S. Novak, "Influence of the processing temperature on the tribological and mechanical properties of poly-ether-ether-ketone (PEEK) polymer," *Tribology International,* vol. 94, pp. 92-97, 2016.

[6] R. Schroeder, F. W. Torres, C. Binder, A. N. Klein, and J. D. B. de Mello, "Failure mode in sliding wear of PEEK based composites," *Wear,* vol. 301, no. 1-2, pp. 717-726, 2013.

[7] S. Bahadur, "The development of transfer layers and their role in polymer tribology," *Wear,* vol. 245, no. 1, pp. 92-99, 2000.

[8] S. Bahadur and D. Tabor, "The wear of filled polytetrafluoroethylene," *Wear,* vol. 98, no. C, pp. 1-13, 1984.

[9] J. Bijwe, S. Sen, and A. Ghosh, "Influence of PTFE content in PEEK–PTFE blends on mechanical properties and tribo-performance in various wear modes," *Wear,* vol. 258, no. 10, pp. 1536-1542, 2005.

[10] S. Biswas and K. Vijayan, "Changes to near-surface region of PTFE during dry sliding against steel," *Journal of Materials Science,* vol. 23, no. 5, pp. 1877-1885, 1988.

[11] B. J. Briscoe, T. A. Lin Heng Yao, and T. A. Stolarski, "The friction and wear of poly(tetrafluoroethylene)-poly (etheretherketone) composites: An initial appraisal of the optimum composition," *Wear,* vol. 108, no. 4, pp. 357-374, 1986.

[12] A. Kapoor and S. Bahadur, "Transfer film bonding and wear studies on CuS-nylon composite sliding against steel," *Tribology International,* vol. 27, no. 5, pp. 323-329, 1994.

[13] C. J. Schwartz and S. Bahadur, "Studies on the tribological behavior and transfer film–counterface bond strength for polyphenylene sulfide filled with nanoscale alumina particles," *Wear,* vol. 237, no. 2, pp. 261-273, 2000.

[14] Q. Wang, Q. Xue, H. Liu, W. Shen, and J. Xu, "The effect of particle size of nanometer ZrO2 on the tribological behaviour of PEEK," *Wear,* vol. 198, no. 1-2, pp. 216-219, 1996.

[15] J. R. Cooper, D. Dowson, and J. Fisher, "The effect of transfer film and surface roughness on the wear of lubricated ultra-high molecular weight polyethylene," *Clinical Materials.,* vol. 14, no. 4, pp. 295-302, 1993.

[16] H. Cai, F. Yan, and Q. Xue, "Investigation of tribological properties of polyimide/carbon nanotube nanocomposites," *Materials Science & Engineering A,* vol. 364, no. 1, pp. 94-100, 2004.

[17] K. A. Laux and C. J. Schwartz, "Effects of contact pressure, molecular weight, and supplier on the wear behavior and transfer film of polyetheretherketone (PEEK)," *Wear,* vol. 297, no. 1-2, pp. 919-925, 2013.

[18] D. R. Haidar, J. Ye, A. C. Moore, and D. L. Burris, "Assessing quantitative metrics of transfer film quality as indicators of polymer wear performance," *Wear,* vol. 380-381, pp. 78-85, 2017.

[19] K. A. Laux, A. Jean-Fulcrand, H. J. Sue, T. Bremner, and J. S. S. Wong, "The influence of surface properties on sliding contact temperature and friction for polyetheretherketone (PEEK)," *Polymer,* vol. 103, pp. 397-404, 2016.

[20] H. Blok, "The flash temperature concept," *Wear,* vol. 6, no. 6, pp. 483-494, 1963.

[21] Q. Wang, Y. Wang, H. Wang, N. Fan, M. Wang, and F. Yan, "Evaluation of fretting Wear Behavior of PEEK by Analyzing the Change of Crystallinity: The High Temperature Effect," *Polymer Engineering and Science,* 2017.

[22] A. Wang *et al.*, "Orientation softening in the deformation and wear of ultra- high molecular weight polyethylene," *Wear,* vol. 203, pp. 230-241, 1997.

[23] R. Ciora and J. Magill, "Rolltruded poly(aryl ether ether ketone) (PEEK) for membrane applications," *Sep. Sci. Technol.,* vol. 32, no. 5, pp. 899-923, 1997.

[24] R. H. Olley, D. C. Bassett, and D. J. Blundell, "Permanganic etching of PEEK," *Polymer,* vol. 27, no. 3, pp. 344-348, 1986.

[25] S. Roy and S. Sundararajan, "The effect of heat treatment routes on the retained austenite and Tribomechanical properties of carburized AISI 8620 steel," *Surface & Coatings Technology,* vol. 308, pp. 236-243, 2016.

[26] A. Wang *et al.*, "Orientation softening in the deformation and wear of ultra-high molecular weight polyethylene," *Wear,* vol. 203, pp. 230-241, 1997.

[27] J. Vande Voort and S. Bahadur, "The growth and bonding of transfer film and the role of CuS and PTFE in the tribological behavior of PEEK," *Wear,* vol. 181, pp. 212-221, 1995.

[28] D. W. Lee, X. Banquy, and J. N. Israelachvili, "Stick-slip friction and wear of articular joints," *Proceedings of the National Academy of Sciences of the United States of America,* vol. 110, no. 7, p. E567, 2013.

[29] G. M. Bartenev, *Friction and Wear of Polymers / G.M. Bartenev and V.V. Lavrentev ; translated by D.B. Payne ; edited by Lieng-Huang Lee and K.C. Ludema*. Amsterdam ; New York : New York: Amsterdam ; New York : Elsevier Scientific Pub. Co. ; New York : Distributors for the U.S. and Canada, Elsevier/North-Holland, 1981.

[30] L. Zhang *et al.*, "Significantly enhanced wear resistance of PEEK by simply filling with modified graphitic carbon nitride," *Materials & Design,* vol. 129, pp. 192-200, 2017.

CHAPTER 4: THE WEAR REDUCING ATTRIBUTES OF POLYETHERETHERKETONE (PEEK) TRANSFER FILM AS A RESULT OF LARGE INITIAL WEAR

A paper to be submitted to *Wear*

Mark D. Placette and Christian J. Schwartz

Abstract

Polyetheretherketone (PEEK) is a high-performance thermoplastic that has applications spanning many industries. One of the fundamental wear characteristics of PEEK is its ability to form transfer film that acts as solid lubrication, but the mechanisms for how this occurs is not well understood. It has been speculated that PEEK transfer film development is a combination of adhesion and mechanical interlocking of polymer material between asperities. However, in practice this does not have explanatory power as these are also potential wear mechanisms. Some studies have suggested interfacial softening, mechanical shear, and sliding orientation with respect to roughness all play key roles in transfer film development. In this study, the effect of roughness orientation is explored in multi-directional sliding. Two test paths biased parallel and perpendicular with respect to roughness orientation were conducted over a varied number of cycles. High resolution coefficient of friction and temperature data was collected for each test. The roughness of the counterface after testing was analyzed with white-light profilometry. When it was found that the temperature differed substantially between the sliding directions in the wear tests, a theoretical framework was established to explain the results. The results indicate that sliding direction with respect to roughness orientation has a significant impact on wear and transfer film development, and large initial wear is required to develop transfer film that results

in long term wear-reducing benefits. The results also indicated that the reason for both the disparity in transfer film and wear between the two sliding orientations was the adhesion strength of the transfer film. The theoretical framework established in this study indicates cyclic loading magnitude resulting from counterface asperities might explain the difference in wear and transfer film behavior between the different roughness orientations.

4.1 Introduction

Polyetheretherketone (PEEK) is a high-performance thermoplastic with applications in several advanced technologies. It is being explored for use in hydrophobic coatings [1], oral and orthopedic implants [2], and control bearings in aircraft [3]. PEEK films are also used as solid lubrication to extend the longevity of both industrial equipment and medical devices [4, 5]. Other than tribology applications, PEEK is being examined for use in cryogenic storage in space [6, 7] and microelectronics fabrication [8, 9]. It is also easy to sterilize, able to operate at high humidity, and readily tailored for specific applications by additives. PEEK is able to achieve such an array of utility by having a combination of a high glass transition temperature (T_g~140°C), tensile strength (~110 MPa), and low chemical reactivity and moisture absorption [10]. Consequently, wear of PEEK is considerably lower than most polymers even at elevated temperatures or corrosive environments. One attribute of PEEK thought to impact good wear performance is the formation of a self-lubricating transfer film. Despite this advantage and the broad use of PEEK, the exact mechanisms for transfer film development are still unclear.

Transfer film formation is an intrinsic property of the PEEK wear cycle. Transfer films consist of polymer material that has been adhered to the counterface. This process is thought to mainly be due to adhesion, and once a transfer film has been developed, it reduces wear by lowering contact stress and protecting the polymer bulk from abrasion by the harder counterface

[11]. In PEEK, transfer films can form almost immediately within the first several cycles when sliding on metals [12]. It is therefore imperative to study PEEK transfer film, but the mechanisms that govern transfer film development are often the same mechanisms responsible for wear. Briscoe et. al found that interfacial softening by either temperature or plastic deformation will increase wear, but will also promote transfer film development depending on normal load [13]. By analyzing the crystallinity of wear debris, one study similarly concluded that interfacial temperatures were promoting not only lubricating effects, but also the wear mechanisms of fatigue delamination, micro-cutting, and adhesion [14, 15]. There also appears to be a mechanical component to the formation of transfer film and its permanence on the counterface. PEEK transfer film is capable of being removed through mechanical shear if the adhesion is weak, so instead of being solid-lubrication, the film generates large wear debris [11]. In contrast, a study investigating PEEK at different chamber temperatures found transfer films were only observed when ploughing was present [16]. Additives can also play a role in both wear and transfer film development by adding lubrication and promoting better adhesion, but are not universally beneficial. PTFE/PEEK blends reduce wear by PEEK adhering to the counterface and PTFE providing the solid lubrication at the interface [17]. It is also well known other additives such as carbon fiber and silica generally reduce wear in PEEK by reinforcing the polymer matrix [18]. However, if a transfer film is not formed, the additives of polymer composites can have wear enhancing effects, or in the case of some PEEK-Carbon Fiber composites, the transfer films can severely abrade the bulk polymer during sliding [19-21]. It is therefore difficult to understand the optimum mechanisms that simultaneously produce transfer film and reduce wear.

One fundamental factor that can influence both transfer film formation and wear in PEEK is roughness orientation. Rough contact is a fundamental contact problem that has long been explored with classical modeling techniques [22, 23]. In PEEK systems, the counterface roughness seems to, in part, determine the mechanisms of wear. Ovaert found that minimum wear and high transfer film development can occur at R_q=0.15 μm [24]. Below this regime, a mirror finished counterface can produce substantially more wear, most likely due to increased adhesive forces from a larger real contact area [25, 26]. Above this optimum roughness, fatigue and abrasive wear become increasingly dominant [24]. The direction of sliding relative to roughness can also have an impact. Changing the direction of sliding orthogonal to roughness has been shown to decrease wear, which could largely be due to the fact transfer film is more readily formed in this direction [27, 28]. Roughness can effectively change the composition of transfer film in composites, where lubrication properties can be hindered or increased [29]. Furthermore, even if the typical measurements of roughness are ignored, the skewness of a surface may influence the formation of transfer film. A study of PEEK coatings thermally sprayed onto stainless steel showed that a distribution of asperity heights with a positive skewness could increase the formation of film, and it was speculated the positive skewness provided more available surface area for adhesion and mechanical interlocking [30]. In multi-directional sliding, roughness orientation can have large effects on the wear cycle and transfer film. Studies of multi-directional sliding of PEEK have shown that transfer film readily develops when sliding perpendicularly to roughness orientation but have very little transfer film in parallel sliding [31, 32]. The exact reason for this difference in film deposition behavior and its influence on wear is unknown, but has profound implications for multi-directional sliding applications of PEEK.

The goal of this paper was to understand the substantial impact of counterface roughness orientation on PEEK transfer film development and bulk wear. In order to evaluate the effects of roughness orientation, rectangular path wear tests were conducted with extreme aspect ratios which biased the predominant sliding direction either parallel or perpendicular to roughness orientation. High resolution coefficient of friction data was collected during testing, and this was closely examined in relationship to thermal images taken by an infrared camera in order to ascertain transfer film behavior. To explain observations in frictional heating and wear, a viscoelastic cyclic heating model is proposed. The model proposed was verified empirically with dynamic mechanical analysis. Finally, a simple finite element contact model was developed to explore any difference sliding perpendicular or parallel had in stress and contact area.

4.2 Materials and Methods

4.2.1 Testing Materials

A 6.35-mm diameter PEEK cylindrical pin (Quadrant Plastics, Ketron PEEK 1000) was cut from stock. The PEEK stock is non-reinforced and unfilled with a tensile strength of 115 MPa and melting temperature of 340°C. The pin was then polished with abrasive paper on a two-axis tribometer to ensure the pin surface would mate well with the counterface surface during testing. The pin was then cleaned in an ultrasonic bath by sequentially bathing the sample in acetone, a soap-water mixture, and deionized water. Finally, the sample was rinsed with ethanol to evaporate all excess water. The sample was then weighed after allowing it to air dry for ten minutes. Upon completion of the wear test, the cleaning procedure was repeated, and the pin was weighed again to determine mass loss. Using the known density of the polymer this was then converted to volumetric wear. All counterface materials were A36 hot rolled-steel with a hardness of 62.4 HRB. The counterfaces were surfaced ground with an automatic surface

grinding machine (Okamoto PSG 63UA) that gave a roughness of approximately 1±0.1 μm. After the wear test, the counterfaces were carefully saved for wear debris and roughness measurements.

4.2.2 Wear Testing

All wear tests were conducted on a two-axis tribometer (Rtec Instruments, San Jose, California) represented by Figure 4.1. The stage was moved with two independent stepper motors (XY) controlled with motion software which also controlled velocity. Load was applied in the z-axis by a controlled linear motor. The load cell was capable of measuring force in all three axes and calculating coefficient of friction at a rate of 1000 samples per second.

The two types of wear paths employed in this study are shown in Figure 4.2. Each wear path was a high aspect ratio rectangle with long side lengths of 80 mm and short side lengths of 10 mm. The wear paths were oriented with the long sides either parallel or perpendicular to roughness orientation. The two wear paths will be referred to as parallel biased since the majority of the total wear path ran parallel to the axis of roughness ridges or perpendicular biased as the majority of the total wear path ran across the asperity cross-section for the remainder of this paper. For each test, a load of 145 N was applied for a 4.58 MPa nominal contact pressure. The average velocity of all tests was 11.58 m/s. In order to examine the effect of roughness orientation on the wear cycle, the number of cycles for each test varied, and in some cases replications of tests were performed. Table 4.1 displays the details each test including the sliding distance and replications. First, the 250 meter tests were performed. It was found that perpendicular biased tests had significantly greater wear than parallel biased tests. Tests were then performed for 18 meters, and the wear of the two biased tests was found to be comparable. A binary search method was then employed to locate the sliding distance in which the two test

types (parallel/perpendicular) had wear volume that diverged. For example, the next test done chronologically was at 134 meters since this was the midpoint between 18 meters and 250 meters. In total, six distinct perpendicular biased tests were conducted, and six distinct parallel biased tests were conducted. With replications, a total of twenty-four wear tests were conducted, and a previously unused PEEK pin was used for each of the twenty-four tests. To further explore the effect of transfer film on wear behavior, it was decided to investigate wear in the presence of a pre-deposited film. The same counterfaces for a 76 meter test were then wear tested for an additional 76 meters with fresh pins. This procedure was conducted once for both parallel and perpendicular bias cases. In addition to gathering the wear volume for all tests, optical microscopic images were taken to inspect both wear debris and transfer film of the 250 meter tests.

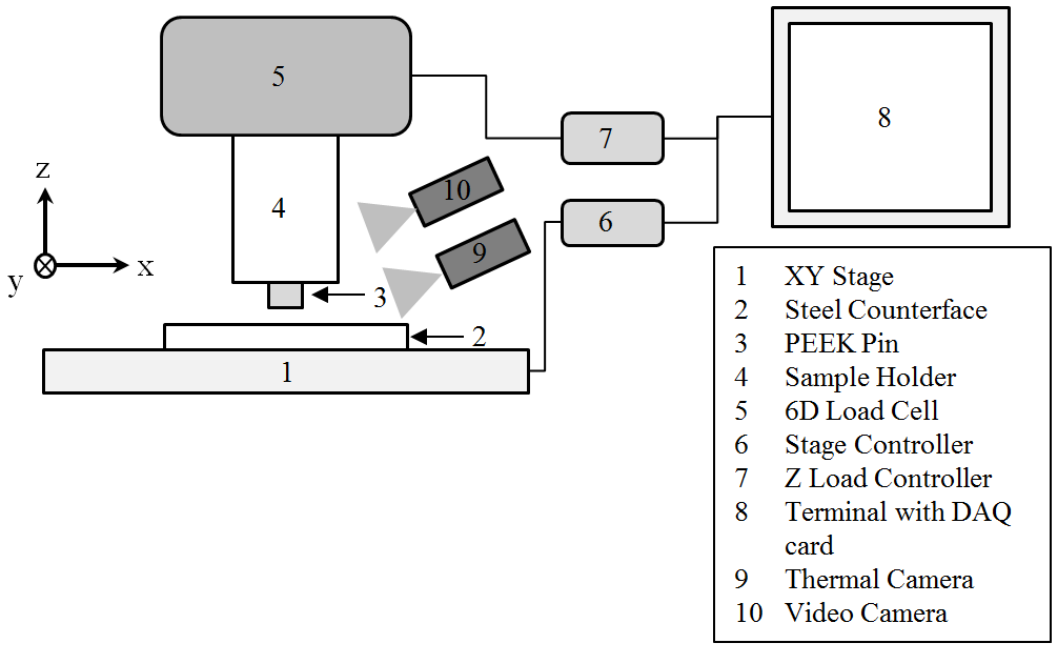

Figure 4.1: Schematic of tribometer and experimental equipment used for all wear tests.

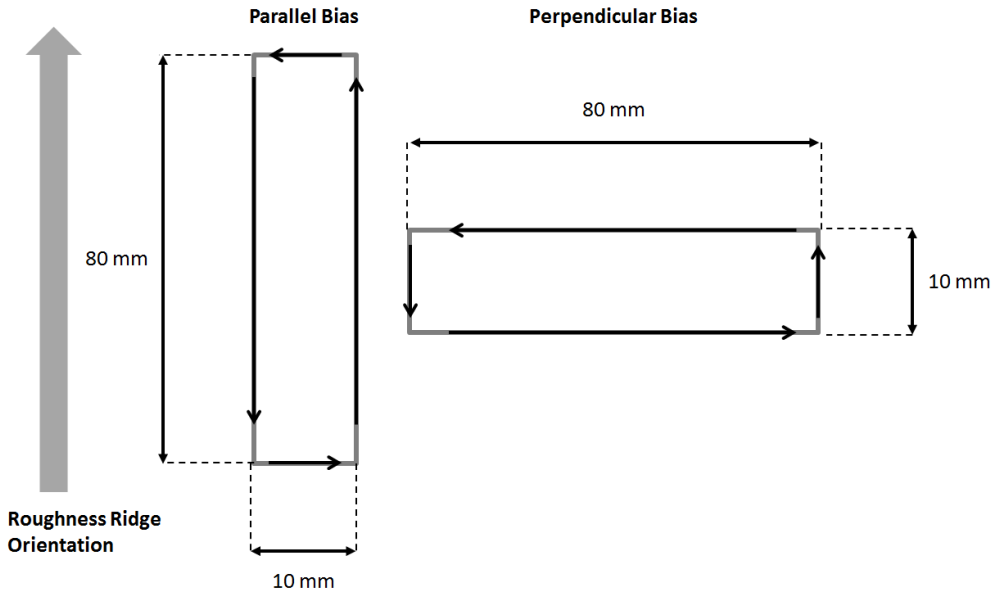

Figure 4.2: Schematic of wear paths with sliding biases parallel and perpendicular with respect to roughness. Each test consisted of an 80 mm X 10 mm rectangular wear path test conducted at a load of 145 N for 6.35 mm diameter pin.

Table 4.1: Summary of wear test parameters with bias, sliding distance, and number of replications indicated. A total of 24 tests were completed.

Sliding Distance (m)	Parallel Bias($\parallel$) No. of samples	Perpendicular Bias($\perp$) No. of Samples
9	2	2
18	2	2
46.98	1	1
76.14	3	3
134.10	1	1
250.02	3	3

4.2.3 White Light Profilometry

In order to explore the effect of sliding direction with respect to roughness orientation, roughness measurements of the counterface and transfer film were conducted with a white light profilometer (Zygo NewView700). Each measurement taken by the profilometer was a 0.47 mm X 0.35 mm sample area. The untouched counterface and one transfer film from a parallel biased and perpendicular biased test was measured five times each and averaged to generate values of

Rzx and Rzy for each surface. Rzx and Rzy give roughness measurements exclusively parallel or perpendicular to roughness orientation respectively. To calculate Rzx, the total sample area is divided into one-pixel wide line segments which run in the x-direction (423 segments total). The average absolute value of the five highest peaks and five lowest valleys is calculated per line segment. This data is gathered for each line segment and average to yield Rzx. Rzy is calculated in a similar way in the y-direction.

4.2.4 Thermal Behavior

A thermal camera (FLIR A600) was used to investigate the temperature rise of pins during linear reciprocating sliding tests. To calibrate the emissivity for the PEEK pin as described by the manufacturer, a cleaned PEEK pin was partially covered with black electrical tape and was thermally soaked for two hours at 40°C. The pin was quickly removed and thermal images were quickly recorded for the sample. Once the measurements were recorded, the emissivity was changed until the PEEK pin agreed with the known temperature of the electrical tape (emissivity ~0.95). This emissivity was found to be approximately 0.44. During each test, black electrical type was applied to the sample holder thermally isolated from the pin. This temperature was recorded for an ambient reference. The emissivity and reference temperature was then entered into the thermal camera software to ensure the temperature of the pin would be accurate. The mean temperature of the bulk PEEK pin was obtained for each frame at 15 frames per second. This thermal imaging technique was utilized for both wear tests and dynamic mechanical analysis.

The investigators hypothesized that there may have been a difference in the interface temperature between parallel and perpendicular sliding due to a difference in the extent of viscoelastic strain magnitude between the two. An existing viscoelastic cyclic heating model is

utilized to explain the results of the wear tests by observing the fundamental differences in loading of the perpendicular and parallel biased tests. This model is well documented in this application by Rittel and Rittel and Rabin [33, 34]. The model is represented by a glassy polymer undergoing cyclic compression. The fundamental heat equation of this polymer is:

$$\rho c_E \dot{T} + (3\lambda + 2\mu)\alpha T_0 \dot{\varepsilon}_{kk} = s_{ij}^{\mu} \dot{d}_{ij}^{\mu} + k\Delta T \tag{4.1}$$

Where ρ is the density of the polymer, c_E is the specific heat, T is temperature, λ and μ are Lamé constants, α is the thermal diffusivity, and ε is strain. $s_{ij}^{\mu} \dot{d}_{ij}^{\mu}$ is the rate of energy dissipation by the product of deviatoric strain and viscous strain. The thermoelastic effect can be neglected as it is significantly low because the elastic volume change is very small. Equation (4.1) then simplifies to:

$$\rho c_E \dot{T} = s_{ij}^{\mu} \dot{d}_{ij}^{\mu} + k\Delta T \tag{4.2}$$

The first term of the right-hand side of the equation is the rate of energy dissipation, and equivalent to the power of a single hysteresis loop. The fraction of mechanical work done that is dissipated as heat is represented by β and must be between 0 and 1. Upon integrating, Equation (4.2) becomes:

$$\dot{T} = \frac{\beta}{\rho c_E} \dot{W}_{in} + k\Delta T \tag{4.3}$$

The work done enclosed by a single hysteresis loop, W_{in}, can be found as follows. Assuming a complex modulus of a viscoelastic material with storage and loss terms, and given sinusoidal behavior, when strain is applied the work done by the hysteresis loop is

$$W_{in} = \int_0^T \sigma d\varepsilon = \int_0^T \omega \varepsilon_0^2 (G_1 \sin \omega t \cos \omega t + G_2 \cos^2 \omega t) dt = \pi G_2 \varepsilon_0^2 \tag{4.4}$$

With $G_2 = (\sigma_0 / \varepsilon_0) \sin \delta$, and the work for only one loading cycle ($2\pi/\omega$) gives

$$\dot{W}_{in} = \frac{1}{2}\omega\sigma_0\varepsilon_0 \sin\delta \tag{4.5}$$

Thus the temperature change per unit volume per cycle of viscoelastic compression for glassy polymers is

$$\dot{T} = \frac{\beta}{2\rho c_E}\omega\sigma_0\varepsilon_0 \sin\delta + k\Delta T \tag{4.6}$$

If adiabatic conditions are assumed and this is integrated with respect to time, the conduction term can be neglected and the solution for temperature rise of one hysteresis cycle is:

$$\Delta T = \frac{\beta\pi}{\rho c_E}\sigma_0\varepsilon_0 \sin\delta \tag{4.7}$$

Thus, the equation is a function of specific heat capacity, the amount of mechanical work converted to heat, density, the amplitude of strain, and the frequency of the cyclic loading. The experimental results were compared to this relation to determine the likelihood that thermal effects influence the transfer film development in the parallel and perpendicular cases.

To empirically verify the predictions of the viscoelastic heating model, dynamic mechanical analysis (DMA) was conducted (RSA-G2 series, TA Instruments). A 5.35-mm notch was cut into a cylindrical PEEK sample (6.35 mm diameter) in order to minimize the volume of material for measurable temperature rise by a thermal camera, leaving a 1-mm thick cross-section. Oscillating sinusoidal strain was then applied to the PEEK sample under 3-point bending for varied frequencies and strain magnitudes. Additionally, a test was conducted under 3-boint bending with a static force load of 15 N. The temperature of the PEEK sample for each DMA test was then recorded with the thermal camera for analysis.

4.2.5 Finite Element Contact Model

Because contact area is a fundamental parameter that governs several tribological mechanisms such as real contact pressure and adhesion, it became necessary to explore the effect of sliding direction relative to roughness orientation on contact area. This was done to ascertain if there would be fundamental differences in the area between parallel and perpendicular sliding. A simple finite element model (FEA) was created to examine this question (ABAQUS). The model used two-dimensional plane strain, linear elements and all materials included were assumed linear elastic. The diagram of the model used is shown in Figure 4.3. A rectangular body representing PEEK was loaded onto a steel counterface with idealized semi-circular asperities. The counterface was fixed, and the x-axis symmetry was used on the sides of the PEEK body. The steel counterface was modeled as a rigid body. The coefficient between the bodies was assumed to be 0.3 as measured by PEEK wear tests. Two loading cases were examined in order to model the perpendicular and parallel biased tests. The first case used strictly normal force with a shear force of zero, and this modeled the parallel bias case as sliding would occur in the z-direction. The second case modelled perpendicular biased sliding and variable shear loads were added from $1/10^{th}$ normal load to $1/3^{rd}$ normal load in the x-direction. The mesh length was varied until convergence of the mesh occurred. The ultimate rectangular element mesh length was 1/200 the total length of the PEEK body. The contact area for each loading case was collected and examined.

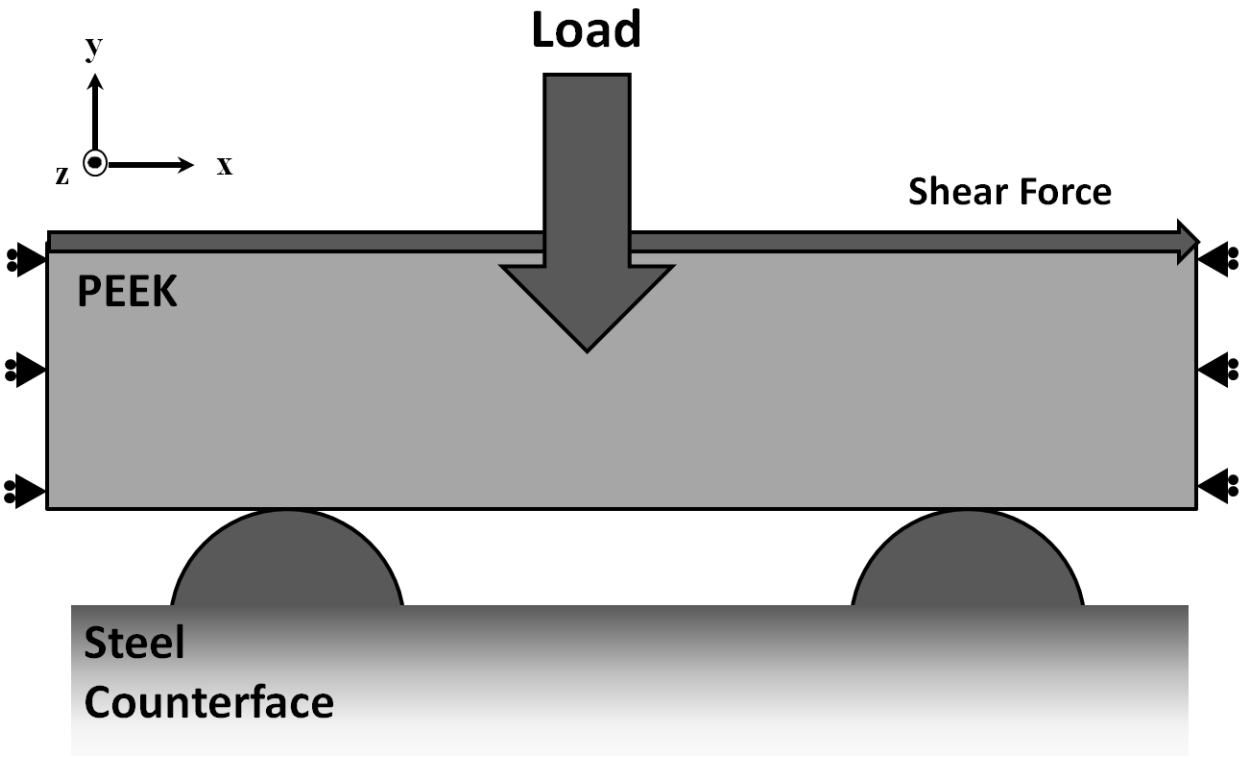

Figure 4.3: Schematic of finite element contact model. The loading parameters considered were strictly normal load and a shear force of zero, and a normal load with a shear force of 1/10, 1/8, 1/5, 1/4, and 1/3 that of the normal load.

4.3 Results and Discussion

4.3.1 Wear Results

The direction of sliding with respect to roughness orientation had an overall significant impact on wear behavior at large sliding distances. The volumetric wear results for every test in Table 4.1 are shown in Figure 4.4, and the mean wear volume of each cycle and the 90% and 95% confidence intervals of the difference in means are shown in Table 4.2. At 9 meters and 18 meters, the wear for both test sliding orientations were comparable. This is shown in the figure and by the fact that zero was near the middle of the confidence intervals of the means. At 76 meters, the test types diverged and perpendicular tests had substantially less wear than sliding in parallel orientation. At 250 meters, the parallel bias tests were substantially higher than the perpendicular bias tests. It was observed that there was a clear difference in the extent and

amount of transfer film between parallel and perpendicular biased tests. The evolution of this film gave insights into why a directional difference was observed.

The considerable reduction in wear rate of the perpendicular tests between 18 meters and 75 meters strongly suggests the development of a transfer film. Before 76 meters, the wear rate in perpendicular sliding was substantially greater than after 76 meters when a low steady-state wear rate was observed. Based on time lapse images taken during the wear test, a transfer film had fully developed by this sliding distance for the perpendicular oriented tests. After this distance, it is hypothesized that transfer film provided protection from further wear. In contrast, parallel biased tests had much less visible transfer film, and the wear rate did not decrease to a lower steady-state from 9 meters to 250 meters. The counterfaces for the 76 meter wear tests were saved and reused with fresh PEEK pins to further demonstrate the effects observed above. Figure 4.5 shows the wear volume of the pre-developed film tests. It is clear from Figure 4.5 that when a transfer film was pre-developed by perpendicular sliding, it lowered wear. This was most likely due to the fact the transfer film was already developed and no initial wear was needed for its formation. Wear in the parallel pre-developed film was comparable to parallel tests without a pre-developed film as shown in the figure. The transfer film developed during parallel sliding did not influence the wear behavior and was completely removed from the counterface by the end of the test.

There is evidence from the visual analysis of transfer film and wear debris that suggests the mechanism determining the difference between wear behaviors of parallel and perpendicular sliding was the adhesion and persistence of transfer film to the counterface. The optical microscopy images of transfer film are shown in Figure 4.6. Investigating the transfer film images in Figure 4.6 revealed the transfer film in perpendicular oriented sliding was thicker, less

transparent, and covered more area. This strongly indicated weaker PEEK adhesion to the counterface and eventual removal for the parallel biased tests. The optical microscopy images of the wear debris are shown in Figure 4.7. Wear debris for both test types was flat and flake-like but the wear debris was larger in the parallel bias tests and was curled, suggesting residual stress. This not only supports that fact that parallel tests had more wear, but also suggests that the wear debris on the parallel tests was once attached to the counterface and had been removed during sliding. From the time lapse images, transfer film was deposited onto the counterface during parallel sliding, but the weakly bonded transfer film was eventually removed. This process was repeated continuously in multiple locations on parallel oriented sliding areas on the counterface. This suggests that the deposition and eventual removal of the transfer film was cyclical in parallel oriented sliding.

A mechanical interlocking concept has been proposed to explain differences in transfer film adhesion to the counterface between the parallel and perpendicular sliding [11], but the concept lacks a strong physical basis nor has it been well investigated. Instead, the authors propose the behavior could be better explained by a difference in film adhesion caused by a difference in wear interface temperatures between the two sliding orientations. This temperature rise may be induced by cyclic viscoelastic loading as predicted by Equation 4.6. If the strain amplitude is higher, then a higher wear interface temperature is predicted which would likely promote greater true contact area and adhesion due to softening. Figure 4.8 shows two positions of an idealized polymer asperity during sliding on a rigid counterface with roughness profile normal to the page. During perpendicular-oriented sliding (corresponding to a left-to-right motion in the figure), the maximum strain is experienced when a polymer asperity is compressed by a ridge (Position 1), while minimum strain occurs when the asperity is between two ridges

(Position 2). The strain difference between these two is the strain amplitude (as opposed to the offset). This alternating strain amplitude is hypothesized to be considerably larger than the alternating strain amplitude in parallel sliding. In an idealized case, there would be no alternating strain when sliding parallel to roughness profile (normal to the page). In reality, there would be minor strain fluctuations in parallel sliding since the ridges and grooves do have height variation, but these would be relatively low compared to the strain amplitude in perpendicular sliding. The higher strain amplitude in perpendicular sliding is hypothesized to induce higher interfacial temperature than parallel sliding per Equation 4.6. This higher interfacial temperature would in turn promote stronger PEEK adhesion to the counterface in perpendicular sliding by increasing true contact area and possibly increasing the intrinsic adhesive bond strength. The results of measuring viscoelastic temperature rise and coefficient of friction were then examined to further explore this hypothesis.

Table 4.2: Wear volume mean and confidence interval for each sliding distance with α=.05 and 0.10 for wear tests that had replications

	Wear Volume (mm^3)		**95% Confidence Interval**	**90% Confidence Interval**
Sliding Distance (m)	$\bar{x}_{\parallel}$	$\bar{x}_{\perp}$	**(Difference of means)**	**(Difference of means)**
9.00	0.205	0.198	(-0.182, 0.195)	(-0.121, 0.134)
18.00	0.326	0.381	(-0.121, 0.231)	(-0.064, 0.175)
76.14	1.054	0.576	(-0.081, 1.037)	(0.05, 0.901)
250.02	**2.707**	1.388	(-0.018, 2.660)	(0.292, 2.35)

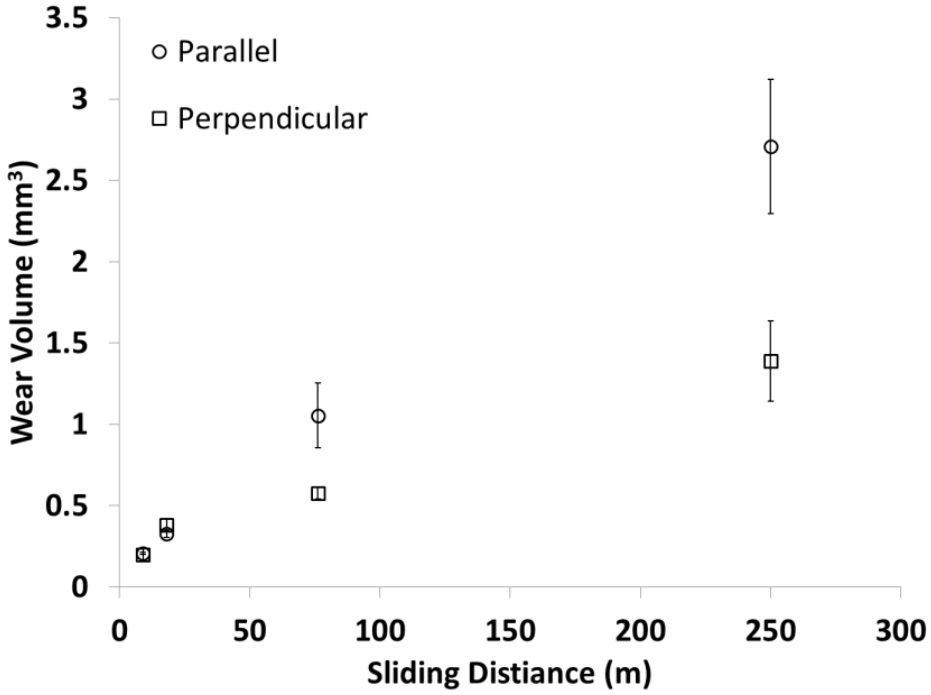

Figure 4.4: The volumetric wear of perpendicular and parallel bias tests. Error bars indicate mean standard error.

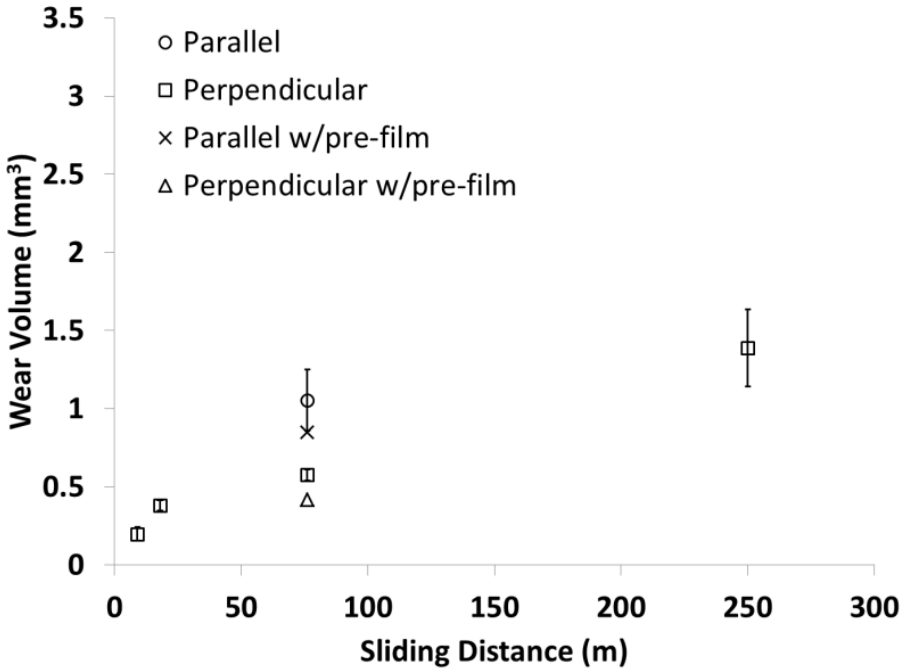

Figure 4.5: Volumetric wear of the pre-film tests with perpendicular bias wear graphed for reference. Error bars indicate mean standard error. The wear volume of perpendicular biased and parallel biased tests are shown for reference.

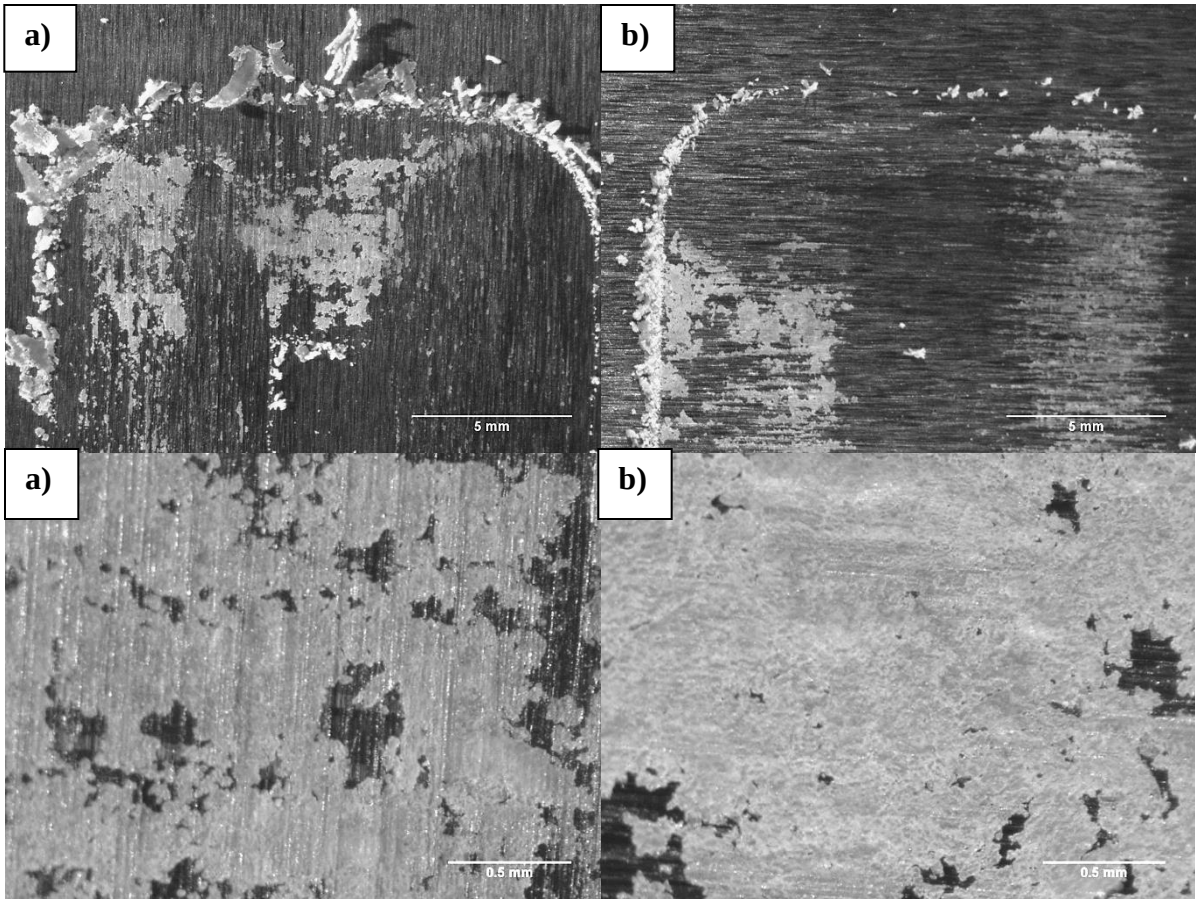

Figure 4.6: Wear debris and transfer film of a) parallel and b) perpendicular biased tests after 250 m of sliding. Scale is indicated in bottom right of image.

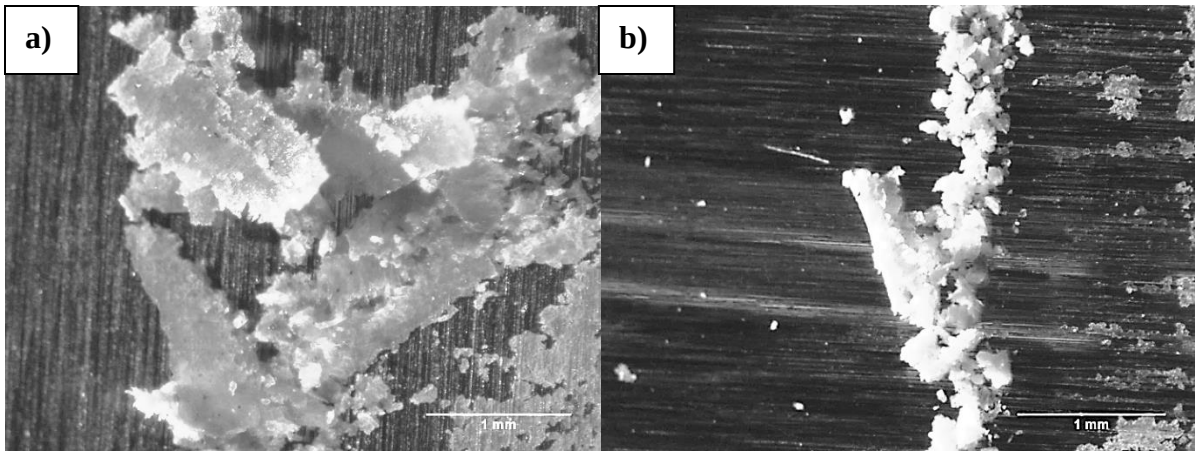

Figure 4.7: Wear debris of a) parallel and b) perpendicular biased tests after 250 m of sliding. Scale is indicated in bottom right of image.

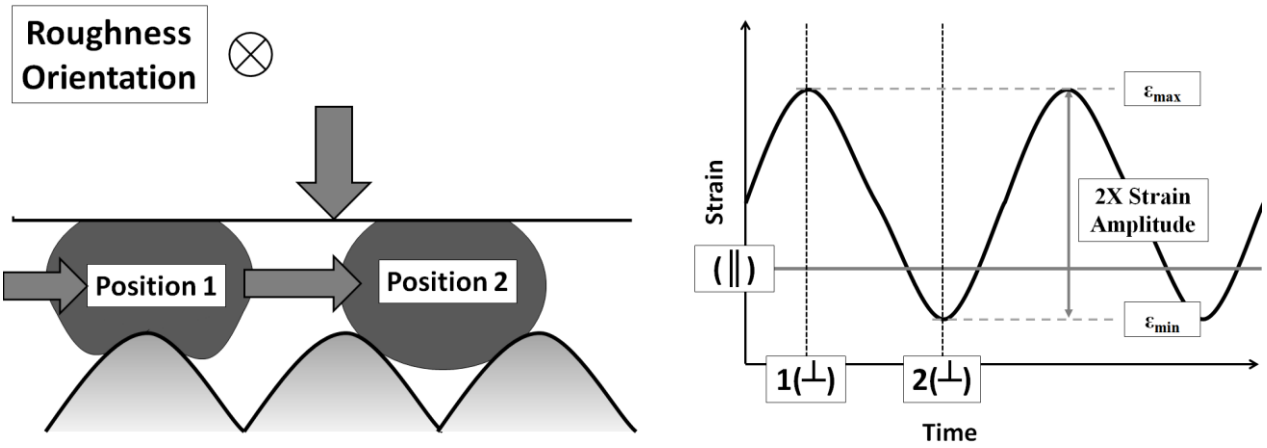

Figure 4.8: An idealized polymer-on-metal interaction with minimum and maximum strain. Sliding from Position 1 to Position 2 corresponds to perpendicular sliding. The plot indicates the theoretical strain history of a single asperity on the polymer surface.

4.3.2 Coefficient of Friction and Frictional Heating

The measured temperature of the bulk during sliding was higher during perpendicular oriented sliding than in parallel, and oscillations of coefficient of friction and temperature suggested a dependence on counterface roughness. Figure 4.9 shows the synchronized thermal radiometry measurement of temperature of the bulk PEEK pin and coefficient of friction at 47 meters for a parallel bias test. The graph shows multiple cycles of the same wear path with vertical lines indicating transitions between the legs of the square. Figure 4.10 shows the same information for the perpendicular case. The graphs designate parallel sliding (∥) and perpendicular sliding (⊥). The sliding distance in the graphs represents the point in the wear cycle where the transfer film was fully developed in perpendicular-oriented sliding. It is clear from comparing the figures that friction increased sharply at most of the corners of the wear path, but the baseline friction was not significantly different between the two sliding orientations. The average overall coefficient of friction was 0.30 for both the perpendicular and parallel cases. It is important to note the thermal camera's position was static and in-line with the bias direction of sliding so the recorded temperatures oscillate between being captured with leading and trailing faces of the pin. The temperature measurements of the short legs of the rectangle are therefore

when the pin was orthogonal to the direction of sliding, and often lower as a result. Temperature of the perpendicular biased tests was markedly greater and shows large cyclic change. This is more evident during the long segments when sliding was perpendicular to roughness orientation. There are also coordinated oscillations between the temperature and coefficient of friction in the perpendicular bias test, and the frequency of these oscillations are shown in Figure 4.10. Parallel tests are relatively stable thermally, and do not have oscillations or large cyclic change. This behavior was verified by examination of the results of several tests at different sliding distances. This could indicate a dependence on counterface roughness as the oscillations are regular and repeating.

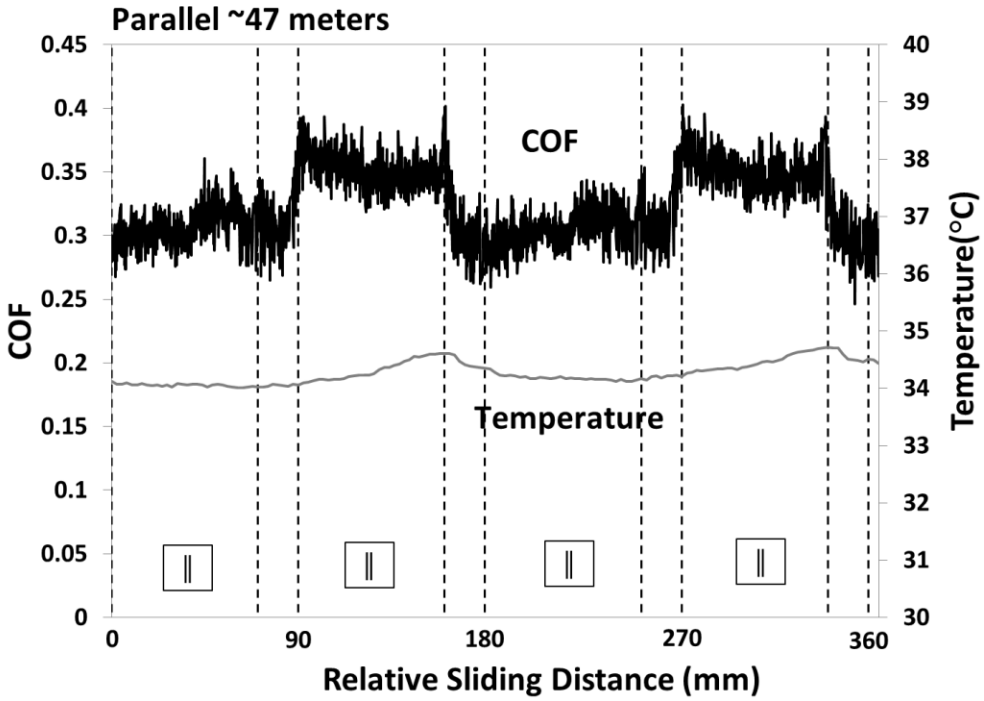

Figure 4.9: Combined coefficient of friction and temperature graphs of parallel tests at a 45 meter sliding. Temperatures were taken with an infrared camera and are displayed in grey. || indicates parallel to roughness orientation sliding.

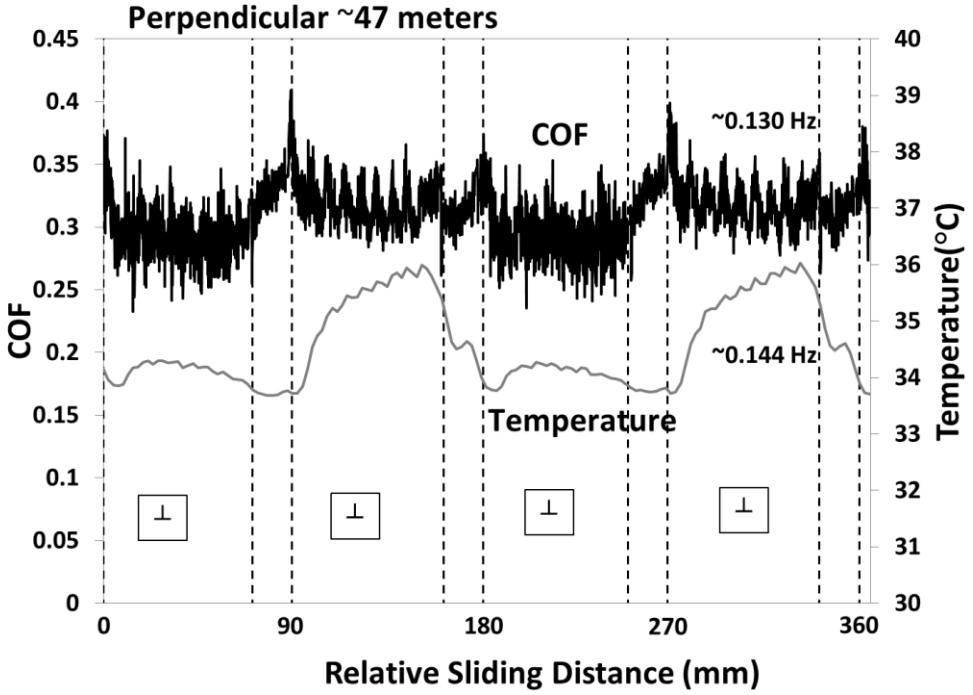

Figure 4.10: Combined coefficient of friction and temperature graphs of perpendicular tests at a 45 meter sliding distance. Temperatures were taken with an infrared camera and are displayed in grey. ⊥ indicates perpendicular to roughness sliding. The spatial frequencies of the oscillations are also shown.

4.3.3 Counterface and Transfer Film Roughness

The counterface roughness measurements give credibility to the possibility of different strain amplitudes depending on sliding direction. To validate that the counterface roughness orientation influenced the temperature, friction, and strain amplitude, two roughness metrics were obtained using white-light profilometry on both the counterface and deposited transfer film. The diagram of these measurements is shown in Figure 4.11. Rzx was measured perpendicular to the roughness orientation, and Rzy was measured parallel to roughness orientation. The results of these measurements are shown in Table 4.3. The measurements show that the transfer film roughened the interface when compared to the bare counterface, even in the perpendicular case which was thought to have a wear-reducing transfer film. This is surprising considering transfer film is usually thought to lower wear by reducing contact stress, roughness, and abrasion. The Rzx and Rzy measurements show that for the bare counterface, parallel roughness was almost

half that of perpendicular roughness. These measurements strongly suggest that there was considerable difference in the alternating strain amplitudes between sliding directions. The transfer film for perpendicular bias tests had an Rzx greater than Rzy, while the parallel had no significant difference in these values. This is likely due to the degree of uniformity of the transfer film. The parallel transfer film was discontinuous, and it had small areas with large pockets of PEEK adhered to the counterface. In the perpendicular wear path, the transfer film was more uniform, but smoother in the direction of sliding. This could possibly be due to the PEEK pin mechanical smoothing the transfer film as it slides. There was clearly a difference in morphology between the two transfer films when sliding perpendicular to roughness orientation. The impact of this morphology on wear is not clear, but the authors speculate the lower roughness in the direction of sliding in perpendicular transfer films contributes to its wear reducing effects.

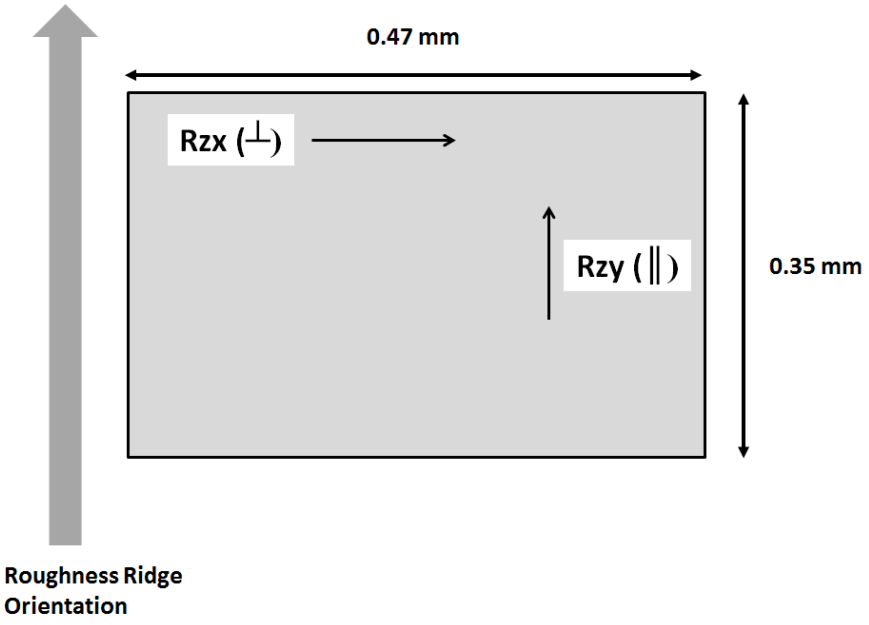

Figure 4.11: Diagram of roughness measurements taken with white-light profilometry.

Table 4.3: Infrared profilometer roughness measurements of bare, unused counterfaces

	Rzx	Rzy
Bare Counterface	5.80	2.72
Perpendicular Bias Wear Path	7.99	11.30
Parallel Bias Wear Path	11.59	11.42

4.3.4 DMA Cyclic Heating

The temperature measurements obtained during the DMA tests strongly supports the hypothesis that the temperature difference between sliding orientations is the result of different strain magnitudes. DMA tests were conducted under 3-point bending with oscillating sinusoidal strain and constant strain. The frequency and strain amplitude was varied to give tests at: 0.74 maximum strain at a frequency of 1 Hz, 0.89 maximum strain at a frequency of 1 Hz, and 0.89 maximum strain at a frequency of 0.5 Hz. Due to the fact sinusoidal strain was applied with a minimum strain of zero, the strain amplitude was half of the max strain. An example of the thermal readings taken during the DMA test is shown in Figure 4.12. The figure shows that there was a hot zone located in the location of the notch that at the given conditions reach 25.2°C. Figure 4.13 shows the temperature after fifteen seconds of loading for a PEEK sample loaded at constant force of 15 N, tests with oscillating strains, and the ambient temperature represented by a horizontal dashed line. The figure shows that the temperatures of oscillating strains were greater than both the static load and the ambient temperature. Furthermore, the 1 Hz, 0.89 strain test produced the highest temperature, and a decrease in strain amplitude and frequency lowered the temperature based on the results of the 1 Hz, 0.74 strain and 0.5 Hz, 0.89 strain tests respectively. These results agree with the trends predicted by Equation 4.6. Given the hypothesis

proposed in previous sections, the static load test had a loading history analogous to the idealized strain experienced by parallel-oriented sliding, while the oscillating strain tests corresponded to perpendicular-oriented sliding. Since temperature measurements of perpendicular sliding and oscillating strain DMA tests were both respectively higher than temperature measurements of parallel sliding and static loading, the results give further support to the hypothesis strain magnitudes are responsible for the temperature difference observed in the different sliding orientations.

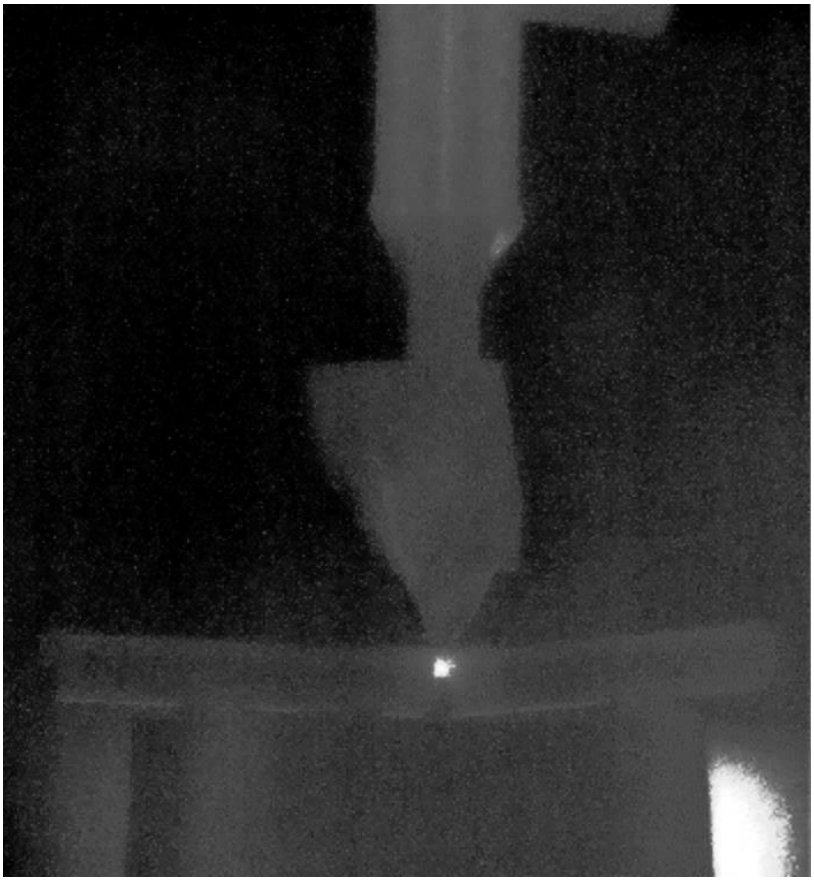

Figure 4.12: Thermal image of a DMA 3-point bending during oscillating strain of 0.89 at 1 Hz. The recorded temperature at the center of the sample was 25.5°C.

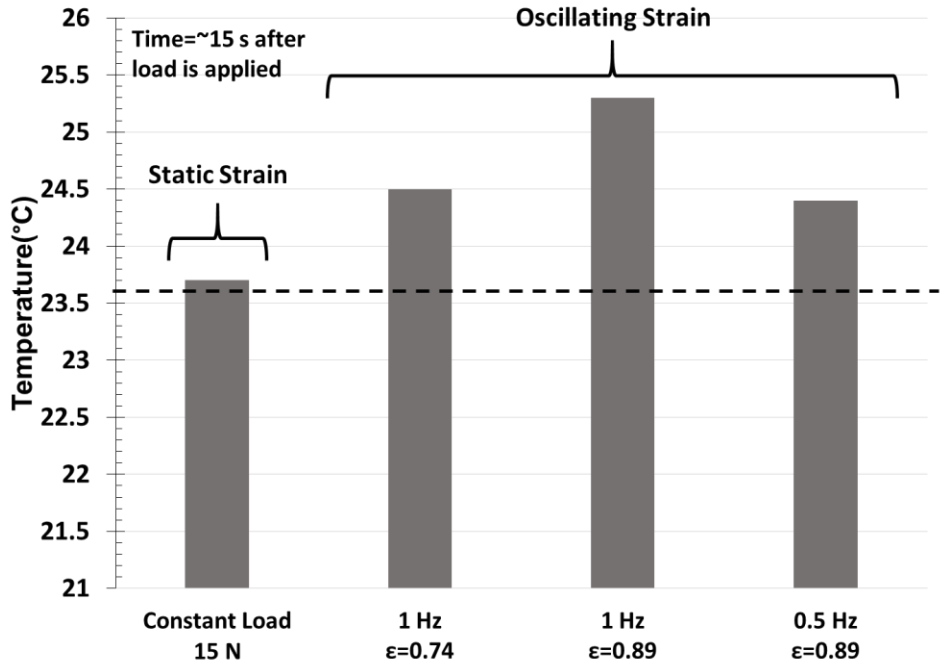

Figure 4.13: Temperatures of PEEK after 15 seconds of strain during DMA testing. The dashed line indicates ambient temperature.

4.3.5 Finite Element Contact Model

An alternative hypothesis to explain the wear behavior of the different sliding directions was proposed, but it was ultimately rejected. Since contact area is a fundamental parameter that influences adhesion, friction, and contact stress, a substantial difference in contact area between the two sliding directions might contribute to the behavior seen in the wear results. A simple, purely mechanical finite element model was developed in order to examine any potential mechanisms that could arise from the difference in contact area when sliding between the two orientations. Figure 4.14 shows the contact area results of this model by comparing parallel and perpendicular sliding. A variety of shear loads were applied, yet the contact area was changed by a maximum of 3%. This indicates that from a purely mechanical standpoint, contact area was not playing a large role in the difference of sliding between the orientations in the model. In reality, plastic deformation, plastic flow, and temperature have significant contributions to contact area,

but these results eliminated contact area difference as a potential hypothesis for the effects observed in the wear tests.

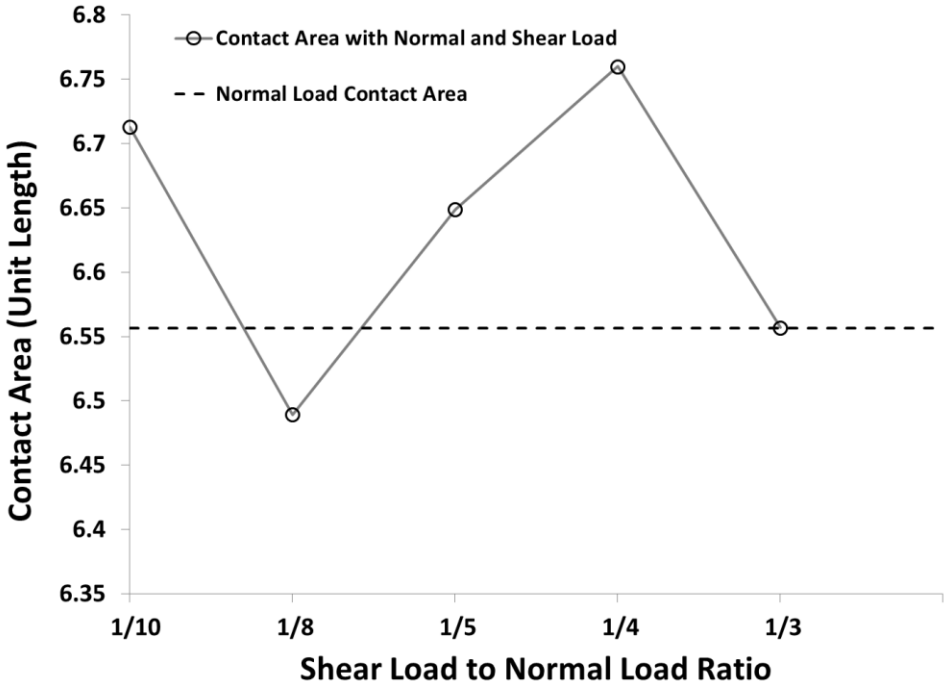

Figure 4.14: Results of finite element contact model. The purely normal load case corresponds to parallel biased sliding, and the normal and shear load case corresponds to perpendicular sliding.

4.4 Conclusions

- The wear behavior of PEEK was greatly impacted by the orientation of sliding with respect to the surface roughness direction of a steel counterface. Once steady-state wear was achieved, the wear amounts produced by sliding perpendicular to roughness direction were substantially less than when sliding parallel to the roughness direction.
- Well developed and tenacious transfer films were evident in perpendicular sliding, whereas they were largely absent in parallel sliding. Debris morphology suggests that perpendicular wear generates fine wear debris while parallel sliding produces large flakes of debris that originate from a poorly-bonded transfer film.

- Wear in perpendicular sliding before the onset of steady state is considerably higher than for parallel sliding, likely due to a sacrificial volume of PEEK that must be deposited early in the wear process to produce a durable transfer film. In contrast, parallel sliding did not show a marked transition to steady state because there appeared to be a continual process of localized film deposition and rapid removal.
- The improved transfer film observed in perpendicular sliding appeared to be governed by favorable thermal conditions which led to a softened PEEK material exhibiting a greater propensity to adhere to the counterface than in parallel sliding.
- The widely cited concept of debris 'interlocking' with asperities is not a useful conceptual model to explain the difference in transfer film adhesion between perpendicular and parallel sliding. This difference in behavior can be better described by the difference in cyclic strain magnitude experienced between the two orientations, and the increased sliding temperature produced in perpendicular sliding due to this basic phenomenon. Greater temperatures foster stronger adhesion of the polymer to the counterface. This predicted temperature rise was confirmed using thermal imagery during dynamic loading of the PEEK material.

4.5 References

[1] H.J. Song, Z.Z. Zhang, and X.H. Men, "Superhydrophobic PEEK/PTFE composite coating," *Applied Physics.*, vol. 91, no. 1, pp. 73-76, 2008.

[2] M. Sampaio, M. Buciumeanu, B. Henriques, F. S. Silva, J. C. M. Souza, and J. R. Gomes, "Comparison between PEEK and Ti6Al4V concerning micro-scale abrasion wear on dental applications," *Journal of the Mechanical Behavior of Biomedical Materials*, vol. 60, no. C, pp. 212-219, 2016.

[3] J. F. Braza and R. E. Furst, "Reciprocating sliding wear evaluation of a polymeric/coating tribological system," *Wear*, vol. 162, no. Part B, pp. 748-756, 1993.

[4] D. Vogel, H. Dempwolf, A. Baumann, and R. Bader, "Characterization of thick titanium plasma spray coatings on PEEK materials used for medical implants and the influence on the

mechanical properties," *Journal of the Mechanical Behavior of Biomedical Materials,* vol. 77, pp. 600-608, 2018.

[5] G. Zhang *et al.,* "Structures and tribological performances of PEEK (poly-ether-ether-ketone)-based coatings designed for tribological application," in *Prog. Org. Coat.* vol. 60, ed, 2007, pp. 39-44.

[6] M. Flanagan *et al.*, "Permeability of carbon fibre PEEK composites for cryogenic storage tanks of future space launchers," *Composites Part A,* vol. 101, pp. 173-184, 2017.

[7] B. R. Murray, A. Doyle, P. J. Feerick, C. O. A. Semprimoschnig, S. B. Leen, and C. R. M. Brádaigh, "Rotational moulding of PEEK polymer liners with carbon fibre/PEEK over tape-placement for space cryogenic fuel tanks," *Materials & Design,* vol. 132, p. 567, 2017.

[8] "T-Series compound finds applications in semiconductor industry," *Plastics, Additives and Compounding,* vol. 9, no. 5, pp. 8-8, 2007.

[9] N. Iyer, N. Saka, and J.-H. Chun, "Contamination of Silicon Surface Due to Contact with Solid Polymers," *IEEE Transactions on Semiconductor Manufacturing,* vol. 14, no. 2, p. 85, 2001.

[10] S. M. Kurtz, *PEEK Biomaterials Handbook* (Plastics Design Library). Burlington: Burlington : Elsevier Science, 2011.

[11] S. Bahadur, "The development of transfer layers and their role in polymer tribology," *Wear,* vol. 245, no. 1, pp. 92-99, 2000.

[12] J. Vande Voort and S. Bahadur, "The growth and bonding of transfer film and the role of CuS and PTFE in the tribological behavior of PEEK," *Wear,* vol. 181, pp. 212-221, 1995.

[13] B. Briscoe, B. Stuart, S. Sebastian, and P. Tweedale, "The failure of POLY (ETHER ETHER KETONE) in high speed contacts," *Wear,* vol. 162, pp. 407-417, 1993.

[14] M. Q. Zhang, Z. P. Lu, and K. Friedrich, "Thermal analysis of the wear debris of polyetheretherketone," *Tribology International,* vol. 30, no. 2, pp. 103-111, 1997.

[15] M. Q. Zhang, Z. P. Lu, and K. Friedrich, "On the wear debris of polyetheretherketone: fractal dimensions in relation to wear mechanisms," *Tribology International,* vol. 30, no. 2, pp. 87-102, 1997.

[16] F. D. Rzatki *et al.*, "Effect of surface finishing, temperature and chemical ageing on the tribological behaviour of a polyether ether ketone composite/52100 pair," *Wear,* vol. 332-333, p. 844, 2015.

[17] T. Onodera, J. Nunoshige, K. Kawasaki, K. Adachi, K. Kurihara, and M. Kubo, "Structure and Function of Transfer Film Formed from PTFE/PEEK Polymer Blend," *J. Phys. Chem. C,* vol. 121, no. 27, pp. 14589-14596, 2017.

[18] X. M. Gao, J. W. Liu, and Y. H. Liu, "Review of Friction and Wear Resistance Properties of Modified PEEK Composites," *Advanced Materials Research,* vol. 1053-1053, pp. 290-296, 2014.

[19] G. Li, H. Qi, G. Zhang, F. Zhao, T. Wang, and Q. Wang, "Significant friction and wear reduction by assembling two individual PEEK composites with specific functionalities," *Materials & Design,* vol. 116, pp. 152-159, 2017.

[20] T. J. Hoskins, K. D. Dearn, S. N. Kukureka, and D. Walton, "Acoustic noise from polymer gears – A tribological investigation," *Materials and Design,* vol. 32, no. 6, pp. 3509-3515, 2011.

[21] S. Qian-Qian and C. Xian-Hua, "Friction and wear of rare earths modified carbon fibers filled PTFE composite under dry sliding condition," *Applied Surface Science,* vol. 253, no. 22, pp. 9000-9006, 2007.

[22] I. J. Ford, "Roughness effect on friction for multi- asperity contact between surfaces," *Journal of Physics D: Applied Physics,* vol. 26, no. 12, pp. 2219-2225, 1993.

[23] J. A. Greenwood, K. L. Johnson, and E. Matsubara, "A surface roughness parameter in Hertz contact," *Wear,* vol. 100, no. 1, pp. 47-57, 1984.

[24] T. C. Ovaert and H. S. Cheng, "Counterface topographical effects on the wear of polyetheretherketone and a polyetheretherketone-carbon fiber composite," *Wear,* vol. 150, no. 1, pp. 275-287, 1991.

[25] D. M. Elliott, J. Fisher, and D. T. Clark, "Effect of counterface surface roughness and its evolution on the wear and friction of PEEK and PEEK-bonded carbon fibre composites on stainless steel," *Wear,* vol. 217, no. 2, pp. 288-296, 1998.

[26] T. C. Ovaert and H. Cheng, "The unlubricated sliding wear behavior of polyetheretherketone against smooth mild-steel counterfaces" *J. Tribol.-Trans. ASME,* vol. 113, no. 1, pp. 150-157, 1991.

[27] K. Friedrich, J. Karger-Kocsis, and Z. Lu, "Effects of steel counterface roughness and temperature on the friction and wear of PE(E)K composites under dry sliding conditions," *Wear,* vol. 148, no. 2, pp. 235-247, 1991.

[28] S. Ramachandra and T. C. Ovaert, "The effect of controlled surface topographical features on the unlubricated transfer and wear of PEEK," *Wear,* vol. 206, no. 1, pp. 94-99, 1997.

[29] G. Zhang, B. Wetzel, B. Jim, and W. Oesterle, "Impact of counterface topography on the formation mechanisms of nanostructured tribofilm of PEEK hybrid nanocomposites," *Tribology International,* vol. 83, pp. 156-165, 2015.

[30] K. Patel, C. S. Doyle, D. Yonekura, and B. J. James, "Effect of surface roughness parameters on thermally sprayed PEEK coatings," *Surface & Coatings Technology,* vol. 204, no. 21, pp. 3567-3572, 2010.

[31] K. A. Laux and C. J. Schwartz, "Influence of linear reciprocating and multi-directional sliding on PEEK wear performance and transfer film formation," *Wear,* vol. 301, no. 1-2, pp. 727-734, 2013.

[32] K. A. Laux and C. J. Schwartz, "Effects of contact pressure, molecular weight, and supplier on the wear behavior and transfer film of polyetheretherketone (PEEK)," *Wear,* vol. 297, no. 1-2, pp. 919-925, 2013.

[33] D. Rittel, "An investigation of the heat generated during cyclic loading of two glassy polymers. Part I: Experimental," *Mechanics of Materials,* vol. 32, no. 3, pp. 131-147, 2000.

[34] D. Rittel and Y. Rabin, "An investigation of the heat generated during cyclic loading of two glassy polymers. Part II: Thermal analysis," *Mechanics of Materials,* vol. 32, no. 3, pp. 149-159, 2000.

CHAPTER 5: TRIBOLOGICAL TESTING OF SILICONE IMPLANTABLE CARDIAC DEVICE LEADS BY INVESTIGATING LOAD, TESTING FLUID, AND SILICA ABRASIVE

A paper to be submitted to *Biotribology*

Mark D. Placette, Adam Himes, and Christian J. Schwartz

Abstract

Many biomedical devices have lifetimes limited by wear of their polymer components. One type of biomedical device, implantable cardiac devices (ICDs), experiences wear on the surface of the insulation of silicone lead wires. An ICD device (pacemaker, defibrillators) is composed of a titanium casing that holds the battery and lead wires that deliver pulses that regulate heart activity. The wear of the silicone insulation produced during regular activity can yield severe patient discomfort or surgical complications upon replacement. Little is known about the wear mechanisms of these silicone wires *in vivo*, but it is known wear occurs between the wires and either titanium casing, other wires, or bodily tissue. This study investigates titanium-on-silicone wear of lead wires used in ICDs. Surgically retrieved silicone wires showed unusual wear scars that are polished and smooth. The goal of this study is twofold: replicate the unique wear scar with a testing apparatus and determine wear mechanisms of the silicone leads. Silicone cardiac lead wires were obtained from the manufacturer and an apparatus was constructed to simulate in-body conditions while accelerating the wear process. Three key parameters were chosen to investigate the wear mechanisms of this system: load, environmental fluid, and third-body abrasive. A full factorial matrix design with two replications was used to test these variables. Wear scars were examined using white light profilometry, optical

microscopy, and scanning electron microscopy (SEM). An analysis-of-variance (ANOVA) showed that all test factors were not significantly affecting the size and depth of the wear scars but revealed key mechanisms that could affect wear *in vivo* on long timescales and other ICD wear configurations.

5.1 Introduction

Pacemakers and cardioverter-defibrillators are cardiac biomedical devices that treat patients with dysrhythmic heartbeat disorders. These implantable cardiac devices (ICDs) generate an electrical signal that stimulates cardiac muscles to facilitate normal heart rhythms. The devices are composed of a titanium casing, which houses the battery and computer monitoring system, and multiple lead wires depending on the required treatment. The titanium housing is implanted under the skin typically in the pectoral region. The lead wires are transvenously inserted and fed into the appropriate chamber in the heart where they monitor and deliver life-saving pulse therapy [1, 2]. While the exact structure can differ, ICD lead wires are generally composed of several layers of insulation separating multiple coils of metal conductors from *in vivo* environment. The outer layer, often referred to as the 'sleeve,' is composed typically either of polyurethane or silicone elastomers that are both biocompatible and mechanically durable in order to handle the internal mechanical stresses of the body [3]. Although lead wear has been observed in explanted devices, little is known about the wear mechanisms of the silicone lead wires *in situ*.

Lead failure poses a critical problem for patient safety and reliability, but it is difficult to ascertain the wear mechanisms of these systems. Wear damage to the insulating sleeve of the leads is of prime concern with regards to potential device failure. When the outer lead insulation is worn, conductor exposure can lead to complete device failure by short circuiting [5]. If the

sensing circuits are affected, over-sensing or under-sensing can result in loss of pacing or loss of sensing completely [6]. Patients can also be administered electrical shocks when ICD leads fail, producing discomfort and pain [7]. The danger of lead wire wear can be impactful even without complete exposure of the internal conductors. Infective endocarditis can occur with very little surface wear of silicone leads [8], and in replacement surgeries, insulation wear can create complications upon extraction and in rare cases death [9]. Tribology studies of these lead wires are rare, but there are four primary categories of potential tribological phenomena proposed. Wire insulation of one lead can wear against the insulation of another lead wire producing a polymer-on-polymer wear system. Internal polymer-on-polymer wear is also possible between two or more insulating layers of a single lead wire [10, 11]. Leads can be worn by bodily tissue from cardiac muscle contractions or other body movements [10]. Finally, the titanium casing is known to contact and slide against lead wires in the confined implantation cavity during patient activity or respiration producing silicone-on-metal sliding, and this wear mode is the focus of the current study. The sleeve material is a factor in all these systems [12]. Typically, polyurethane and polyurethane co-polymers are more wear resistant but are often degraded in the body which can produce large cracking, but silicone, although a more biocompatible and chemically stable material, is less resistant to abrasion and generally has higher friction [1]. Thus, investigating the wear of silicone leads is therefore a worthwhile endeavor for patient safety and product reliability; however, determining the wear mechanisms of silicone leads can be challenging. Wear *in situ* is not easily observed, and there is no clear empirical data for the amount of load or stress the leads encounter in the body. Moreover, lead wear is a slow process occurring over several years [4].

There are several wear modes commonly reported of elastomers including: viscoelastic rolling, complex abrasion, and fatigue tearing. Viscoelastic rolling produces characteristic ridges on the wear track of elastomers [14, 15]. However, as the wear cycle continues, the ridges can detach and form wear debris [16]. In addition, fatigue cracking may be initiated in the elastomer at high loading conditions or a long number of cycles [17]. For the leads of ICDs, fatigue and creep of the sleeve are speculated to occur, with concerning effects as layers of silicone leads can be can detached or tear so that the conductors are exposed [1, 3]. ICD silicone insulation may have additional wear modes that are initiated by *in vivo* conditions. An ICD device resides in a small, fibrous cavity in the chest only slightly larger than the titanium casing [2]. This is hypothesized to produce high concentrations of entrapped wear debris due to the lack of ambient fluid to carry away wear particles. At the same time, the ambient fluid contains proteins, such as albumin, in significant concentrations. It is not clear what effect albumin is having on the wear process for this system, although biological proteins are known to have lubrication effects in many implants [13] [19, 20]. Furthering the complexity of the tribological system, silicone leads are often reinforced with silica particles to improve mechanical performance. This leads to the potential significant third-body abrasion once silica is liberated from silicone and retained in the interface region the high concentration in the isolated cavity. The impact of albumin and silica long-term may also play a role in wear as aging can also increase hardness and crack growth in medical grade silicone [18]. Wear scars of silicone leads retrieved from patients are unusual. Creep and material flow of silicone is present, indicated by material smeared away from point of contact, but the wear scar has a polished-like sheen and is very smooth. This polished appearance may be indicative of third-body abrasion or lubricated sliding since silicone can be polished by

glass abrasives in aqueous solutions [21]. It is therefore necessary to investigate the impact of several factors that could potentially affect the wear of silicone leads.

In this study, the wear of ICD silicone sleeves on titanium was examined thoroughly. The goal of this study was to determine the wear mechanisms of silicone leads by exploring key parameters that were theorized to play a role: load, environmental fluid, and third-body abrasive. These three parameters were investigated using a full factorial experimental design with replication. Silicone cardiac lead wires were obtained from the manufacturer and a testing apparatus was constructed to simulate *in vivo* conditions on a two-axis tribometer. Wear scars were examined using white light profilometry, optical microscopy, and scanning electron microscopy (SEM). An analysis-of-variance (ANOVA) was conducted to test the significance of the key parameters' contributions to wear of the silicone leads. Finally, additional tests were conducted for a longer number of cycles in which only the environmental fluid was altered.

5.2 Materials and Methods

5.2.1 Experimental Materials

Silicone ICD lead wires were obtained from the manufacturer (Medtronic, Minneapolis Minnesota). Lead wires were cut to approximately 90 mm to fit in the testing apparatus. Before each test, the leads were cleaned with ethanol and gently wipe with a lent-free cloth before being rinsed with distilled water and allowed to air dry for ten minutes. To simulate the mechanical system of device enclosure contact with the leads, titanium counterfaces were formed in a U-shape to form a semi-circular counterface with a bend radius of approximately 4.0 mm and a length of 40 mm. The counterface was attached to a load cell with a testing fixture and an acrylic spacer as seen in Figure 5.1. This titanium alloy was identical to that used in the device

enclosure. The titanium counterfaces were also cleaned with ethanol and distilled water prior to testing.

A full factorial testing matrix was developed based on the results of the pilot testing under various load and motions. The experimental factors were: load, test fluid, and third-body abrasive. Table 5.1 organizes these factors into a testing matrix with all possible test settings. Load was maintained at either 0.1 N or 0.3 N, and the fluid in which the wear test was conducted was either distilled water or BSA. Silica was added to the testing fluid, or the testing fluid was left unaltered. The tests in Table 5.1 were conducted twice in randomized order which produced a factorial matrix with two replications for a total of sixteen tests which could be analyzed statistically. An analysis of variance (ANOVA) test was conducted with a significance level of 0.05 to test whether any change in load, fluid, or third body would affect the size of the wear scar. Additional experiments were conducted after the first sixteen tests. These tests were performed to isolate the testing fluid parameters (BSA, distilled water) and to test the effect of a greater sliding distance. Each of the extended tests was conducted at a 0.3 N load for 400 meters in either BSA or distilled water, and no silica was added to any test. Four extended tests were performed in total: two tests with BSA and two tests with distilled water at the conditions provided.

Two additives were investigated for the testing fluid used in this study. Because the silicone leads used in this study are composites of silicone and silica, the researchers investigated the possibility of third-body abrasion by liberated silica particles. Solutions of silica micro-particles (~1 μm diameter) were prepared to artificially accelerate this process for the wear tests. 0.05 grams of silica micro-particles were added to 50 mL distilled water solution yielding a concentration of 1 mg/mL. The solution was placed in a heated ultrasonic bath for 1 hour at 35°C

to disperse the silica particles. The solution was added to the testing fluid as per the factorial matrix.

To investigate the potential for protein lubrication on wear mechanisms, bovine Serum Albumin (BSA) was prepared by mixing bovine albumin powder (Sigma-Aldrich, A7906) in distilled water or the silica solution at a concentration of 3 g/dL. The experiments included tests with and without protein supplement. For those tests requiring protein in the wear fluid, 1.5 grams of albumin powder was added to 50 mL of distilled water of water/silica dispersion, and the mixture was slowing stirred and heated at 37°C for 30 minutes before testing. In some tests, both silica and albumin were not needed, and instead distilled water was heated to 37°C for 30 minutes and used as the testing fluid.

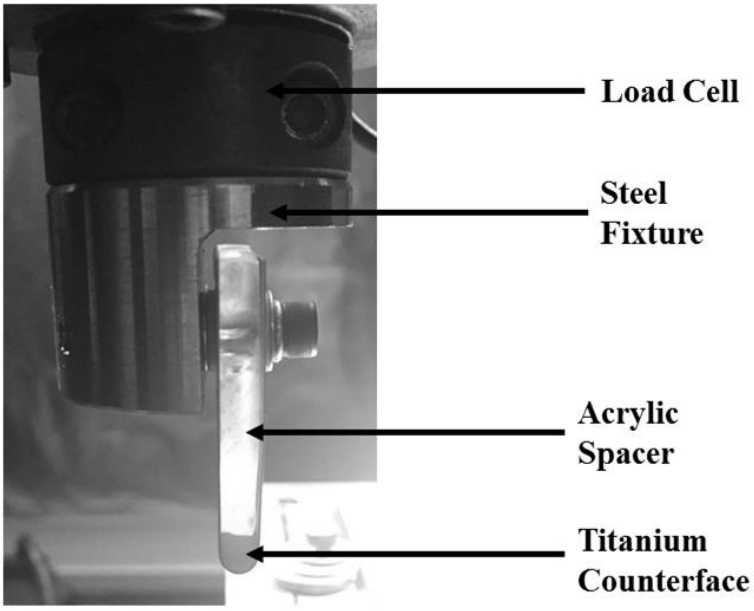

Figure 5.1: Test fixture attaching the titanium counterface to the load cell.

Table 5.1: Test settings for 180 m wear tests. Two of each unique test setting was conducted.

	Setting	
Factor	**'Low'**	**'High'**
Normal Load	0.1 N	0.3 N
Testing Fluid	No Albumin	With Albumin
Third-Body Abrasive	None	Added Silica

5.2.2 Wear

All tests were conducted using a two-axis tribometer (Rtec Instruments, San Jose, California) with a heated basin seen in Figure 5.2. The stage was moved with two independent stepper motors (XY). Load was applied in the z-axis by a controlled linear motor. The load cell was capable of measuring force and torque in six dimensions. Velocity and wear path were regulated through motion control software. An acrylic basin filled with distilled water housed a mounting platform that held the lead in place by being clamped at the lead ends. This mount was then attached to the interior bottom of the basin. An adhesive heating element was attached to the exterior bottom of the basin to heat the entire apparatus to 37°C, which is maintained by a solid-state relay temperature controller. A plastic bag filled with testing fluid (BSA, silica dispersion) was mounted around the testing area of the wire to simulate the limited capsule volume which encloses the ICD *in vivo*. The wear path for all tests involved linear reciprocation of the titanium counterface perpendicular to wire as shown in Figure 5.3. The travel distance of the counterface was 5 mm back and forth for a total sliding distance of 10 mm per cycle. The average speed of the counterface movement was 9.09 mm/s. This accounts for the short distance of deceleration and motion reversal of the counterface during the reciprocating wear cycle.

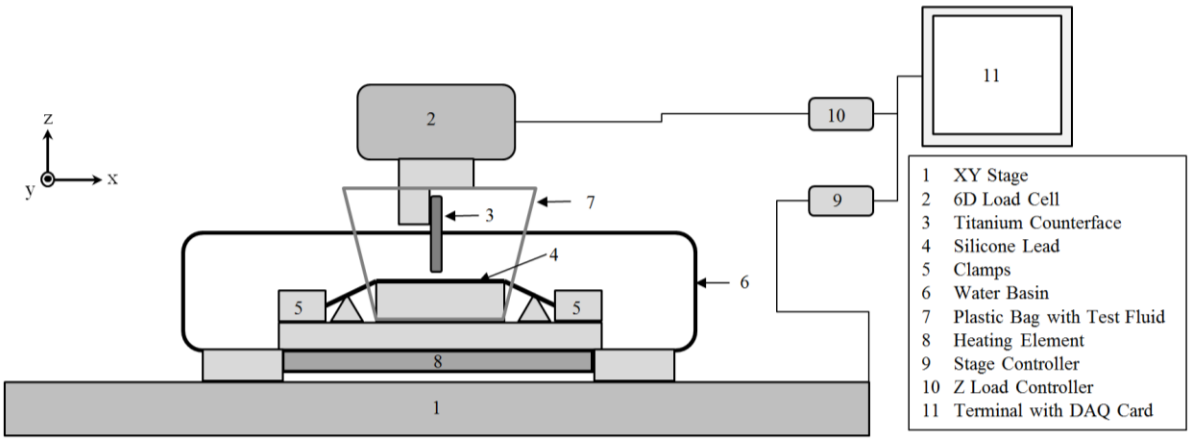

Figure 5.2: Schematic of experimental setup of silicone lead wear tests. The lead was clamped at the ends while being immersed in a heated basin.

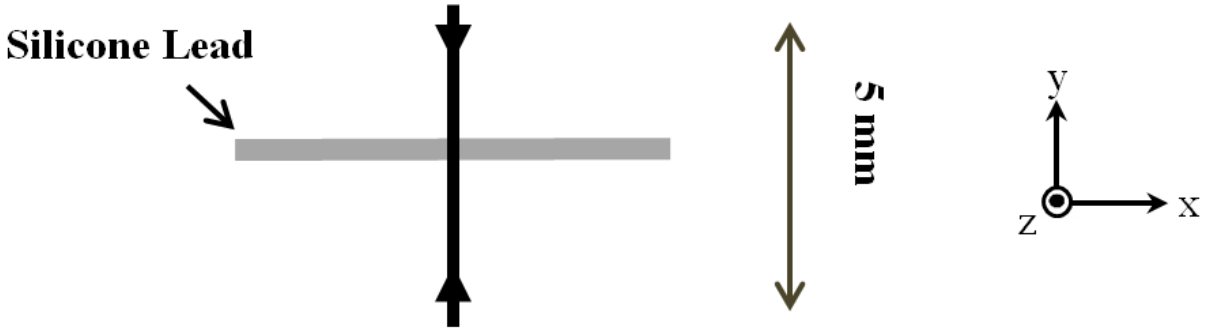

Figure 5.3: Silicone lead wear path. The titanium counterface was slid perpendicular to the wire at 9.09 m/s for a 5 mm wear path for a total cycle distance of 10 mm. Tests were conducted at 180 meters and 400 meters total sliding distance.

5.2.3 Wear Analysis

A white-light profilometer (Zygo NewView700) was used to measure the height data at the wear scar produced by the wear tests described above. An example of these measurements and the data gathered from the wear scar height map is shown in Figure 5.4. To compare the wear scars of each test, a line scan of the center of the wear scar for each test specimen was collected as seen in Figure 5.4a. The height data along this line scan was gathered and analyzed. Two types of data were collected from this profile data: maximum depth and the area produced enclosed by the parabolic wear scar as seen in Figure 5.4b. This data was then analyzed with an analysis-of-variance (ANOVA) to find the significance of the three testing parameters on the wear depth and profile area. To further investigate possible wear modes, SEM was conducted on selected lead wires. The lead wires were first washed with distilled water, wiped with a lint-free cloth, and rinsed again. After air drying for twenty minutes, the samples were coated with a uniform 2 nm thick layer of iridium for use in high vacuum SEM. Various images were obtained and reviewed for possible wear modes. The final wear analysis method investigated viscoelastic

creep of the silicone leads. Viscoelasticity may play an important role in the wear process of rubbery polymers. To determine if the silicone lead was producing wear scars from experiencing viscoelastic creep effects, a dynamic mechanical analysis (DMA, TA Instruments) was conducted on the silicone lead in 3-point bending. The lead was positioned on top of an aluminum counterface and the load was applied at 50°C for eight hours. Two tests were conducted at 0.5 N and 1.5 N loads, and the lead wires were examined using SEM after being cleaning be the procedure described above and coated with a 2-nm layer of iridium.

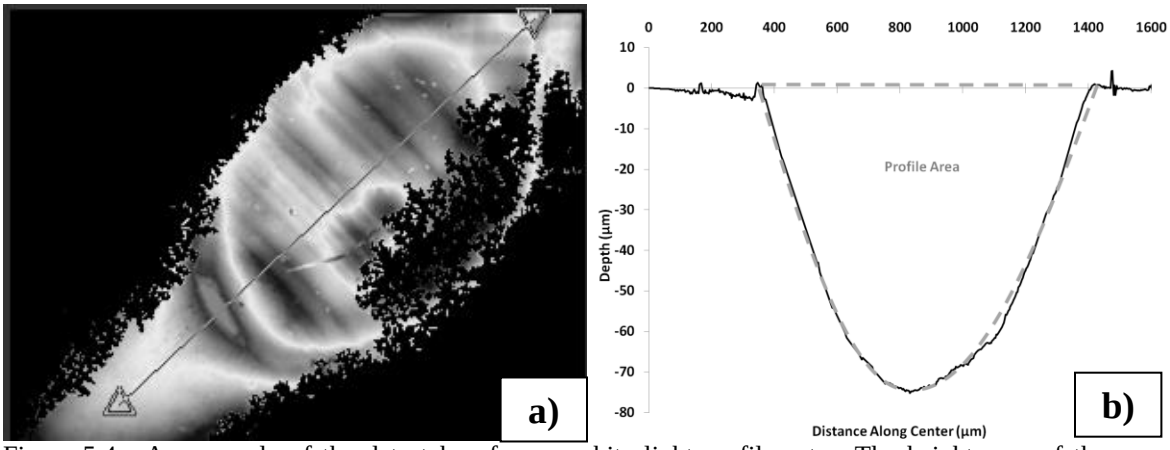

Figure 5.4: An example of the data taken from a white light profilometer. The height map of the wear scar is displayed along with the profile height data taken from the center line. The area enclosed by the parabola was calculated for comparison.

5.3 Results

5.3.1 Wear Results

The three key factors of load, silica abrasive, and albumin protein do not have significant effect on wear. After the wear tests, the ICD silicone lead was analyzed using white light profilometry to measure the maximum depth and area of the profile produced by the wear scar. The results of the wear scar measurements are shown in Figure 5.5 for both the depth and profile areas of the wear scars. The results show that there were no significant wear effects from the parameters examined. To examine the effects of the parameters statistically, an analysis of variance (ANOVA) test was conducted to further asses the results for signs of interactions. Both

scan depth and profile area was used as a response variable. The P-values for all three parameters are shown in Table 5.2 for the main effects as the table indicates neither load, protein, or silica significantly affected the wear scar depth or area profile within the parameter ranges used in this study. However, silica did affect the wear scar appearance and was shown to have profound effect on topography which will be discussed in the next section. While this was an unexpected result, there are reasonable explanations that can be proposed. These results suggest which experimental parameters may need to be changed. The loads used may, in fact, be significantly larger than those applied to the lead in the body. Thus, these results may be well above a reasonable threshold compared to field retrievals. Secondly, the wear tests were conduct a total sliding distance of 180 meters, and the length of time of the wear tests was approximately 16 hours. *In vivo,* wear has a timescale of several years in the body where aging and creep might play a more dominant or noticeable role.

Based on the results of the static load test, there is no evidence that viscoelastic creep is a significant wear mode of silicone leads in the tests performed. Viscoelastic creep has been known to cause severe damage to silicone insulation [1, 3]. No damage to the insulation was observed in the lead after eight hours at 37°C for a load of 1.5 N. While there is no evidence that viscoelastic creep is having an effect on the wear of silicone leads at this temperature and loading condition, it cannot be dismissed as a possible mechanism *in vivo*. While the wear metrics did not show clear factor effects, the analysis of the wear scars gave insights into the wear mechanisms.

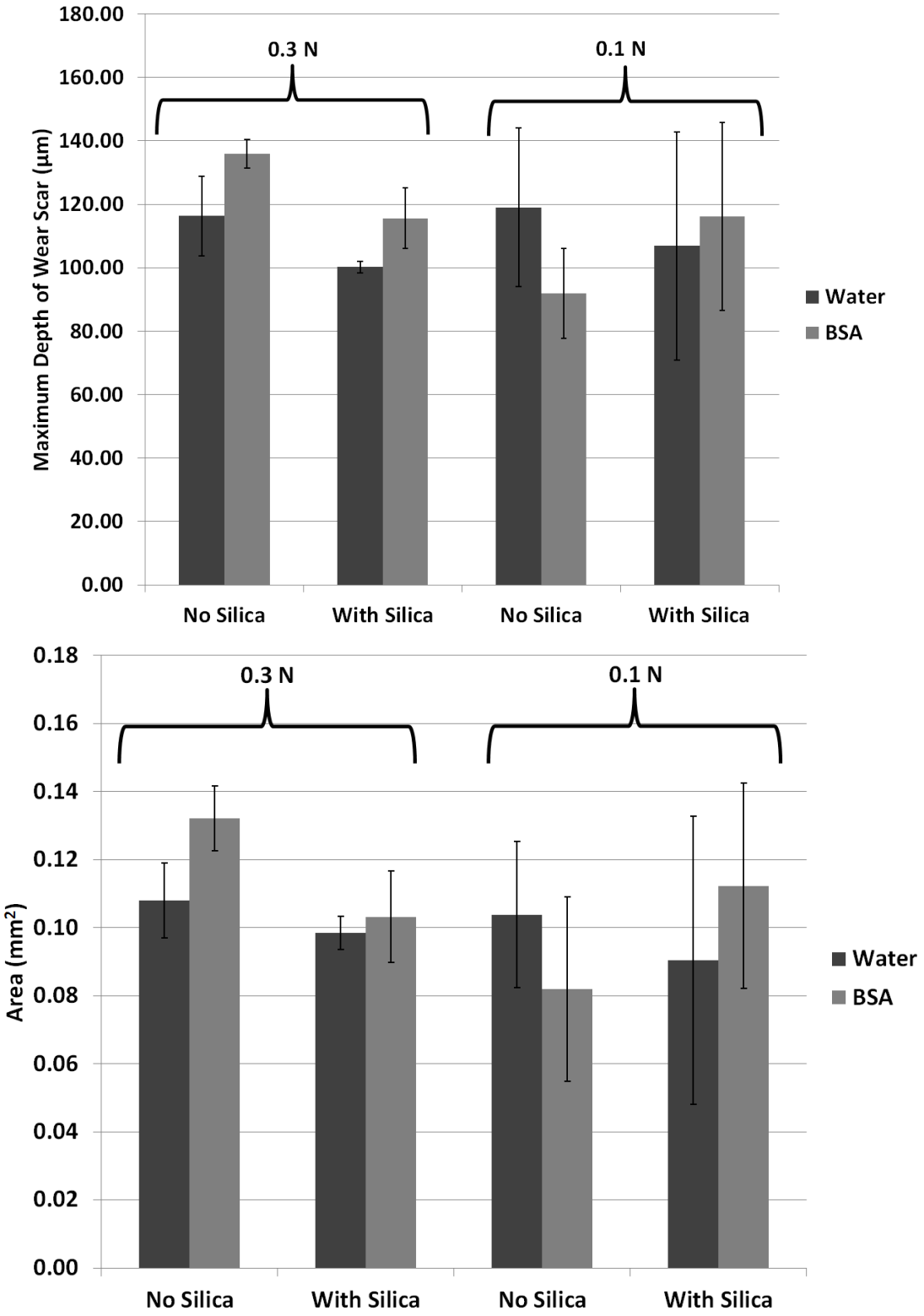

Figure 5.5: Area and maximum depth of wear scars from wear tests with settings in Table 5.1. The mean is graphed, and errors bars indicate mean standard error.

Table 5.2: Results of ANOVA comparing the effect of load, fluid, and abrasive on wear scar area and depth.

	P-Value	
	Profile Area	**Max. Depth**
Load	0.391	0.532
Fluid	0.638	0.753
Abrasive	0.726	0.654

5.3.2 Wear Scar Analysis

The analysis of the lead wear scars by optical microscopy and SEM showed that silica particle enrichment of the testing fluid had a profound effect on the appearance and topology of the scars. The results strongly suggest that the silica particles polished the surfaces of the silicone lead. Figure 5.6 and Figure 5.7 display SEM images of tests with no silica added and silica enriched solution in the testing fluid respectively. Without silica, Figure 5.6 shows characteristic elastomer ridges likely due to a viscoelastic adhesion and fatigue driven wear process. These ridges are still present but appear to have been smoothed in Figure 5.7 when silica was present in the testing fluid. Extending the sliding distance from 180 meters to 400 meters without the addition of silica particles, showed that returned wear debris can produce a similar. Figure 5.8 shows SEM images of the 400-meter sliding distance test with no silica added to the testing fluid. It is apparent that the embedded silica particles in the elastomer matrix also play a role in supporting the load and shielding the surrounding soft bulk from aggressive wear damage. The figure shows a particle surrounded by a surface regime exhibiting considerably less damage than the rest of the wear sample. Highly defined ridges are observed in Figure 5.8, but a wear particle has appeared to have polished these ridges. EDS of this wear debris particle confirmed it as silica. This strongly suggests silica was removing material as a third-body abrasive in the 400-meter tests despite not being added to the testing fluid.

Further SEM analysis was conducted for titanium counterfaces with and without silica in solution. There is no evidence in either case silica was being embedded or attached to the counterface at the wear interface. This gives evidence to support that silica is not affecting the wear of the titanium counterface. Consequently, it also strongly supports that the titanium counterface is not significantly worn during lead on enclosure wear, which is confirmed by anecdotal reports of field retrievals with worn leads. Given the experiments in this study and field retrievals, this gives evidence to suggest that silica plays a dual role as third body abrasive as well as localized wear shielding. Furthermore these results suggest that liberated silica from the elastomer matrix is primarily responsible for the polished appearance of field retrievals.

The presence of BSA in solution led to wear debris being attached to the wear scar, and this appeared to facilitate abrasion. Figure 5.9 shows the wear scar of a silicone lead tested with albumin in the testing fluid. There was a clear difference in surface morphology in Figure 5.8 compared to Figures 5.6 and 5.7, where the wear scars appeared relatively regular and free of wear debris. Figure 5.9 appeared to have large flakes of silicone wear debris adhered to the surface and complex abrasive patterns compared to the wear scars without albumin. There were also large particles of debris (white in the Figure) that are rich in silica despite having no silica added to the testing fluid. This silica must then have been extracted from the silicone matrix. It is unclear what effect the silica-rich wear particles are having, but the authors speculate that the complex abrasion patterns seen in Figure 5.9 is the result of these particles abrading the wear scar once they have been extracted and relocated at the interface.

Wear through of silicone leads occurred between 180 meters and 400 meters, and there was strong evidence this was the result of insulation compression between the counterface and conductor metal. Referring to the wear scars in Figure 5.8 (obtained at 400 meters), wear through

of the sleeve and exposure of the conductors in the lead occurred at the center of the wear scar. This was found for all tests with a sliding distance at 400 meters. This strongly suggests that these failures are only seen beyond a 180-meter sliding distance. The fatigue tears spatially correlated to the internal conductors of the silicone lead and were only located at the center of the wear scar. The authors speculate that the center of the silicone insulation at the center of the wear scar would experience high compressive stresses between the counterface and the conductor since the leads are cylindrical. This would facilitate higher stress at this location and promote wear through.

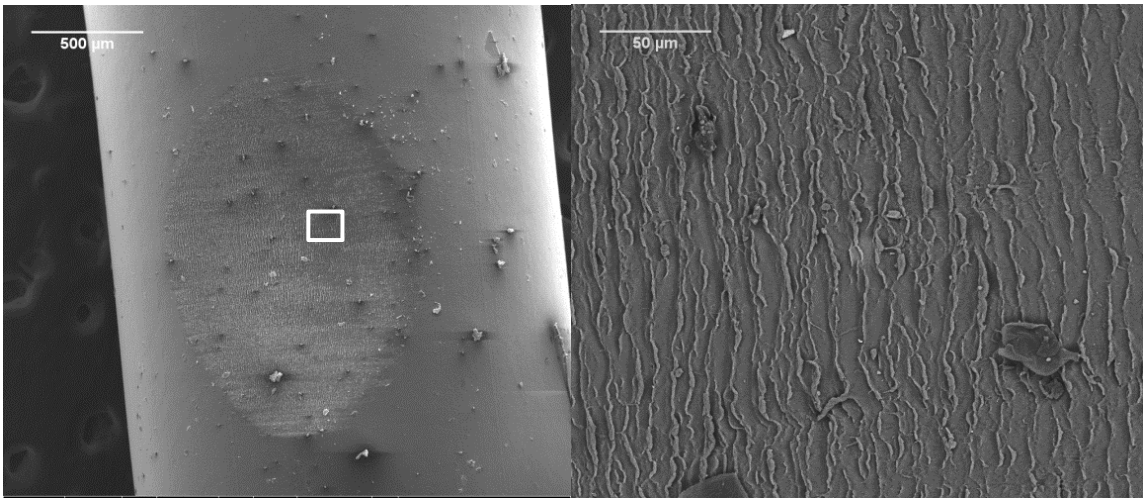

Figure 5.6: SEM micrographs of silicone lead with test settings of 0.3 N, distilled water, and no silica (180 meters).

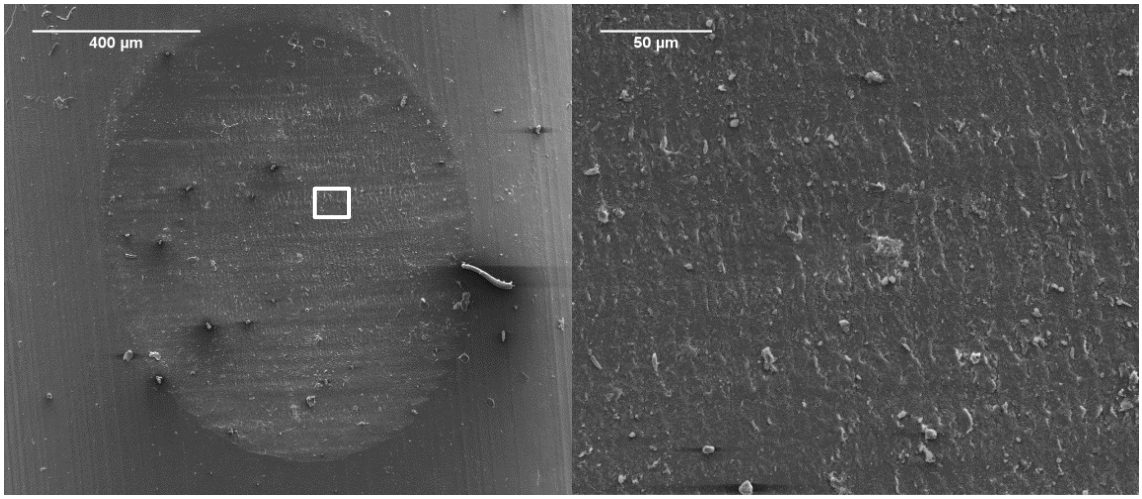

Figure 5.7: SEM micrographs of silicone lead with test settings of 0.1 N, distilled water, and with silica (180 meters).

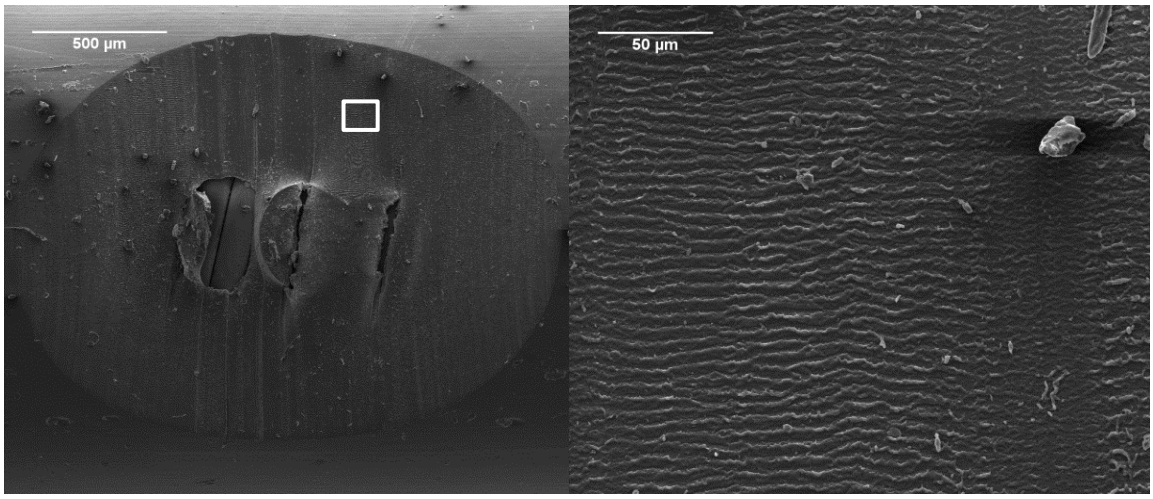

Figure 5.8: SEM micrographs of silicone lead with test settings of 0.3 N, distilled water, and no silica (400 meters).

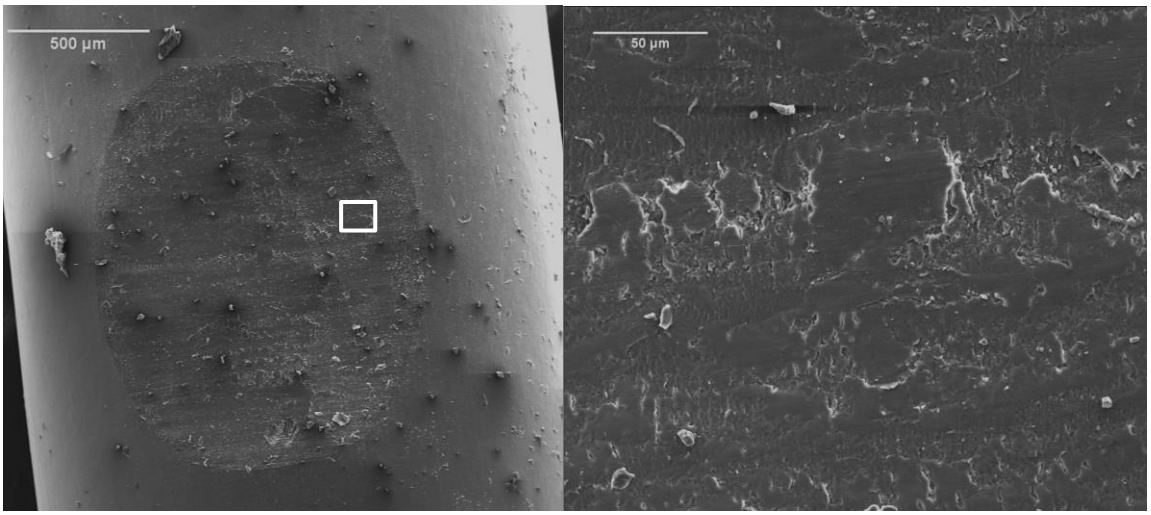

Figure 5.9: SEM micrographs of silicone lead with test settings of 0.3 N, BSA, and no silica (180 meters).

5.3.3 Optical Microscopy of Silicone Leads

Optical microscopy of the wear scars indicated that the silica was having a polishing effect similar to that of retrieval lead wires. Figure 5.10 displays images taken by an optical microscope of wear scars with silica enriched testing fluid. There was a shine that was visible on the outer edge of the scar, but this shine is not without silica enrichment. Since silica was shown by SEM to polish viscoelastic-induced ridges, silica may have been microscopically polishing the wear scar which optically produced a glossy-finish to the wear scar. In SEM images of retrievals, the wear scar is very smooth, and optically the wear scars of retrievals have a shine.

Although this was not explicitly replicated in the wear tests, this gives evidence to suggest polishing by silica is the source of the optical appearance and morphology of retrieval wires.

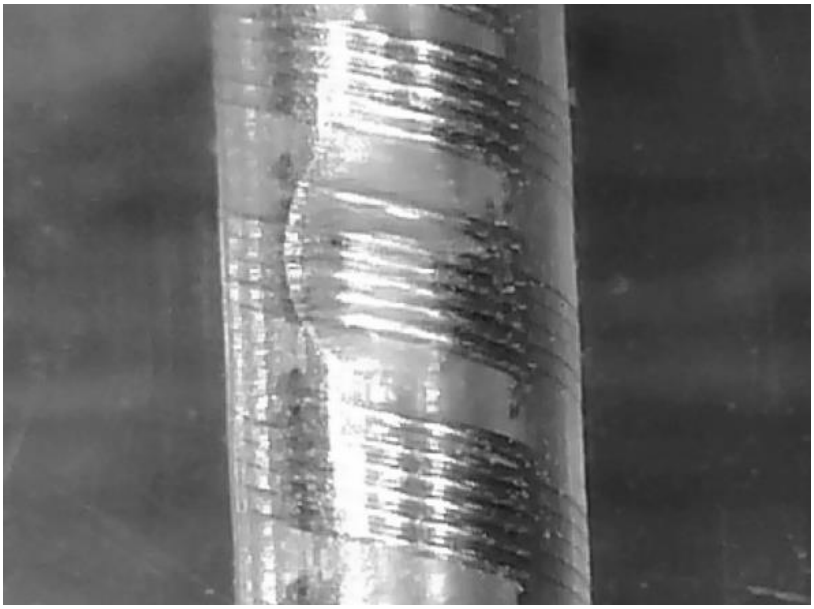

Figure 5.10: Optical Microscope image of silicone lead wear scar after doping with silica.

5.4 Conclusions

- Within the parameter range of the study, neither load, protein content, nor silica enrichment had a significant effect on the wear of the silicone leads when sliding against titanium. However, there was marked differences in the appearance of the wear scars which may be important for longer duration wear tests.
- Retained silica at the wear interface drastically impeded the topology of the wear scar. This suggests that liberated silica from the elastomers matrix plays a role during *in vivo* wear.
- Albumin protein increased adhesion of wear debris to the surface of the silicone lead. The wear debris was rich in silica and promoted complex abrasion patterns.

- Severe wear through and exposure of conductors before 400 meters in linear reciprocating tests were exhibited. This further suggests that lower normal loads would be most appropriate for accelerated wear testing.

5.5 References

[1] H. M. Haqqani and H. Mond, "The Implantable Cardioverter-Defibrillator Lead: Principles, Progress, and Promises," in *PACE-Pacing Clin. Electrophysiol.* vol. 32, ed, 2009, pp. 1336-1353.

[2] D. R. Ramsdale, *Cardiac Pacing and Device Therapy by David R. Ramsdale, Archana Rao*. London : Springer London : Imprint: Springer, 2012.

[3] C. D. Swerdlow, G. Kalahasty, and K. A. Ellenbogen, "Implantable Cardiac Defibrillator Lead Failure and Management," *Journal of the American College of Cardiology,* vol. 67, no. 11, pp. 1358-1368, 2016.

[4] T. Kleemann *et al.*, "Annual rate of transvenous defibrillation lead defects in implantable cardioverter-defibrillators over a period of >10 years," *Circulation,* vol. 115, no. 19, p. 2474, 2007.

[5] M. O. Sweeney, "Exploding implantable cardioverter defibrillator," *Journal of Cardiovascular Electrophysiology,* vol. 12, no. 12, p. 1422, 2001.

[6] R. Gradaus, G. Breithardt, and D. Bocker, "ICD leads: Design and chronic dysfunctions," in *PACE-Pacing Clin. Electrophysiol.* vol. 26, ed, 2003, pp. 649-657.

[7] N. Oza, M. Taylor, and S. Kalbfleisch, "The Impact of Inappropriate Shocks from Implantable Cardiac Defibrillator Lead Failure on Cardiovascular Morbidity and Mortality," *Circulation,* vol. 128, no. 22, 2013.

[8] K. Kolodzinska, A. Kutarski, M. Grabowski, I. Jarzyna, B. Małecka, and G. Opolski, "Abrasions of the outer silicone insulation of endocardial leads in their intracardiac part: a new mechanism of lead-dependent endocarditis," *Europace : European pacing, arrhythmias, and cardiac electrophysiology : journal of the working groups on cardiac pacing, arrhythmias, and cardiac cellular electrophysiology of the European Society of Cardiology,* vol. 14, no. 6, p. 903, 2012.

[9] S. M. Kurtz *et al.*, "Implantation Trends and Patient Profiles for Pacemakers and Implantable Cardioverter Defibrillators in the United States: 1993-2006.(Report)," *Pacing and Clinical Electrophysiology,* vol. 33, no. 6, p. 705, 2010.

[10] A. Himes and C. Wilson, "Wear of cardiac lead outer insulation due to internal cable motion," *Tribol. Int.,* vol. 62, pp. 177-185, 2013.

[11] C. Wilson and A. Himes, "Tribology of Insulation Materials Within Implantable Cardioverter-Defibrillator Leads," in *International Joint Tribology Conference*, Denver, Colorado, USA, 2012.

[12] U. Dorwarth *et al.*, "Transvenous defibrillation leads: high incidence of failure during long-term follow-up," *Journal of Cardiovascular Electrophysiology*, vol. 14, no. 1, p. 38, 2003.

[13] Sreekanth and P. S. S. R. Kanagaraj, "Wear of Biomedical Implants," ed, 2013, pp. 657-674.

[14] K. Friedrich, *Friction and Wear of Polymer Composites / edited by Klaus Friedrich*. Amsterdam ; New York: Amsterdam ; New York : Elsevier, 1986.

[15] A. K. Bhowmick, "Ridge Formation during the Abrasion of Elastomers," *Rubber Chemistry and Technology.*, vol. 55, no. 4, pp. 1055-1062, 1982.

[16] A. N. Gent and C. T. R. Pulford, "Mechanisms of rubber abrasion," *J. Appl. Polym. Sci.*, vol. 28, no. 3, pp. 943-960, 1983.

[17] A. N. Gent and C. T. R. Pulford, "Wear of Metal by Rubber," *Rubber Chemistry and Technology*, vol. 53, no. 1, pp. 176-185, 1980.

[18] F. A. Alnaimat, D. E. T. Shepherd, and K. D. Dearn, "Crack growth in medical-grade silicone and polyurethane ether elastomers," *Polymer Testing*, vol. 62, pp. 225-234, 2017.

[19] A. P. Serro, M. P. Gispert, M. C. L. Martins, P. Brogueira, R. Colaço, and B. Saramago, "Adsorption of albumin on prosthetic materials: Implication for tribological behavior," *Journal of Biomedical Materials Research.*, vol. 78, no. 3, pp. 581-589, 2006.

[20] M. P. Gispert, A. P. Serro, R. Colaço, and B. Saramago, "Friction and wear mechanisms in hip prosthesis: Comparison of joint materials behaviour in several lubricants," *Wear*, vol. 260, no. 1-2, pp. 149-158, 2006.

[21] D. J. Nelson, "Method for polishing silicone products," United States, 1993.

CHAPTER 6: GENERAL CONCLUSIONS

The conclusions of this dissertation can be categorized into two topics: Identifying the friction and wear mechanisms of 1) Polyetheretherketone and its relationship to transfer film development and 2) Silicone considering the parameters of load, albumin protein, and third-body silica abrasion.

The study described in Chapter 2 proposed a finite element model to determine the utility of the roughness parameter Ra in describing the contact behavior of rough surfaces between polymers and metals by developing two different surface types, a fractal based surface and a semi-cylindrical shaped asperity surface. These difference surface types were then used in a finite element contact model were the values of contact area and asperities in contact were collected. It was found that Ra is a weak descriptor of contact behavior as the surface types had geometrical differences that governed the relationship between contact length and load behavior. It was also concluded that the model could accurately describe the empirically tested Greenwood-Williamson model, but only at lower loads, and all surfaces failed in excessive principle strain. The conclusion that geometry of the asperities plays a large role in contact behavior despite surfaces having similar Ra demonstrates the possibility that surfaces in multi-directional sliding can have significantly different contact behavior depending on the direction of sliding with respect to roughness orientation.

The effects of roughness orientation in multi-directional sliding of the high-performance thermoplastic polyetheretherketone were then explored in Chapters 3 and 4. Emphasis was placed on the development of transfer film in relation to sliding direction with respect to roughness orientation. Chapter 3 investigated the effect of roughness orientation and explored linear and multi-directional wear paths. Several hypotheses to explain the disparity in transfer

film development between perpendicular and parallel-oriented sliding. It was determined that directional strengthening of the polymer chains or wear debris compaction was not responsible for the disparity seen in transfer film, but there was significant evidenced that frictional heating was playing a key role in transfer film volume. One key finding of how transfer film effects the wear cycle was that a thin, uniform transfer film appeared to reduce wear, and it was concluded that reciprocation plays a dominant role in the wear of PEEK.

Chapter 4 extended the study in Chapter 3 by investigating the transfer film development of PEEK at different sliding distances to better understand the relationship between transfer film and the wear cycle. It was determined that the direction of sliding with respect to roughness orientation greatly impacted wear at large sliding distances, and an effective PEEK transfer film required a large amount of sacrificial wear to be developed. There was evidence to suggest transfer film in perpendicular-oriented sliding was more strongly bonded to the counterface than parallel sliding. A model was proposed that described the difference in adhesive behavior of the two sliding orientations that predicted temperature rise as a function of cyclic strain magnitude of the asperities. Future work that investigates the dependence of counterface temperature on the development of transfer film in multi-direction sliding while accounting for roughness orientation would benefit the understanding of PEEK transfer film development.

Chapter 5 addressed the second topic of this dissertation, the friction and wear mechanisms of silicone, by performing wear tests on silicone leads used in an implantable cardiac device application by examining the effects of loading conditions, albumin protein, and silica as a third-body abrasive during sliding on titanium. By using statistical techniques and methods of analyzing the wear scars of the silicone leads, it was found that none of these parameters contributed significantly to the wear depth and profile area of the wear scar.

However, it was determined that silica may have acted as a polishing agent on the surface of the wear interface and albumin protein promoted the adhesion of wear debris to the interface and complex abrasion wear. Wear through and exposure of the conductors in the leads was influenced by load shielding at sliding distances of 400 meters. This study examined only one known wear mode of silicone leads, silicone-on-titanium, and future work that explores the other wear modes such as silicone-on-silicone sliding could provide further information on the friction and wear mechanisms experienced by silicone in this application.